
Electronic Thesis and Dissertation Repository

4-22-2021 10:30 AM

Implication of city growth on wind-induced loads for cladding and structural design

Hadil M. Abdallah, *The University of Western Ontario*

Supervisor: Girma Bitsuamlak, *The University of Western Ontario*

Co-Supervisor: Ayman El Ansary, *The University of Western Ontario*

A thesis submitted in partial fulfillment of the requirements for the Master of Engineering Science degree in Civil and Environmental Engineering

© Hadil M. Abdallah 2021

Follow this and additional works at: <https://ir.lib.uwo.ca/etd>



Part of the [Aerodynamics and Fluid Mechanics Commons](#), [Civil Engineering Commons](#), [Other Civil and Environmental Engineering Commons](#), and the [Structural Engineering Commons](#)

Recommended Citation

Abdallah, Hadil M., "Implication of city growth on wind-induced loads for cladding and structural design" (2021). *Electronic Thesis and Dissertation Repository*. 7740.
<https://ir.lib.uwo.ca/etd/7740>

This Dissertation/Thesis is brought to you for free and open access by Scholarship@Western. It has been accepted for inclusion in Electronic Thesis and Dissertation Repository by an authorized administrator of Scholarship@Western. For more information, please contact wlsadmin@uwo.ca.

Abstract

As cities grow, the urban topology changes in density resulting in continuous variations in wind flow. The interaction of flow with this changing surrounding environment drives the aerodynamics to become more complex and varying, subjecting the building to significant changes in wind-induced-loads both on structural and non-structural elements. In this study, a series of boundary layer wind tunnel tests are conducted to investigate the impact of city growth on cladding and structural loading by using a typical tall building adopted from the Commonwealth Advisory Aeronautical Council (CAARC) building model. The city growth is represented by five different generic surrounding configurations, varying in height ratios compared to the study building of height (H). The configuration includes isolated case (0000SH), surrounded with 0.25H height (0025SH), 0.5H height (0050SH), 0.75H height (0075SH) and H height (0100SH) of surrounding buildings, respectively. Based on the study analysis, the city growth has different impact on structural and non-structural elements from wind hazard perspectives. The overall recorded mean wind pressures are reduced while fluctuations within these pressures are increasing as the urban environment becomes denser creating wake induced turbulence. Due to Bernoulli and Venturi effect, local pressure increases are observed for certain cases. The results show 40% and 20% increase in the negative peak pressures \check{C}_p for cases 0025SH and 0050SH respectively compared to the isolated case scenario 0000SH at $AoA=120^\circ$ and 90° which subject the building to higher risk of cladding failure. From the main wind force resisting system, the mean and fluctuating base moments reduced by 20% for case 0050SH and 50% for case 0075SH which consequently decreased the peak base moments and top peak acceleration on the structural system.

Keywords

City development; urban growth; high-rise buildings; wind loads; surrounding buildings; wind tunnel testing; cladding design; structural design

Summary for Lay Audience

The limited land in urban areas has pushed people to build tall, flexible, and slender buildings, where wind is the governing design load. Several factors can affect the behavior of the building's structural and non-structural elements. One of the main factors contributing to the behavior of tall buildings is the surrounding layout. While a typical wind tunnel study can involve the actual representation of existing surrounding buildings, it does not take into consideration the effect of future city growth on the behavior of tall buildings. As cities grow, the surrounding layout change, making the wind phenomenon more complex and the flow of wind alters significantly. This variation in wind flow is due to the interaction of fluid flow with the new built environment. This study presents an experimental investigation on the impact of city growth on the behavior of the structural and non-structural elements of tall buildings. The city growth is represented by five surrounding configurations, varying in height ratios. The configurations are divided into 2 phases: first, experimenting a reference isolated model having a height (H). The second phase is experimenting four different surrounding configurations. This includes $0.25H$ height (0025SH), $0.5H$ height (0050SH), $0.75H$ height (0075SH) and H height (0100SH) of surrounding buildings, respectively in suburban terrain. Results have shown different impacts on structural and non-structural elements of tall buildings. For instance, the mean wind pressures on cladding are reduced with the increase of surrounding ratios. On the other hand, a fluctuation increase within the measured pressures was noticed as the urban environment becomes denser. This increase at certain critical configurations was observed to impact the cladding (non-structural) elements which in return subject the cladding elements to higher wind risks through damage accumulations. On the other hand, the structural assessment has shown an overall decrease in base moments with the increase in surrounding heights which consequently reduces the peak base moments and top accelerations, especially for higher surroundings heights.

Acknowledgments

Firstly, I would like to thank ALLAH, the Almighty, the Most Gracious and the Most Merciful who empowered me with strength and knowledge to accomplish this work.

I would like to express my sincere gratitude to my supervisor, Prof. Girma Bitsuamlak. He is an exceptional professor and a remarkable mentor. He guided me throughout my journey and opened my eyes to explore new things. He introduced me to the field of wind engineering, where I had the chance to work on great projects with wonderful people. Without his guidance and persistent help this dissertation would not have been possible.

This gratitude and respect need to be extended to Dr. Ayman El Ansary my co-supervisor. Dr. El Ansary is a knowledgeable professor and a great advisor. I am grateful for his confidence in me and his continuous support. I will always learn from him and look up to him academically and personally.

I would like to thank Dr. Ahmed El Shaer and Christopher Howlett for their support and help in my research. I want also to thank all my colleagues (Hang You, Anant, Kim, Thomas, Tsinuel, Eric, Matiyas, Muna, Meseret, Tibebu, Abiy, Anwar, Matt, Cody, Barilelo, Tewadros, Ameyo) for sharing their valuable experiences and knowledge with me.

Above ground, I am indebted to my family for their continuous love and care. Thanks to my husband “Moustafa” for believing in me and encouraging me achieving my goals. you’ve been a wonderful husband and an awesome dad to our beautiful son “Selim” who was part of this journey from the beginning. I would like to dedicate all the work I have done to them and thank Allah for your presence in my life. My deepest appreciation goes to my parents, sister, and little brother (Prof. Abdallah, Amel Lotfy, Dina, and Adel) for their endless love, support, and encouragement. Thank you for giving me the strength to chase my dreams. My in-laws (Prof. A. Aboutabikh, Wafaa, Farah, Marwa and Dr. Salah El-Fitiany) deserve my wholehearted thanks as well, you’ve always been there when I needed you the most.

Finally, I would like to thank all my friends in Canada and overseas, you encouraged me and supported me in every way you could. You all contributed greatly to my life and to this work.

Table of Contents

Abstract	ii
Summary for Lay Audience	iii
Acknowledgments	iv
Table of Contents	v
List of Tables	viii
List of Figures	ix
Chapter 1	1
1 Introduction	1
1.1 Background and literature review	1
1.2 Research objectives	6
1.3 Overview of thesis	7
1.4 References	9
Chapter 2	13
2 Methodology and analysis procedure	13
2.1 Wind tunnel testing	13
2.1.1 Description of test building and experimental setup	15
2.1.2 Test configurations	16
2.2 Aerodynamic data analysis	19
2.2.1 Mean pressure coefficient	19
2.2.2 Peak pressure coefficient	19
2.2.3 Area averaging	21
2.2.4 Base moments	22
2.2.5 Dynamic response	22
2.3 References	24

Chapter 3.....	25
3 Implications of city development on cladding loads.....	25
3.1 Introduction.....	25
3.2 Experimental setup.....	29
3.2.1 Model description and wind profile.....	29
3.2.2 Pressure measurements and statistics.....	30
3.2.3 Test configurations and cases	33
3.3 Results and discussion	35
3.3.1 Mean and fluctuation pressure distributions	35
3.3.2 Peak pressure distribution	40
3.3.3 Effect of height ratio on the local peak pressure coefficients.	45
3.3.4 Pressure power spectra.....	50
3.4 Conclusion	57
3.5 References.....	58
Chapter 4.....	61
4 Implications of city development on structural loads	61
4.1 Introduction.....	61
4.2 Experimental setup methodology	64
4.2.1 Wind tunnel testing	64
4.2.2 Pressure measurements	66
4.2.3 Dynamic response evaluation	69
4.2.4 Surrounding configurations	70
4.3 Results and discussion	71
Wind loading.....	71
4.3.1 Mean and rms pressure distribution.....	71
4.3.2 Base moment time histories and spectra.....	78

4.3.3	Mean, rms and peak base moments	80
4.3.4	Top floor acceleration	81
4.4	Conclusion	82
4.5	References	83
Chapter 5	86
5	Conclusion	86
5.1	Summary	86
5.2	Recommendation for future work	87
Curriculum Vitae	88

List of Tables

<i>Table 1-1: Scope and main findings of previous studies focused on the effect of surroundings on high-rise buildings</i>	<i>4</i>
<i>Table 2-1: Test plan and phases of testing</i>	<i>17</i>
<i>Table 2-2: Numerical coefficients of the BLUE method for (n=10).....</i>	<i>20</i>
<i>Table 3-1: Main findings of previous studies focused on the effect of surroundings on high-rise buildings from cladding point of view</i>	<i>28</i>
<i>Table 3-2: Test configurations and their corresponding cases for the surroundings buildings</i>	<i>33</i>
<i>Table 4-1: Scope and main findings of previous studies focused on the effect of surroundings on high-rise buildings</i>	<i>62</i>
<i>Table 4-2: Dynamic properties of the study building</i>	<i>68</i>
<i>Table 4-3: Mass distribution.....</i>	<i>70</i>
<i>Table 4-4: Test phases and configurations at different wind directions.</i>	<i>70</i>

List of Figures

<i>Figure 2-1: Principle of wind flow in a wind tunnel testing (Davenport 1967).....</i>	<i>13</i>
<i>Figure 2-2: Simulated wind parameters in wind tunnel for suburban terrain: (a) normalized mean wind speed, (b) turbulence intensity profiles (TI%).....</i>	<i>14</i>
<i>Figure 2-3:CAARC model installed at (UWO wind tunnel I) for the isolated case 0000SH at AoA=0° at a scale ratio of (1:400)</i>	<i>15</i>
<i>Figure 2-4: Model setup before installation in wind tunnel</i>	<i>16</i>
<i>Figure 2-5: Plan view with the alignment of the surrounding buildings and the spacing around the CAARC study model</i>	<i>17</i>
<i>Figure 2-6: Surrounding configurations where a) represents the study concept and b) wind tunnel installation</i>	<i>18</i>
<i>Figure 2-7: Elevation and side view tap locations with dimensions scaled to 1:400 in centimeters.</i>	<i>21</i>
<i>Figure 3-1: Simulated wind parameters in wind tunnel for suburban terrain: (a) normalized mean wind speed, (b) turbulence intensity profiles (TI%).....</i>	<i>30</i>
<i>Figure 3-2: Elevation and side view tap locations with dimensions scaled to 1:400 in centimeters.</i>	<i>32</i>
<i>Figure 3-3: Model setup before installation in wind tunnel connected to scanners for data recording.....</i>	<i>32</i>
<i>Figure 3-4: Installation of the surrounding configurations at UWO (wind tunnel I) for the 5 different cases at AoA = 45°</i>	<i>33</i>
<i>Figure 3-5: Alignment of the surrounding buildings with equal spacing around the CAARC study model.</i>	<i>34</i>

<i>Figure 3-6: Experimental model installed at (UWO wind tunnel I) for the isolated case 0000SH at AoA=0°.</i>	34
<i>Figure 3-7 Wind flow separation and eddies generation for different AoA hitting (a) frontal wall (b) corner walls.</i>	35
<i>Figure 3-8: Mean pressure coefficients (C_p) on the northern wall for all cases at AoA= 0°, 60°, 90°, 120°, 180°.</i>	38
<i>Figure 3-9: Root mean square of pressure coefficients (C_p) on the northern wall for all cases at wind directions θ= 0°, 60°, 90°, 120°, 180°.</i>	40
<i>Figure 3-10: Largest minimum \check{C}_p tap locations for a) case 0000SH, b) case 0050SH</i>	41
<i>Figure 3-11: Maximum peak pressure coefficients (\hat{C}_p) on the northern wall for all cases at AoA= 0°, 60°, 90°, 120°, 180°.</i>	43
<i>Figure 3-12: Minimum peak pressure coefficients (\check{C}_p) on the northern wall for all cases at AoA= 0°, 60°, 90°, 120°, 180°.</i>	45
<i>Figure 3-13: Variation in a) Maximum and b) Minimum pressure coefficient peaks for various configurations at AoA (θ).</i>	46
<i>Figure 3-14: a) specific tap locations at the northern and eastern facades and b) AoA(θ) according to tap location.</i>	48
<i>Figure 3-15: Variation of the positive peak pressure (\hat{C}_p) at the center line of the north facade for all cases at different AoA: (a) Tap A₁; (b) Tap A₂; (c) Tap A₃.</i>	48
<i>Figure 3-16: Variation of the negative peak pressure (\check{C}_p) at the center line of the north facade for all cases at different AoA: (a) Tap A₁; (b) Tap A₂; (c) Tap A₃.</i>	48
<i>Figure 3-17: Variation of the positive peak pressures (\hat{C}_p) at the corner edge of the east facade for all cases at different AoA: (a) Tap B₁; (b) Tap B₂; (c) Tap B₃.</i>	49
<i>Figure 3-18: Variation of the negative peak pressures (\check{C}_p) at the corner edge of the east facade for all cases at different AoA: (a) Tap B₁; (b) Tap B₂; (c) Tap B₃.</i>	49

<i>Figure 3-19: Variation of the positive peak pressures (\hat{C}_p) at the center line of the east facade for all cases at different AoA: (a) Tap C₁; (b) Tap C₂; (c) Tap C₃</i>	<i>49</i>
<i>Figure 3-20: variation of the negative peak pressures (\check{C}_p) at the center line of the east facade for all cases at different AoA: (a) Tap C₁; (b) Tap C₂; (c) Tap C₃</i>	<i>49</i>
<i>Figure 3-21: Power spectral densities of pressure at model height of 2/3H of the study building height for case 0000SH in suburban terrain at AoA=0°.</i>	<i>52</i>
<i>Figure 3-22: Power spectral densities of pressure at model height of 2/3H of the study building height for case 0025SH in suburban terrain at AoA=0°.</i>	<i>53</i>
<i>Figure 3-23: Power spectral densities of pressure at model height of 2/3H of the study building height for case 0050SH in suburban terrain at AoA=0°.</i>	<i>54</i>
<i>Figure 3-24: Power spectral densities of pressure at model height of 2/3H of the study building height for case 0075SH in suburban terrain at AoA=0°.</i>	<i>55</i>
<i>Figure 3-25: Power spectral densities of pressure at model height of 2/3H of the study building height for case 0100SH in suburban terrain at AoA=0°.</i>	<i>56</i>
<i>Figure 4-1: Experimental model in BLWTL for the isolate case 0000SH for a wind AoA=0°</i>	<i>65</i>
<i>Figure 4-2: Wind tunnel profiles for suburban terrain: (a) normalized mean wind speed, (b) turbulence intensity profiles (TI%)</i>	<i>65</i>
<i>Figure 4-3: a) perspective view and b) a longitudinal section of the constructed 3D printed model</i>	<i>66</i>
<i>Figure 4-4: Tributary area distribution on the pressure layout for the north and east elevations.</i>	<i>68</i>
<i>Figure 4-5: Mass distribution layout on the CAARC building</i>	<i>70</i>

<i>Figure 4-6: Installation of the CAARC model and the five different surrounding configurations of at the University of Western Ontario Boundary layer wind tunnel I (BLWT I).</i>	71
<i>Figure 4-7: mean pressure distribution (C_p) for the north, east and south facades at $AoA=0^\circ$</i>	74
<i>Figure 4-8: mean pressure distribution (C_p) for the north, east and south facades at $AoA=45^\circ$</i>	75
<i>Figure 4-9: Rms pressure distribution (C_p) for the north, east and south facades at $AoA=0^\circ$</i>	76
<i>Figure 4-10: Rms pressure distribution (C_p) for the north, east and south facades at $AoA=45^\circ$</i>	77
<i>Figure 4-11: CAARC building axis definition</i>	78
<i>Figure 4-12: Base moments time histories for M_x, M_y and M_z at $AoA=0^\circ$</i>	78
<i>Figure 4-13: Power spectral density of the base moment for a) M_x and b) M_y at $AoA=0^\circ$</i>	79
<i>Figure 4-14: Mean, rms, and peak base moment for M_x, M_y, M_z for different surrounding configurations for different wind AoA</i>	80
<i>Figure 4-15: Top floor acceleration along the x-axis, y-axis and the torsional</i>	81

Chapter 1

1 Introduction

1.1 Background and literature review

The development of cities and the rapid growth of our communities directed the designers to focus on vertical expansion more than ever. The urge for urbanization is the reason behind building more tall, flexible, and slender structures where wind is the governing design parameter (Holmes 2018). However, the current methods of design of structural and nonstructural elements for high-rise buildings are not accurately representing the real developing environment of city growth. It is mainly derived for isolated building cases with limited guidelines about the effect of the surroundings. In most cases, they provide either a conservative estimate of the along-wind peak loads or an underestimated prediction for the local peak pressures on building surfaces leading to cladding failure. As a result, wind tunnels have been significantly involved over the past decades to assure accuracy of the design, especially with code limitations with respect to building height, shape, and surrounding configurations. Typically, a wind tunnel study on a structure, as presented by (Davenport 2002), includes the evaluation of local wind climate for the structure, simulation of the corresponding boundary layer taking the terrain roughness and topography into consideration and modeling the aerodynamic characteristics of the building shape and the potential for load increase.

As the city grows, the wind phenomenon becomes more complex and the flow of wind changes significantly than usual. This variation in wind flow is due to the interaction of fluid flow with the built environment (Krishna 1995) and (Holmes 2002). As a result, the change in the urban topology can either significantly increase or decrease not only the overall wind loads on the building structure but might also affect the local peak pressures acting on the nonstructural components as cladding elements. Several studies were performed on the effect of existing surrounding buildings on high-rise building loads. This topic gained attention starting in the early seventies, when the three out of eight natural draft cooling towers at Ferrybridge, England in 1965 were collapsed. The reasons where

highly associated to the existing built environment (Amrit 1980). Since then, several experimental tests took place, exploring the effect of twin buildings, square in shape (one acted as the shielding body while, the other was the instrumented study model), assuming a tandem arrangement and an open terrain exposure (Lee and Fowler 1975). Studies found in the literature also investigated and assessed the behavior of high-rise buildings under different urban topologies. (Bailey and Kwok 1985) performed a series of boundary layer wind tunnel tests to study the enhanced dynamic response of a Highrise square building under the effect of a neighboring twin building. (Stone 1987) studied the effect of a group of upstream buildings on the loading of a high-rise building. Different building aspect ratios and their shielding effect on the study building were also investigated by (English 1990). Using flow visualization tests, (Taniike 1991) examined the effect of turbulence on the aerodynamic interference by indicating that the fluctuating drag on the study building increased as the size of the surrounding building increased because, the larger the width of the surrounding building, the larger the size of the shed vortices. (Atul C. Khanduri, Stathopoulos, and Bédard 2000) classified the behavior of drag and lift coefficients over several wind tunnel experiments of varying aspect ratios, height of surrounding buildings at different terrain exposures. Dynamic response of a high-rise building due to surrounding effects for multiple wind tunnel model types (i.e., force balance test, aeroelastic test) were also compared (Huang and Gu 2005). Moreover, (Lam, H. Leung, and Zhao 2008) investigated the structural response on the study model immersed in a row of closely spaced, square high-rise buildings. (Mara et al. 2014) also assessed the interference effect caused by a twin building to the study model showing reduction in the mean and rms- along wind moments for a single upstream interfering building.

Most of the past mentioned studies were limited in terms of surrounding configurations intended to investigate 2 or more buildings mainly on the same row or shielding one layer around the building which is specific to certain cases not quite representing the real situation. Their work focused on the effect of shape differences, aspect ratios and type of arrangement on the overall loading from structural perspective. Only few studies tackled the impact of changing wind loads on non-structural elements such as claddings components. For instance, (Irwin 1998) studied the effect of future buildings on cladding pressure changes and developed a methodology to adjust wind tunnel results to compensate

the obtained uncertainty. (Surry and Mallais 1983) performed pressure tests and determined the cladding pressures on a high-rise building with and without surrounding buildings with a fixed spacing. They reported high suction near the ground and at the top corner of the studied building. In the late 90s, (Surry and Djakovich 1995) explored the highest peak suctions developed on the building surfaces of an isolated case only and their relation to the building geometry and turbulence intensity. (Kim et al. 2011) performed a series of wind tunnel tests to study the effect of sheltering on the local peak pressures of two high rise buildings with different spacing, height configurations and with different building shapes. (Hui et al. 2013) and also investigated the interference effects between two high-rise buildings with same heights but different shapes and arrangement, the results show an increase in the negative pressures for some cases up to 50% larger than in the isolated case and decrease of around 30% in other cases depending on the wind direction.

On the other hand, computational fluid dynamics (CFD) simulations were also utilized to predict wind-induced responses in high-rise buildings. For instance, (Zhang and Gu 2008) performed a CFD study to investigate the effect of a neighboring building on an adjacent tall building in a staggered arrangement at different wind azimuths. The results show good agreement with wind tunnel results in terms of mean C_p , base moments, and base forces. (Cóstola et al. 2009) also compared CFD simulations to different wind tunnel results, full scale measurements and databases using building energy simulation and airflow network programs. The study investigated different parameters that affect the distribution of pressure coefficients on building surfaces as different building shapes, facade detailing and degree of sheltering of identical building configurations at several wind directions. (Dagneu and Bitsuamlak 2014), evaluated the aerodynamic response of a typical tall building with and without surrounding buildings (i.e. isolated building, two adjacent buildings) showing a good agreement of pressure, top displacement, top accelerations, and base moments with wind tunnel results. (Elshaer et al. 2016), (Elshaer et al. 2017), also investigated the aerodynamic response and the structural analysis of a typical tall building with and without surrounding buildings.

However, most of previous work had limitations in term of the number of surrounding buildings, orientation, height ratios and most importantly the prediction of city growth and

future development. In this thesis, several wind tunnel tests were performed on a typical high-rise building (CAARC), including generic surrounding configurations representing city growth to study the impact of city development on wind-induced loads on building components (structural and nonstructural elements). The generic configurations cover an area of 500m in radius in full scale, varying in height ratios, representing the predicted city development. Table 1-1 summarizes the main findings focusing on the effect of surround on high-rise buildings in terms of structural and cladding design.

Table 1-1: Scope and main findings of previous studies focused on the effect of surroundings on high-rise buildings

Authors	Model	Study purpose	Surrounding Environment	Comments
Surray and Mallais (1982)	BLWT	Cladding design	2 buildings	Performed pressure tests to determine the cladding pressures on a typical high-rise building with and without an interference building with fixed spacing.
Bailey and kwok (1985)	BLWT	Structural design	2 buildings	Studied the dynamic response of a high-rise building due to the effect of an adjacent twin building.
Stone (1987)	BLWT	Structural design	Multiple buildings	Studied the effect of a group of upstream buildings on the loading of a high-rise building
English (1990).	BLWT	Structural design	2 buildings	Investigated different aspect ratios and their shielding effect on the study building.
Taniike (1991)	BLWT	Cladding design	2 buildings	Investigated the effect of changing the aspect ratio of an upstream building on the structural response of a typical high-rise building, the results show an increase in the fluctuating drag as the size increases.
Surry and Djakovich (1995)	BLWT	Cladding design	Isolated building	Explored the highest peak suction developed on the building surfaces of an isolated building with changing the building geometry.

Irwin (1998)	BLWT	Cladding design	Isolated / 2 buildings	Studied the variation in the negative pressure and developed a correction value for wind tunnel results.
Khanduri et al. (2000)	BLWT	Structural design	2 buildings	Investigated the structural response of a high-rise building surround by an interference building with different aspect ratios, height of surrounding building and terrain exposures.
Huang and Gu (2005)	BLWT	Structural design	2 buildings	Compared the dynamic response of a downstream building surrounded by an adjacent a typical building with different experimental techniques (i.e. HFFB, aeroelastic).
Zhao and Lam (2008)	BLWT	Structural design	Row of square buildings	Studied the structural response on a high-rise building surrounded by a set of square-based buildings closely spaced in a row.
Zhang and Gu (2008)	CFD	Cladding design	2 buildings	Examined the Aerodynamic behavior of buildings with staggered arrangement showing good agreement with wind tunnel results in terms of mean C_p , base moments, and base shear.
Cóstola et al. (2009)	CFD	Cladding design	1 layer of surrounding buildings	Investigated different parameters that affect the distribution of pressure coefficients on building surfaces (i.e. building geometries, façade detailing and degree of exposure) adopting identical building configurations at several wind directions.
Kim et al. (2011)	BLWT	Cladding design	2 buildings	Investigated the effect of different heights, spacing and wind directions of a surrounding building to assess the local peak pressures on interference effect
Hui et al. (2012)	BLWT	Structural design	Isolated building	Studied the effect of geometry on a high-rise building due to the effect of an adjacent surrounding building.

Hui et al. (2013)	BLWT	Structural design	2 buildings	Investigated the flow field and the pressure distribution of interference effects on external pressures between two high-rise buildings of exact height.
Dagnew and Bitsuamlak (2014)	CFD	Structural design	2 buildings	Investigated the effect of sheltering of a neighboring building. Also, examined three different turbulence models showing agreement of the synthetic method with the BLWT.
Mara et al. 2014	BLWT	Structural design	2 buildings	Assessed the interference effect caused by a neighboring building showing reduction in the mean and rms- along wind moments for a single upstream interfering building
Elshaer et al (2016)	CFD	Structural design	Isolated and Complex building surroundings	Investigated the aerodynamic response of a typical tall building with and without surrounding buildings showing a decrease in mean by 50% and an increase in rms by 40%.
Elshaer et al (2017)	CFD	Structural design	1 layer of surrounding buildings	Examined the changes in the design of wind loads on tall buildings with urban development showing a reduction in the mean and fluctuating base moments by 50% and 20%, respectively, with the increase in surrounding height .

1.2 Research objectives

The research objective is to develop a generic configuration of surroundings varying in height ratios and covering a wider surrounding radius around the study building that mimic the real development of cities. This can provide a representation of urbanization aiming to monitor the complex behavior of wind and its impact on building structural and non-structural elements such as cladding. It also intends to deliver a better understanding on the interaction of wind flow while provide a fair comparison between different configurations in relation to the isolated case scenario. The focus of the experimental work is to outline the resulting load effect on nonstructural components for cladding design through the

evaluation of local peak pressures on the building surfaces and from a structural perspective evaluating the base forces, spectra and top floor acceleration through city development. Therefore, in this study, boundary layer wind tunnel tests were performed to investigate and evaluate the impact of city growth on the behavior of a typical high-rise building adopted from the Commonwealth Advisory Aeronautical Research Council (CAARC) building model. The city growth is represented by five different generic surrounding configurations, varying in height ratios compared to the study building of height (H). The configuration includes an isolated case (0000SH), surrounded with 0.25H height (0025SH), 0.5H height (0050SH), 0.75H height (0075SH) and H height (0100SH) of surrounding buildings, respectively in suburban terrain.

The outlined tests were performed to:

- Evaluate the impact of urban growth on wind pressure distribution on building facades with change in wind directions.
- Assess the minimum and maximum local peak pressures for cladding design purposes
- Verify structural base forces and moments F_x , F_y , and M_x , M_y , M_z time histories and evaluate the energy distributed spectra with city development
- Compare the expected acceleration at the top of the study model in isolated case and with the increase of surrounding height ratios.

1.3 Overview of thesis

The structure of this study is organized as follows:

- Chapter 1 introduces the impact of city development on wind induced loads and provides a full review on previous literature from structural and non- structural perspectives. It identifies the research gaps and gives an outline of the planned work to be addressed thoroughly in the following chapters.
- In Chapter 2, a detailed description of the experimental approach is addressed through boundary layer wind tunnel testing. It outlines the test procedures, model

creation and preparation of the wind tunnel to accommodate different surrounding configurations.

- In Chapter 3, analyzed wind tunnel data are presented and discussed in comparison with the isolated case scenario. It focuses on the effect of surrounding on wind-induced loads for cladding design purpose through extreme value analysis.
- Chapter 4 focuses on the analysis of wind tunnel data to discuss the impact of city development on wind-loads from structural perspective through analyzing base forces and moments time histories and comparing top floor accelerations in x and y directions.
- Finally, chapter 5 concludes the study by summarizing the results and discussing the research values to be considered for proper design prediction of loads, while considering the study limitations and possible future application.

1.4 References

- ASCE. 2012. “Wind Tunnel Testing for Buildings and Other Structures.” In . American Society of Civil Engineers.
- Bailey, P A, and K C S Kwok. 1985. “Interference Excitation of Twin Tall Buildings.” *Journal of Wind Engineering and Industrial Aerodynamics* 21 (3): 323–38.
- Bezabeh, M. A., G. T. Bitsuamlak, M. Popovski, and S. Tesfamariam. 2020. “Dynamic Response of Tall Mass-Timber Buildings to Wind Excitation.” *Journal of Structural Engineering* 146 (10): 04020199. [https://doi.org/10.1061/\(asce\)st.1943-541x.0002746](https://doi.org/10.1061/(asce)st.1943-541x.0002746).
- Chen, Xinzhong, and Ahsan Kareem. 2005. “Dynamic Wind Effects on Buildings with 3D Coupled Modes: Application of High Frequency Force Balance Measurements.” *Journal of Engineering Mechanics* 131 (11): 1115–25. [https://doi.org/10.1061/\(asce\)0733-9399\(2005\)131:11\(1115\)](https://doi.org/10.1061/(asce)0733-9399(2005)131:11(1115)).
- Cheung, J C K. 1984. “Effect of Tall Building Edge Configurations on Local Surface Wind Pressures.” In *3rd International Conference on Tall Buildings, Hong Kong and Guangzhou*, 10–15.
- Codes, National Research Council of Canada. Canadian Commission on Building and Fire. 2015. “National Building Code of Canada: 2015.” National Research Council of Canada. Canadian Commission on Building and Fire Codes.
- Cóstola, D., B. Blocken, and J. L.M. Hensen. 2009. “Overview of Pressure Coefficient Data in Building Energy Simulation and Airflow Network Programs.” *Building and Environment* 44 (10): 2027–36. <https://doi.org/10.1016/j.buildenv.2009.02.006>.
- Dagnew, Agerneh K., and Girma T. Bitsuamlak. 2014. “Computational Evaluation of Wind Loads on a Standard Tall Building Using Les.” *Wind and Structures, An International Journal* 18 (5): 567–98. <https://doi.org/10.12989/was.2014.18.5.567>.
- Davenport, A G. 1967. “The Treatment of Wind Loading on Tall Buildings.” In *Tall*

Buildings, 3–45. Elsevier.

Davenport, Alan G. 2002. “Past, Present and Future of Wind Engineering.” *Journal of Wind Engineering and Industrial Aerodynamics* 90 (12–15): 1371–80.

[https://doi.org/10.1016/S0167-6105\(02\)00383-5](https://doi.org/10.1016/S0167-6105(02)00383-5).

Elshaer, Ahmed, Haitham Aboshosha, Girma Bitsuamlak, Ashraf El Damatty, and Agerneh Dagnew. 2016. “LES Evaluation of Wind-Induced Responses for an Isolated and a Surrounded Tall Building.” *Engineering Structures* 115: 179–95.

<https://doi.org/10.1016/j.engstruct.2016.02.026>.

Elshaer, Ahmed, Anant Gairola, Kimberley Adamek, and Girma Bitsuamlak. 2017.

“Variations in Wind Load on Tall Buildings Due to Urban Development.”

Sustainable Cities and Society 34 (December 2016): 264–77.

<https://doi.org/10.1016/j.scs.2017.06.008>.

English, Elizabeth C. 1990. “Shielding Factors from Wind-Tunnel Studies of Prismatic Structures.” *Journal of Wind Engineering and Industrial Aerodynamics* 36: 611–19.

ESDU. 2001. *Engineering Sciences Data Unit. Characteristics of Atmospheric Turbulence near the Ground. Part II: Single Point Data for Strong Winds*. 85320th ed.

Holmes, John D. 2018. *Wind Loading of Structures*. CRC press.

Holmes, John D, Yukio Tamura, and Prem Krishna. 2008. “Wind Loads on Low, Medium and High-Rise Buildings by Asia-Pacific Codes,” no. May: 29–31.

Huang, Peng, and Ming Gu. 2005. “Experimental Study on Wind-Induced Dynamic Interference Effects between Two Tall Buildings.” *Wind and Structures, An International Journal* 8 (3): 147–61. <https://doi.org/10.12989/was.2005.8.3.147>.

Hui, Yi, Akihito Yoshida, and Yukio Tamura. 2013. “Interference Effects between Two Rectangular-Section High-Rise Buildings on Local Peak Pressure Coefficients.” *Journal of Fluids and Structures* 37: 120–33.

- Kareem, Ahsan. 1992. "Dynamic Response of High-Rise Buildings to Stochastic Wind Loads." *Journal of Wind Engineering and Industrial Aerodynamics* 42 (1–3): 1101–12. [https://doi.org/10.1016/0167-6105\(92\)90117-S](https://doi.org/10.1016/0167-6105(92)90117-S).
- Khanduri, A. C., T. Stathopoulos, and C. Bédard. 1998. "Wind-Induced Interference Effects on Buildings - A Review of the State-of-the-Art." *Engineering Structures* 20 (7): 617–30. [https://doi.org/10.1016/S0141-0296\(97\)00066-7](https://doi.org/10.1016/S0141-0296(97)00066-7).
- Khanduri, Atul C., Theodore Stathopoulos, and Claude Bédard. 2000. "Generalization of Wind-Induced Interference Effects for Two Buildings." *Wind and Structures, An International Journal* 3 (4): 255–66. <https://doi.org/10.12989/was.2000.3.4.255>.
- Kijewski, T; Kareem, A. n.d. "Dynamic Wind Effects - A Comparative Study (1998).Pdf." *Wind & Structures*.
- Kim, Wonsul, Yukio Tamura, and Akihito Yoshida. 2011. "Interference Effects on Local Peak Pressures between Two Buildings." *Journal of Wind Engineering and Industrial Aerodynamics* 99 (5): 584–600. <https://doi.org/10.1016/j.jweia.2011.02.007>.
- Krishna, Prem. 1995. "Wind Loads on Low Rise Buildings - A Review." *Journal of Wind Engineering and Industrial Aerodynamics* 54–55 (C): 383–96. [https://doi.org/10.1016/0167-6105\(94\)00055-I](https://doi.org/10.1016/0167-6105(94)00055-I).
- Lam, K. M., M. Y. H. Leung, and J. G. Zhao. 2008. "Interference Effects on Wind Loading of a Row of Closely Spaced Tall Buildings." *Journal of Wind Engineering and Industrial Aerodynamics* 96 (5): 562–83. <https://doi.org/10.1016/j.jweia.2008.01.010>.
- Lee, B E, and G R Fowler. 1975. "The Mean Wind Forces Acting on a Pair of Square Prisms." *Building Science* 10 (2): 107–10.
- Lieblein, Julius. 1974. "Efficient Lillithods of Extreme-Value Methodology," no. October.

- Mara, T. G., B. K. Terry, T. C.E. Ho, and N. Isyumov. 2014. "Aerodynamic and Peak Response Interference Factors for an Upstream Square Building of Identical Height." *Journal of Wind Engineering and Industrial Aerodynamics* 133: 200–210. <https://doi.org/10.1016/j.jweia.2014.06.010>.
- Melbourne, W. 1980. "Comparison of Measurements on the CAARC Standard Tall Building Model in Simulated Model Wind Flows." *Journal of Wind Engineering and Industrial Aerodynamics* 6: 73–88.
- Stone, Gary K. 1987. *Aerodynamic Interference Effects on Wind Loads and Responses of Tall Buildings*. Faculty of Engineering Science, University of Western Ontario.
- Surry, D., and D. Djakovich. 1995. "Fluctuating Pressures on Models of Tall Buildings." *Journal of Wind Engineering and Industrial Aerodynamics* 58 (1–2): 81–112. [https://doi.org/10.1016/0167-6105\(95\)00015-J](https://doi.org/10.1016/0167-6105(95)00015-J).
- Surry, David, and William Mallais. 1983. "Adverse Local Wind Loads Induced by Adjacent Building." *Journal of Structural Engineering* 109 (3): 816–20. [https://doi.org/10.1061/\(asce\)0733-9445\(1983\)109:3\(816\)](https://doi.org/10.1061/(asce)0733-9445(1983)109:3(816)).
- Xie, J, and P A Irwin. 1998. "Application of the Force Balance Technique to a Building Complex." *Journal of Wind Engineering and Industrial Aerodynamics* 77: 579–90.
- Xie, Z. N., and M. Gu. 2007. "Simplified Formulas for Evaluation of Wind-Induced Interference Effects among Three Tall Buildings." *Journal of Wind Engineering and Industrial Aerodynamics* 95 (1): 31–52. <https://doi.org/10.1016/j.jweia.2006.05.003>.
- Xie, Z. N., and Minggu Gu. 2004. "Mean Interference Effects among Tall Buildings." *Engineering Structures* 26 (9): 1173–83. <https://doi.org/10.1016/j.engstruct.2004.03.007>.
- Zhang, Aishe, and Ming Gu. 2008. "Wind Tunnel Tests and Numerical Simulations of Wind Pressures on Buildings in Staggered Arrangement." *Journal of Wind Engineering and Industrial Aerodynamics* 96 (10–11): 2067–79. <https://doi.org/10.1016/j.jweia.2008.02.013>.

Chapter 2

2 Methodology and analysis procedure

2.1 Wind tunnel testing

For the current study, wind tunnel experimental tests were conducted on a high-rise building with different surrounding configurations representing the city development. The Experimental work took place at the University of Western Ontario's Boundary Layer Wind Tunnel I (BLWT I). The tunnel consists of 4 main parts; the inlet (flow preprocessing), the working section (flow processing section), the test area and the exhaust, see Figure 2-1. The inlet draws in air and passes it through a honeycomb screen to generate a smooth flow. This flow then passes through the working section, which is approximately 2.44m wide, 24.4m in length and a height range from 1.7 to 2.3m. It includes three 0.8m high trapezoidal spires, a barrier and cube shaped roughness elements on the floor with various sizes between 2 and 5 cm. Meanwhile, the walls and ceiling are constructed using smooth wood panels and plexiglass for minimum flow friction on the sides and top. The combination of the spires, the barrier and the roughness blocks generate the turbulence needed in the flow to convert the laminar flow at the inlet into turbulent flow to achieve the desired atmospheric boundary layer (ABL) profile, see Figure 2-2. The level of exposure is then determined through adjusting the height and number of blocks obstructing the flow. As for the test section, the model is installed and mounted on a rotating round table to accommodate different wind directions. It is connected to the data acquisition for raw data extraction.

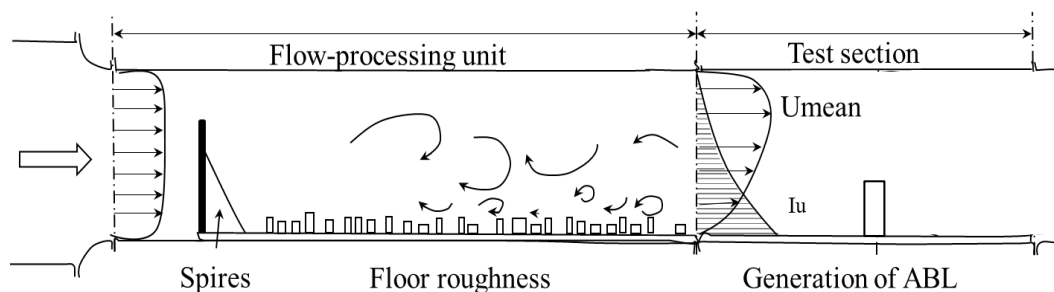


Figure 2-1: Principle of wind flow in a wind tunnel testing (Davenport 1967)

The time series are measured using the pitot tubes, see Figure 2-3. It is an instrument that measures the dynamic velocity in u , v , and w directions with a frequency of 1250Hz. It also has a port to measure the static pressure in unit Pa. The extracted information is in the form of sample numbers, sample frequency, date, and time of measurement. The reference wind speed is measured using pitot tubes. It is hanged from the ceiling at a standard height of 147cm adjusted at the wind gradient height. It measures the relative atmospheric pressure difference and convert it into voltage to be able to record the digital signals as time series. Then the signals are converted from volt to unitless coefficient of pressure C_p for analysis.

The flow fields generated in the current investigation are properly adjusted according to the geometry scale ratio (1:400). In wind tunnel testing, the actual scale and the model scale velocities, time, and length are adjusted for reliable results. For this study, the scaling will replicate the Engineering Science Data Unit (ESDU 2001) models. The tests were carried out in suburban exposure for all the surrounding configurations to represent the city-topology. The wind profiles: the mean wind speed profiles and turbulence intensity of the simulated suburban exposure are shown in Figure 2-2 .

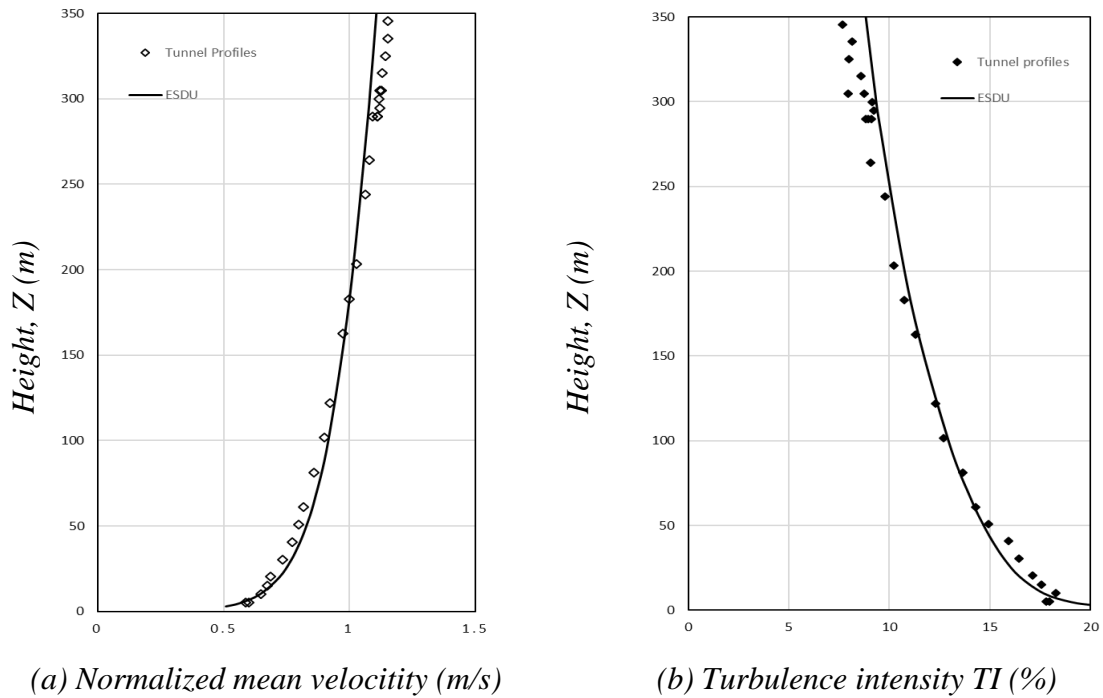


Figure 2-2: Simulated wind parameters in wind tunnel for suburban terrain: (a) normalized mean wind speed, (b) turbulence intensity profiles (TI%)

2.1.1 Description of test building and experimental setup

The study model was adopted from the Commonwealth Advisory Aeronautical Research Council (CAARC) building (Melbourne 1980). It has a rectangular footprint of 45.72 m (150 ft) * 30.48 m (100 ft) and a height of 182.88 m (600ft) in full scale as shown in Figure 2-3.

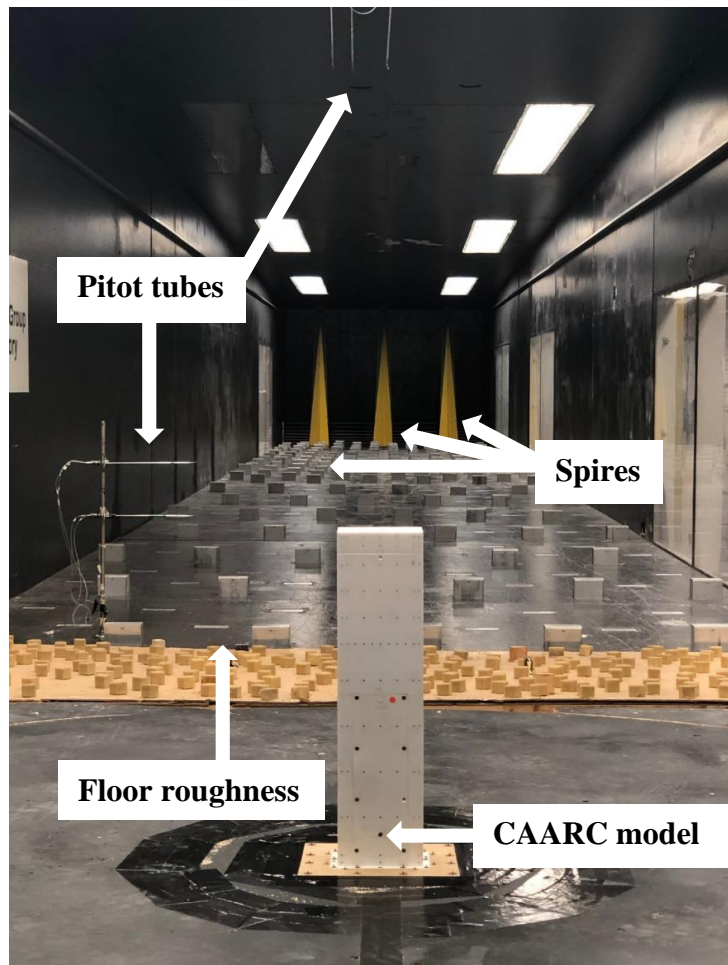


Figure 2-3: CAARC model installed at (UWO wind tunnel I) for the isolated case 0000SH at $AoA=0^\circ$ at a scale ratio of (1:400)

The tests included 5 different surrounding configurations: first, experimenting a reference isolated model having a height (H). The second phase is experimenting four different surrounding configurations. This includes 0.25H height (0025SH), 0.5H height (0050SH), 0.75H height (0075SH) and H height (0100SH) of surrounding buildings, respectively in suburban terrain. Detailed description of the test configurations is found in Table 2-1. High Frequency Pressure Integration test (HFPI) was adopted for the current test to capture the

variation of wind-induced pressures on the CAARC model surfaces throughout the surrounding growth. The wind pressure on the model surface are measured using a multi-pressure sensing system installed using pressure taps at specific location on the model surfaces. It was constructed to have a hollow interior to allow a room for the pressure acquisition system to be mounted inside the model. A total number of 367 taps were installed on the model surfaces including 51 roof taps. Pressure readings were conducted for 23 wind directions from 0 – 180 degrees at 10-degree increment. The pressure time history for all taps were measured simultaneously at a sampling frequency of 400 Hz with 51200 data points recorded for all the surface pressure taps. The pressure time histories for each wind direction was recorded for 128s at model scale which corresponds to 3.5 hours at full-scale. Each tap is connected to an electronic pressure scanner through 600-mm-long plastic tubing of approximately 1.5 mm internal diameter, see Figure 2-4. The pressure taps are designed to be distributed over 12 layers along the height of the building with denser points towards the corners for maximum capturing of vortices at the building edges. The surface pressure measurements are expressed in unitless coefficient of pressure C_p , relative to the roof height mean wind speed. They are recorded in the form of time series.



Figure 2-4: Model setup before installation in wind tunnel

2.1.2 Test configurations

The surrounding models were made from high-density foam blocks. They surround the pressure model with 5 layers of sheltering buildings, representing a generic form of the city

development varying in height ratios. They act as wind barrier around the study model (CAARC); thus, no pressure taps are required to be installed in these models, see Figure 2-6. These sheltering blocks have exact same footprint as the CAARC model, equally spaced from each other with a gap distance of 7.6cm in model scale as shown in Figure 2-5. The testing was divided into two phases: (a) testing the CAARC model in its isolated case without any surrounding. (b) testing the CAARC under the influence of surrounding elements with different configuration,

Table 2-1: Test plan and phases of testing

Configurations	Case	Height of surrounds H_s (m)	Height Ratios ($H_r=H_s/H$)	Exposure (z_0)
Isolated	0000SH	0.00	0.00	<i>Suburban (0.30)</i>
With Surrounding Buildings	0025SH	45.72	0.25	<i>Suburban (0.30)</i>
	0050SH	91.44	0.50	<i>Suburban (0.30)</i>
	0075SH	137.16	0.75	<i>Suburban (0.30)</i>
	0100SH	182.88	1.00	<i>Suburban (0.30)</i>

Note: wind pressure measurements were taken for 0-180° AoA @ 10° increment to additional AoA (45°, 135°, 225°, 315°) were also tested.

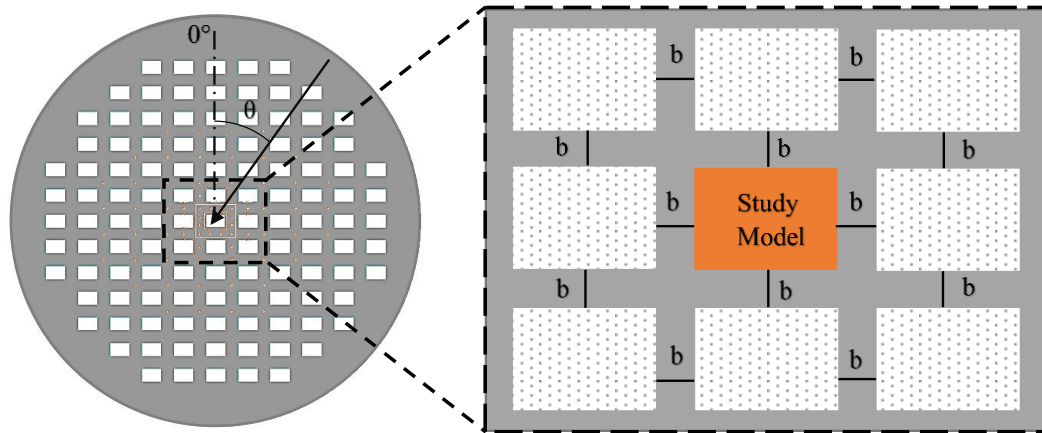


Figure 2-5: Plan view with the alignment of the surrounding buildings and the spacing around the CAARC study model

$b = 30.0$ m in full scale [$b = 7.6$ cm in model scale 1:400]

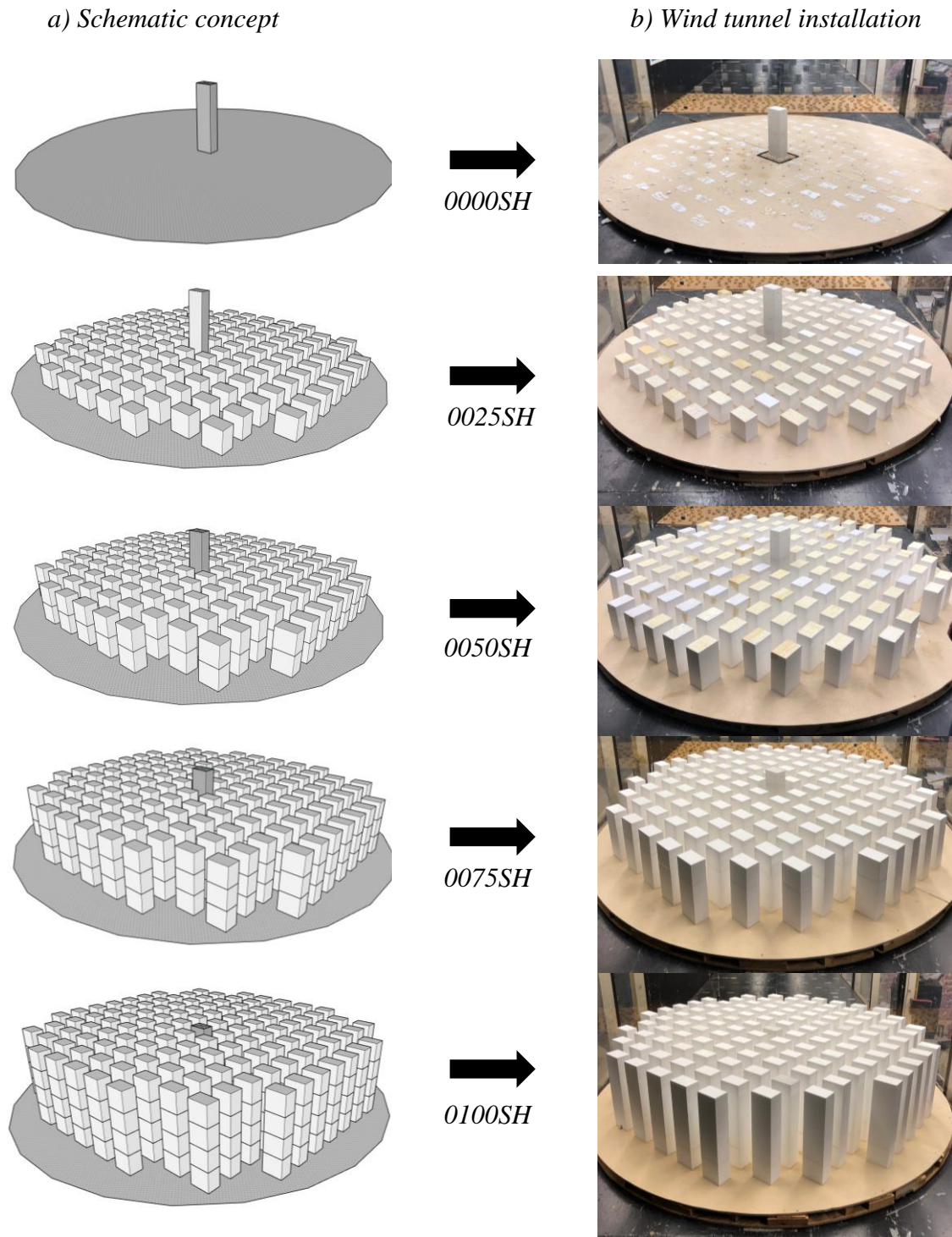


Figure 2-6: Surrounding configurations where a) represents the study concept and b) wind tunnel installation

2.2 Aerodynamic data analysis

2.2.1 Mean pressure coefficient

Pressure coefficients are normalized pressures relative to the mean wind speed at the building roof height U_h . They are recorded in the form of time series, which require further analysis for load evaluation. Different distinctions of pressure coefficients can be extracted as the mean, root mean square fluctuations, maximum and minimum values (Holmes et al. 2008),

$$\bar{C}p_i = \frac{p_i - p_0}{\frac{1}{2} \rho_a \bar{U}_h^2} \quad 2-1$$

$$\hat{C}p_i = \frac{\sqrt{\dot{p}_i^2 - p_0}}{\frac{1}{2} \rho_a \bar{U}_h^2} \quad 2-2$$

$$\hat{C}p_i = \frac{\hat{p}_i - p_0}{\frac{1}{2} \rho_a \bar{U}_h^2} \quad 2-3$$

$$\check{C}p_i = \frac{\check{p}_i - p_0}{\frac{1}{2} \rho_a \bar{U}_h^2} \quad 2-4$$

where, the denominator represents the dynamic pressure obtained from the mean wind speed at roof top of the building \bar{U}_h and air density ρ_a . The reference pressure is expressed in p_0 , where the instantaneous pressure p_i is the varying pressure and the tap location is expressed in i . These measurements are then extracted from the building surfaces to be stored in an excel sheet with given specific numbers corresponding to their location and their attached scanners, see Figure 2-4. Wind loads can then be obtained through multiplying the pressure values to its corresponding tributary areas assigned for each tap location.

2.2.2 Peak pressure coefficient

The peak pressures play an important role in cladding design. Thus, extreme value analysis is required to determine the peak pressures for proper evaluation of loads on building surfaces. For the current investigation, the generated extreme pressure values were

obtained using the liblein Best Linear Unbiased Estimator (BLUE) method, (Lieblein 1974). This method is well-developed and used widely in the wind engineering industry. The technique is an estimator for the Gumble method represented by the following cumulative distribution function (c.d.f.),

$$Prob \{X \leq x\} = e^{e^{-(x-u)/b}} \quad 2-5$$

where, x is the set of data and (u, b) are the numerical values for the best linear unbiased estimators (BLUE) representing location and scale parameters, respectively. The liblein Blue technique is achieved through dividing the data set into 10 segments. For each subset, the positive peaks and the negative peaks are extracted and reordered in ascending or descending order depending on the extracted value type. Then by substituting in the following linear functions,

$$u_n' = \sum_{i=1}^{10} a_i \cdot x_i \quad 2-6$$

$$b_n' = \sum_{i=1}^{10} b_i \cdot x_i \quad 2-7$$

where u_n' and b_n' represent the location and scale parameters and a_i and b_i are the numerical coefficients obtained from the table below for $n \leq 16$ (n is the number of samples), see Table 2-2.

Table 2-2: Numerical coefficients of the BLUE method for (n=10)

n	a_i	b_i
1	.222867	-.347830
2	.1623088	-.091158
3	.133845	-.019210
4	.112868	.022179
5	.095636	.048671
6	.080618	.066064
7	.066988	.077021
8	.054193	.082771
9	.041748	.083552
10	.028929	.077940

2.2.3 Area averaging

The tributary area of the model surface pressures was defined using a simple grid mesh applied using AutoCAD and a python code covering the entire surfaces of the CAARC model. The mesh is created so that it divides the space between each two adjacent taps in x and y-directions to forms an enclosed cell around each tap, where the mesh centroid is positioned exactly at the center of each tap, see Figure 2-7

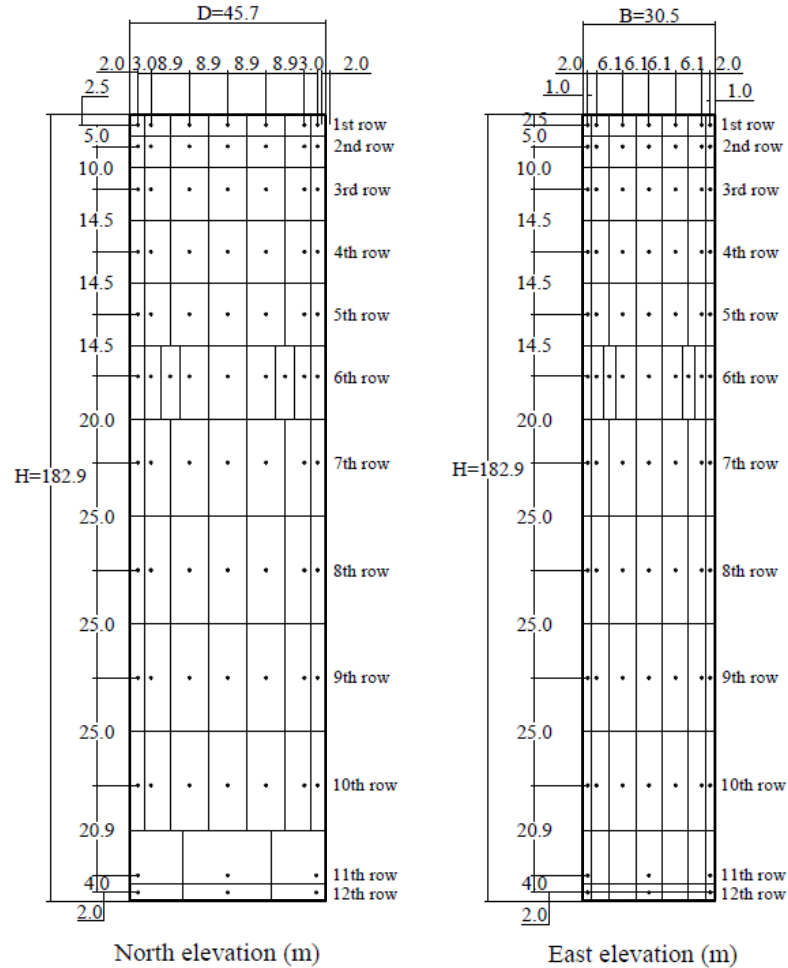


Figure 2-7: Elevation and side view tap locations with dimensions scaled to 1:400 in centimeters.

To obtain the wind-induced responses on the CAARC study building, the force for each pressure tap is computed using the following equations and multiplied by their corresponding tributary areas.

$$f_{xi}(t) = \frac{1}{2} \rho \bar{U}_h^2 C p_i(t) a_{xi}$$

$$f_{yi}(t) = \frac{1}{2} \rho \bar{U}_h^2 C p_i(t) a_{yi} \quad 2-8$$

$$f_{zi}(t) = \frac{1}{2} \rho \bar{U}_h^2 C p_i(t) a_{Ri}$$

where, ρ is the air density, \bar{U}_h is the mean wind velocity at building height and a_{xi} , a_{yi} are the tributary areas at pressure tap i projected from x and y respectively.

2.2.4 Base moments

The base moment time histories are calculated for all the building surrounding configurations using the computed forces as follows.

$$M_x = \sum_{i=1}^N f_{xi}(t) h_i$$

$$M_y = \sum_{i=1}^N f_{yi}(t) h_i$$

$$M_z = \sum_{i=1}^N f_{zi}(t) r_i$$

2-9

where h_i is the height of the pressure and r_i is the moment arm for pressure tap i .

2.2.5 Dynamic response

The dynamic response of the study building is evaluated to investigate the impact of the surrounding growth (Davenport 1967). The first two sway modes were assumed to be linear while the torsional mode was constant. The center of mass and rigidity of the building are assumed to coincide. The structural response of the building is computed using random

vibration theory. The building is approximated by a discrete lumped mass system where each lumped mass has three degrees-of-freedom, two sway and one rotation. It is assumed that the modes shapes are orthogonal and can be considered uncoupled.

The uncoupled system can be represented in modal coordinate by the following equations:

$$\ddot{q}_j + 2\xi_j\omega_j\dot{q}_j + \omega_j^2q_j = \frac{F_j(t)}{m_j} \quad 2-10$$

where ξ_j , ω_j are the j th mode damping and circular frequency, respectively. q_j is the j th mode generalized displacement vector, $F_j(t)$ is the j th mode generalized force, computed using the modes shapes and the forces at each pressure tap

$$F_j(t) = \int f_{xi}(t) \phi_{xj}(h)dh + \int f_{yi}(t) \phi_{yj}(h)dh + \int f_{zi}(t) \phi_{zj}(h)dh \quad 2-11$$

m_j is the j th mode generalized mass which was computed from the mode shapes, discretized mass $m(h)$ and story mass of inertia, $I(h)$

$$m_j = \int m(h) \phi_{xj}^2(h)dh + \int m(h) \phi_{yj}^2(h)dh + \int I(h) \phi_{zj}^2(h)dh \quad 2-12$$

Using random vibration theory, the variance of the j th mode generalized acceleration $\sigma_{\ddot{q}j}^2$ was computed using the spectral density of the generalized forces $S_{FFj}(\omega)$

$$\sigma_{\ddot{q}j}^2 = \int_0^\infty \omega^4 \left| \frac{1}{m_j} \left(\frac{1}{(\omega_j^2 - \omega^2) + 2i\xi_j\omega_j\omega} \right) \right|^2 S_{FFj}(\omega) d\omega \quad 2-13$$

2.3 References

- ESDU. 2001. *Engineering Sciences Data Unit. Characteristics of Atmospheric Turbulence near the Ground. Part II: Single Point Data for Strong Winds*. 85320th ed.
- Holmes, John D, Yukio Tamura, and Prem Krishna. 2008. “Wind Loads on Low, Medium and High-Rise Buildings by Asia-Pacific Codes,” no. May: 29–31.
- Lieblein, Julius. 1974. “Efficient Lillithods of Extreme-Value Methodology,” no. October.
- Melbourne, W. 1980. “Comparison of Measurements on the CAARC Standard Tall Building Model in Simulated Model Wind Flows.” *Journal of Wind Engineering and Industrial Aerodynamics* 6: 73–88.
- Davenport, A G. 1967. “The Treatment of Wind Loading on Tall Buildings.” In *Tall Buildings*, 3–45. Elsevier.
- Davenport, A G, and T Tschanz. 1981. “The Response of Tall Buildings to Wind: Effects of Wind Direction and the Direct Measurement of Dynamic Force.” In *Proceedings*, 205–23.
- Bezabeh, M. A., G. T. Bitsuamlak, M. Popovski, and S. Tesfamariam. 2020. “Dynamic Response of Tall Mass-Timber Buildings to Wind Excitation.” *Journal of Structural Engineering* 146 (10): 04020199. [https://doi.org/10.1061/\(asce\)st.1943-541x.0002746](https://doi.org/10.1061/(asce)st.1943-541x.0002746).
- Chen, Xinzhong, and Ahsan Kareem. 2005. “Dynamic Wind Effects on Buildings with 3D Coupled Modes: Application of High Frequency Force Balance Measurements.” *Journal of Engineering Mechanics* 131 (11): 1115–25. [https://doi.org/10.1061/\(asce\)0733-9399\(2005\)131:11\(1115\)](https://doi.org/10.1061/(asce)0733-9399(2005)131:11(1115)).
- Kareem, Ahsan. 1992. “Dynamic Response of High-Rise Buildings to Stochastic Wind Loads.” *Journal of Wind Engineering and Industrial Aerodynamics* 42 (1–3)

Chapter 3

3 Implications of city development on cladding loads

3.1 Introduction

The development of cities and the continuous growth of high-rise buildings will continue transforming the topology of our modern cities significantly. The urge for expansions and urbanization has pushed people to build more tall, flexible, and slender buildings where wind is the governing design load. However, the traditional methods of design of structural and nonstructural elements for high-rise buildings are not accurately representing the real developing environment. Most designs derived for isolated building cases excluding the effect of surroundings. Only brief warnings were introduced to few codes as the (ASCE 2012) and the (NBCC 2015). In most cases, they provide either a conservative estimate of the along-wind peak loads or an underestimated prediction of the local peak pressures on building surfaces leading to cladding failure. As a result, wind tunnels have been significantly involved over the past decades to assure accuracy of the design, especially with code limitations with respect to building height, shape, and surrounding configurations. Typically, a wind tunnel study on a structure, as presented by (Davenport 2002), includes the evaluation of local wind climate for the structure, simulation of the corresponding boundary layer taking the terrain roughness and topography into consideration and modeling the aerodynamic characteristics of the building shape and the potential for load increase.

As the city grows, the wind phenomenon becomes more complex, changing directions according to the obstructing element. This variation in wind flow is due to the interaction of fluid flow with the built environment (Holmes 2018). As a result, the change in the urban topology can either increase or decrease both the global wind loads on the building structure and the local peak pressures acting on the nonstructural components such as cladding elements. Several studies were performed on the effect of existing surrounding buildings on high-rise building loads. It started in the early seventies after the collapse of the three natural draft cooling towers at Ferrybridge, England in 1965 which was highly correlated to the existing built environment (Amrit 1980). Since then, several experimental

and numerical studies available in the literature were investigating and assessing the behavior of high-rise buildings under different urban topologies. (Bailey and Kwok 1985) performed a series of boundary layer wind tunnel tests to study the dynamic response of a square high-rise building under the effect of a neighboring twin building. (Stone 1987) studied the effect of a group of upstream buildings on the loading of a high-rise building. Different building aspect ratios and their shielding effect on the study building were also investigated by (English 1990). Using flow visualization tests, (Taniike 1991) examined the effect of turbulence on the aerodynamic interference by indicating that the fluctuating drag on the study building increased as the size of the surrounding building increased because, the scale of the shed vortices tends to increase as the surrounding building width increased. (Khanduri et al. 2000) classified the behavior of drag and lift coefficients over several wind tunnel experiments of varying aspect ratios, height of surrounding buildings at different terrain exposures. The dynamic response of a high-rise building due to surrounding effects for multiple wind tunnel model types (i.e., force balance test, aeroelastic test) were also compared by (Huang and Gu 2005). Moreover, (Lam et al. 2008) investigated the structural response of the study model immersed in a row of closely spaced, square high-rise buildings

Most of the past mentioned studies focused mainly on the overall wind loads and the wind-induced structural responses due to surrounding effect aiming for structural design. However, only few literatures were found supporting the design of nonstructural elements for the effect of future buildings on the built environment. For instance, (Irwin 1998) studied the variation in cladding pressure due to effect of future buildings and developed a methodology to adjust wind tunnel results to compensate the obtained uncertainty. (Surry and Mallais 1983) performed pressure tests and determined the cladding pressures on a high-rise building with and without surrounding buildings with a fixed spacing. They reported high suction near the ground and at the top corner of the studied building. (Surry and Djakovich 1995) explored the highest peak suctions developed on the building surfaces of an isolated case only and their relation to the building geometry and turbulence intensity. (Kim et al. 2011) performed a series of wind tunnel tests to study the effect of interference on the local peak pressures of two high-rise buildings with different spacing, height configurations and with different building shapes. (Hui et al. 2013) also investigate the

interference effects between two high-rise buildings with same heights but different shapes and arrangement, the results show an increase in the negative pressures for some cases up to 50% larger than in the isolated case and decrease of around 30% in other cases depending on the wind direction.

On the other hand, computational fluid dynamics (CFD) simulations were also utilized to predict wind-induced responses in high-rise buildings. For instance, (Zhang and Gu 2008) performed a CFD study to investigate the effect of a neighboring building on an adjacent tall building in a staggered arrangement at different wind azimuths. The results show good agreement with wind tunnel results in terms of mean C_p , base moments and base force. (Cóstola et al. 2009) also compared CFD simulations to different wind tunnel results, full scale measurements and databases using building energy simulation. The study investigated different parameters that affect the distribution of pressure coefficients on building surfaces as different building shapes, facade detailing and degree of sheltering of identical building configurations at several wind directions. (Dagnew and Bitsuamlak 2014), (Elshaer et al. 2016) and (Elshaer et al. 2017) evaluated the aerodynamic response of a typical tall building with and without surrounding buildings (i.e. isolated building, two adjacent buildings, complex surrounding buildings) using computational fluid dynamics. The sheltering effect of the surrounding buildings reduced the overall mean force while increasing the fluctuations component of the aerodynamic wind loads. They investigated different numerically generated inflow boundary conditions to assess their suitability for Large Eddy Simulations (LES). The results showed good agreement with wind tunnel data, see, Table 3-1 for a summary of the previous studies .

However, previous research was limited to a defined number of surrounding buildings with fixed heights not taking into consideration the predicted city growth which did not represent the real development of a surrounding city. Therefore, in this paper, boundary layer wind tunnel tests were performed to investigate and evaluate the impact of city growth on cladding load of a typical high-rise building adopted from the Commonwealth Advisory Aeronautical Research Council (CAARC) building model. The city growth is represented by different generic surrounding configurations, varying in height ratios compared to the study building. The configurations include an isolated case scenario

(0000SH), and surrounding buildings of 25% increase (0025SH), 50% increase (0050SH), 75% increase (0075SH) and 100% increase (0100SH) in surrounding height ratios. Maximum positive and minimum negative peak pressures are presented for each tap (i) and evaluated from the cladding design point of view.

Table 3-1: Main findings of previous studies focused on the effect of surroundings on high-rise buildings from cladding point of view

Authors	Model	Study purpose	Surrounding Environment	Comments
Surray and Mallais (1983)	BLWT	Cladding design	2 buildings	Wind tunnel pressure tests to determine the cladding pressures on a typical high-rise building with and without an interference building with fixed spacing.
Taniike (1991)	BLWT	Cladding design	2 buildings	Investigated the effect of a changing the aspect ratio of an upstream building on the structural response of a typical high-rise building, showing an increase in the fluctuating drag as the size increases.
Surry and Djakovich (1995)	BLWT	Cladding design	Isolated building	Explored the highest peak suction developed on the building surfaces of an isolated building with changing the building geometry.
Irwin (1998)	BLWT	Cladding design	Isolated / 2 buildings	Studied the variation in the negative pressure and developed a correction value for wind tunnel results.
Zhang and Gu (2008)	CFD	Cladding design	2 buildings	Examined the aerodynamic behavior of buildings with staggered arrangement showing good agreement with wind tunnel results in terms of mean C_p , base moments, and base forces.
Cóstola et al. (2009)	CFD	Cladding design	1 layer of surrounding buildings	Investigated different parameters that affect the distribution of pressure coefficients on building surfaces (i.e. building geometries, facade detailing and degree of exposure) adopting

				identical building configurations at several wind directions.
Kim et al. (2011)	BLWT	Cladding design	2 buildings	Investigated the effect of different heights, spacing and wind directions of a surrounding building to assess the local peak pressures on interference effect.
Hui et al. (2013)	BLWT	Structural design	2 buildings	Investigated the flow field and the pressure distribution of interference effects on external pressures between two high-rise buildings of exact height.
Dagneu and Bitsuamlak (2014)	CFD	Structural design	2 buildings	Investigated the effect of sheltering of a neighboring building. Also, examined three different turbulence models showing agreement of the synthetic method with the BLWT than the random and the recycling flow methods.
Elshaer et al (2016)	CFD	Structural design	Isolated and Complex building surroundings	Investigated the aerodynamic response of a typical tall building with and without surrounding buildings showing a decrease in mean by 50% and a higher rms by 40%.
Elshaer et al (2017)	CFD	Structural design	1 layer of surrounding buildings	Examined the changes in the design of wind loads on tall buildings with urban development showing a reduction in the mean and fluctuating base moments by 50% and 20%, respectively, with the increase in surrounding height.

3.2 Experimental setup

3.2.1 Model description and wind profile

Wind tunnel experiments on a high-rise building with several surrounding configurations of varying height ratios, were conducted at the Boundary Layer Wind Tunnel Laboratory (BLWTL I) at the University of Western Ontario as shown in Figure 3-6. The tunnel has a working section approximately 2.44m wide by 2.3m tall at the working section with a

length of 24.4m from the downstream inlet to the building located at the center of the turn table. A High Frequency Pressure Integration (HFPI) test was applied for the current study to evaluate the effect of surrounding growth on building components during the flow of wind on a tall building with a rectangular foot print of 45.72 m (150 ft) * 30.48 m (100ft) and a height of 182.88 m (600ft) in full scale, see Figure 3-4. The test was carried out adopting a suburban exposure for all surrounding configurations to represent the city-environment. The specified exposure was generated by the combined effect of the three 0.8 m tall trapezoidal spires and the arrangement of the roughness blocks of various sizes between 2 and 5 cm. The building model was constructed with a geometrical scale of 1:400. The mean wind speed and the turbulence intensity profiles of the simulated suburban exposure were matched with the ESDU profiles as shown in Figure 3-1.

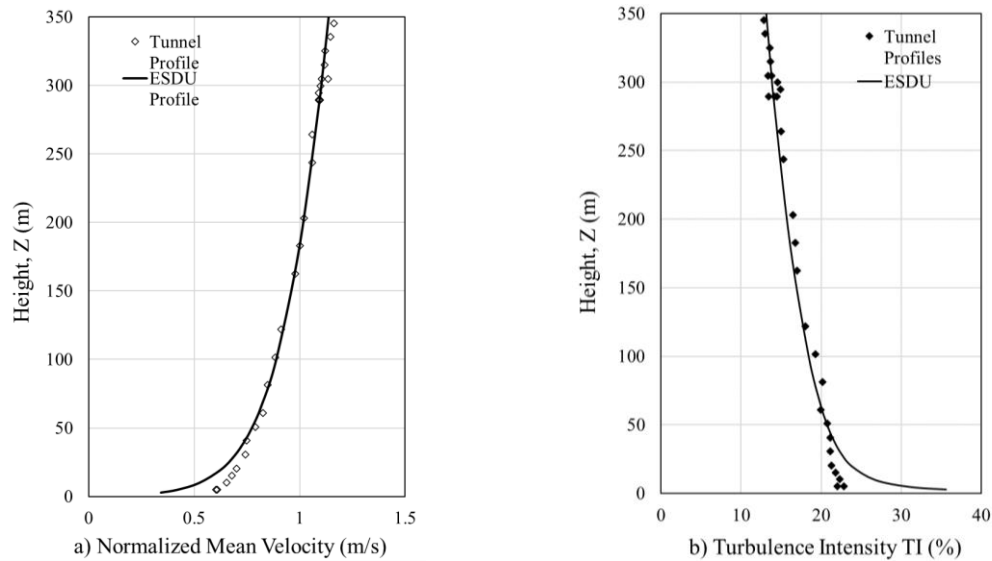


Figure 3-1: Simulated wind parameters in wind tunnel for suburban terrain: (a) normalized mean wind speed, (b) turbulence intensity profiles (TI%)

3.2.2 Pressure measurements and statistics

A High Frequency Pressure Integration (HFPI) test was applied for the current study to capture the variations of the wind-induced pressures on the model surfaces. Pressure readings were extracted from the tests for each wind direction of a total of 23 wind directions from 0° - 180° at 10° increment including AoA= 45° , 135° , 225° and 315° . The wind tunnel model included 367 taps, 51 placed along the roof and the rest are distributed over 12 layers on the building surfaces. Taps were placed more densely near the edges of the buildings to allow capturing the strong pressure gradients that commonly occur at the

corners according to the expected distribution of C_p 's and more taps were also concentrated at $2/3 H$ of the building height for validation purposes, see Figure 3-2 The exact locations of the taps were recorded in an excel sheet and given specific numbers which correspond to their attached scanners. Each tap was connected to an electronic pressure scanner through 600-mm-long plastic tubing of approximately 1.5 mm internal diameter see, Figure 3-3. The pressure time history for all taps were measured simultaneously at a sampling frequency of 400 Hz with 51200 data points recorded for all the surface pressure taps. The pressure time histories for each wind direction was recorded for 128s at model scale which corresponds to 3.5 hours at full-scale. The surface pressure readings are expressed into unitless coefficient of pressure C_p obtained by normalizing the measured surface pressure with the mean dynamic pressure at model height. The mean and root mean square of pressure coefficients are computed as followed:

$$\bar{C}_p = \frac{p_i - p_0}{\frac{1}{2} \rho_a \bar{U}_h^2} \quad \hat{C}_p = \frac{\sqrt{\hat{p}_i^2 - p_0}}{\frac{1}{2} \rho_a \bar{U}_h^2} \quad 3-1$$

where the denominator represent the dynamic pressure found from the mean wind speed at building height \bar{U}_h and the air density ρ_a . The reference pressure is denoted by p_0 , while the varying pressure p_i , is specified to each tap i.

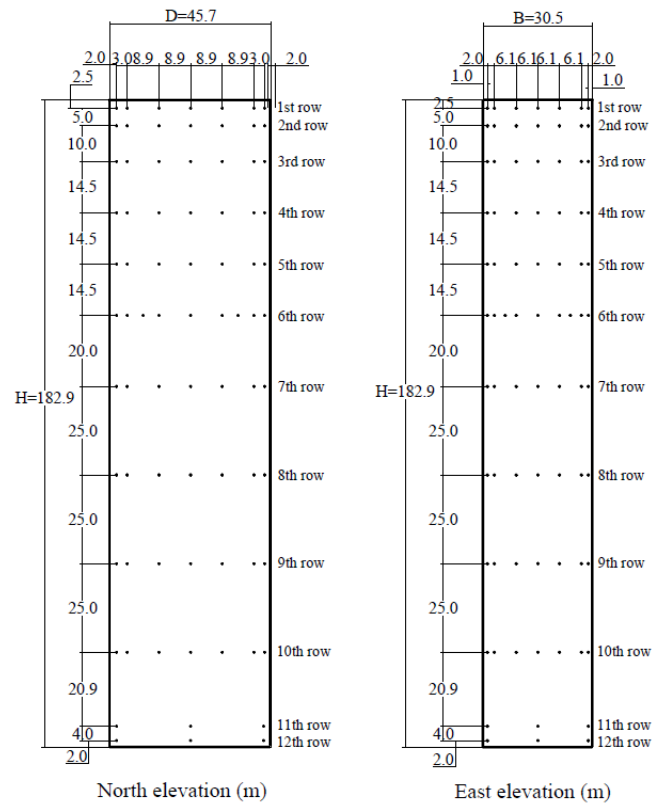


Figure 3-2: Elevation and side view tap locations with dimensions scaled to 1:400 in centimeters.

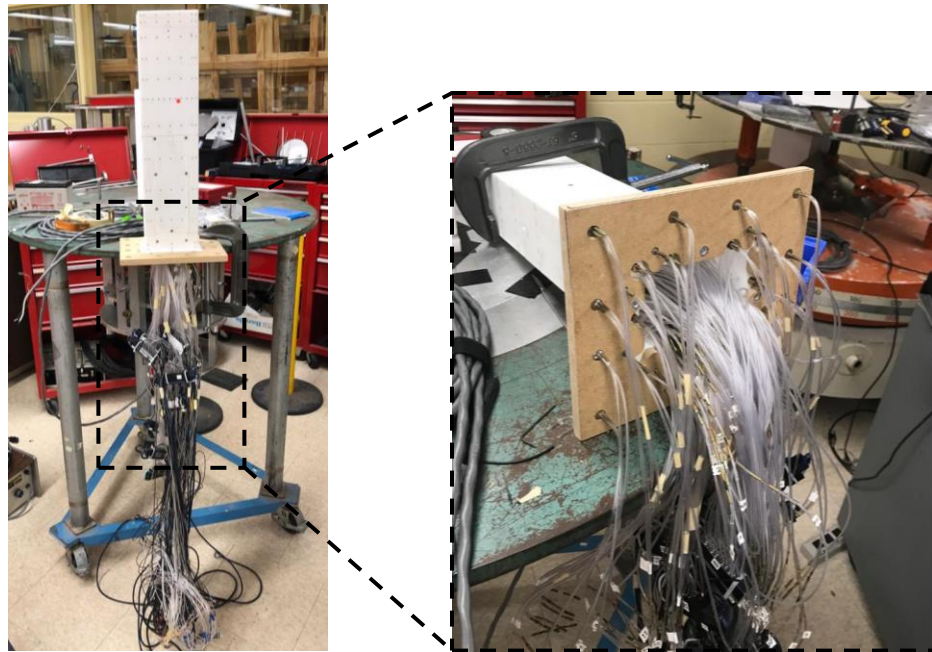


Figure 3-3: Model setup before installation in wind tunnel connected to scanners for data recording.

3.2.3 Test configurations and cases

The surrounding models were made from high-density foam with different heights, see Table 3-2. They cover an area around the study building of around 500m radius in full scale). They represent a generic scenario of city growth and they act as sheltering bodies to the wind flow; thus, no taps were required to be installed, see Figure 3-4. The considered CAARC model was tested under two different configurations in suburban exposure, (a) testing it as isolated case without any surroundings and (b) testing it with neighboring buildings having the same foot print and located in a regular arrangement, surrounding the study building with a gap distance of 7.6cm in model scale as shown in Figure 3-5. For the current study, there are 5 different cases of surrounding buildings varying in height ratios with respect to the study building as shown in Table 3-2.

Table 3-2: Test configurations and their corresponding cases for the surroundings buildings

Configurations	Case	Height of surrounds H_s (m)	Height Ratios ($H_r=H_s/H$)	Exposure (z_o)
Isolated	0000SH	0.00	0.00	<i>Suburban (0.30)</i>
With Surrounding Buildings	0025SH	45.72	0.25	<i>Suburban (0.30)</i>
	0050SH	91.44	0.50	<i>Suburban (0.30)</i>
	0075SH	137.16	0.75	<i>Suburban (0.30)</i>
	0100SH	182.88	1.00	<i>Suburban (0.30)</i>

Note: wind pressure measurements were taken for 0-180° AoA @ 10° increment to additional AoA were also tested (45°, 135°, 225°, 315°)

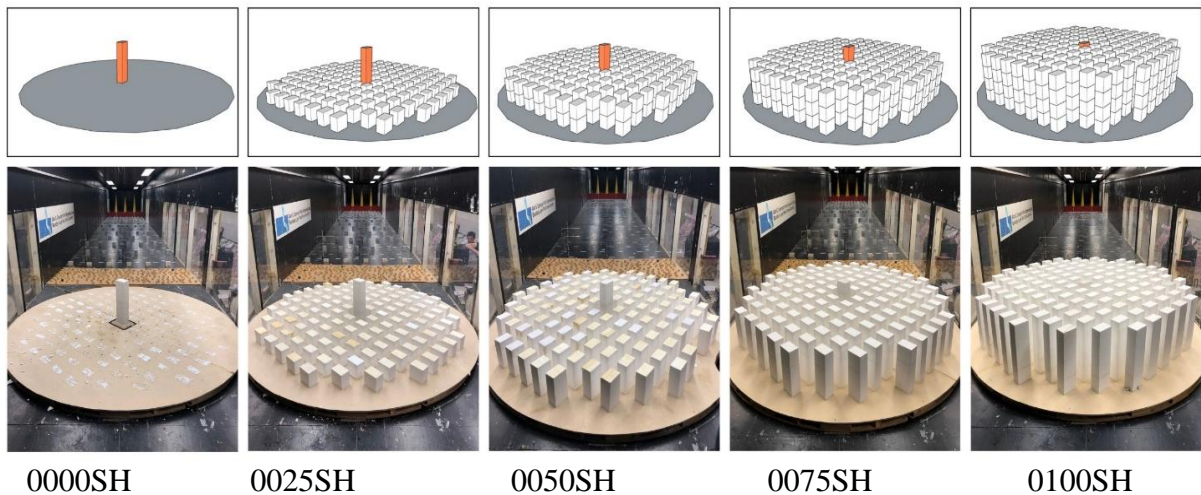
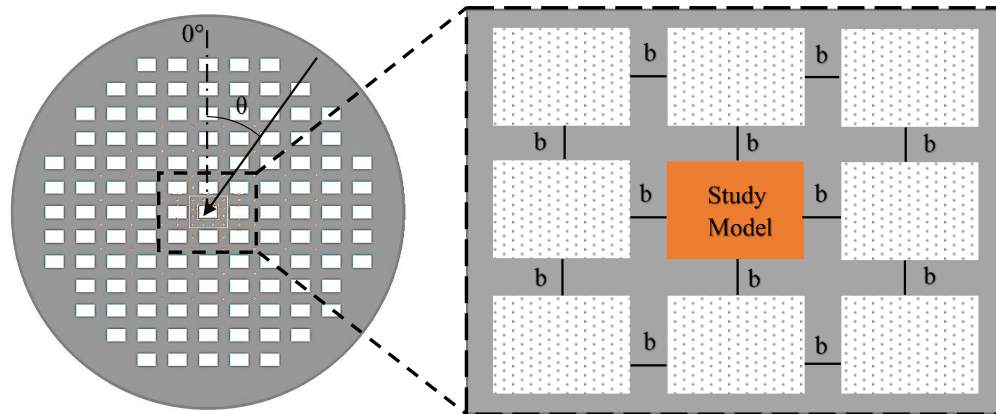


Figure 3-4: Installation of the surrounding configurations at UWO (wind tunnel I) for the 5 different cases at AoA = 45°



$b = 30 \text{ m}$ in full scale [$b = 7.6 \text{ cm}$ in model scale 1:400]

Figure 3-5: Alignment of the surrounding buildings with equal spacing around the CAARC study model.

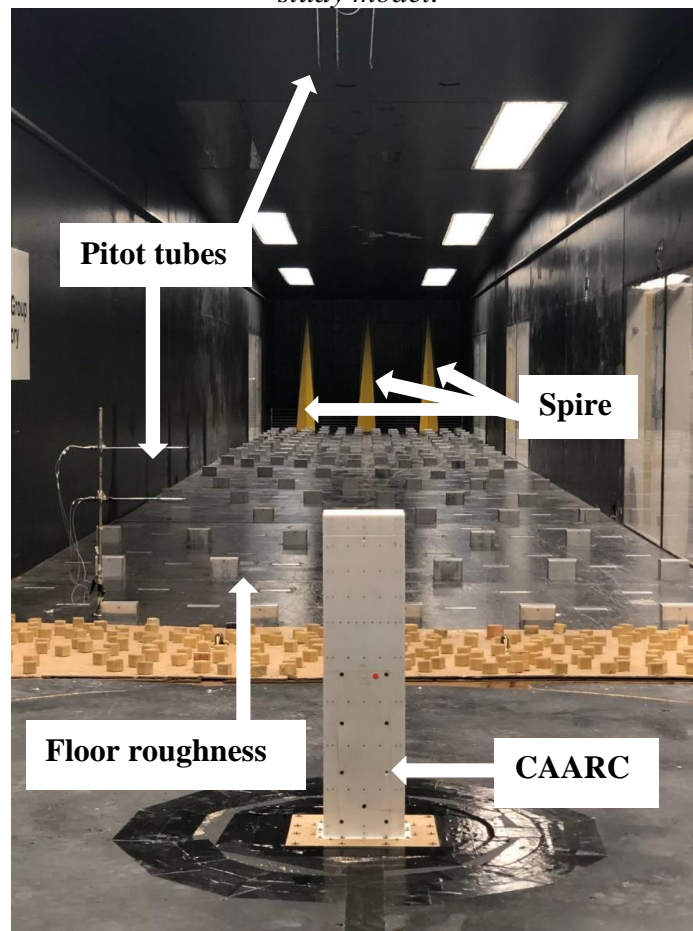


Figure 3-6: Experimental model installed at (UWO wind tunnel I) for the isolated case 0000SH at $AoA = 0^\circ$.

3.3 Results and discussion

3.3.1 Mean and fluctuation pressure distributions

There is a significant change in the mean pressure coefficient distribution on the windward wall of the CAARC building with the increase in surrounding heights as shown in Figure 3-8. For case 0000SH, the highest positive mean C_p at $AoA = 0^\circ$ was at $0.6 H$ of the building height with a C_p mean value of $+0.8$. However, as the upstream surrounding buildings increase in height for the same wind direction, it was observed that the highest positive mean C_p decreases gradually and were shifted upwards. The decreasing C_p value can be attributed to the shielding effect of the upwind surroundings while the upward shift is caused by the wind flowing over the roofs of the surroundings. Meanwhile, a drop in C_p mean values were noticed at the lower regions of the study building near the base. This is due to the presence of the study building in the wake of the upstream building. However, in cases 0075SH and 0100SH, the pressure decreased significantly turning into suction (negative pressures) for the middle and lower parts for case 0075SH and fully suction for the whole surface for case 0100SH with a maximum suction of around -0.8 at about $0.8H$ of the building height as shown in Figure 3-8. Similarly, the rms of the mean C_p at $AoA = 0^\circ$, shows a matching trend with the mean C_p .

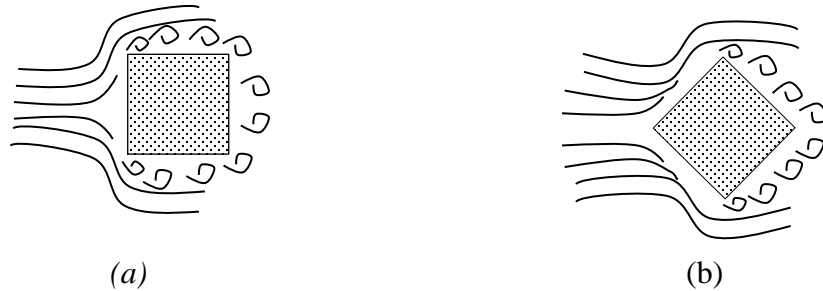
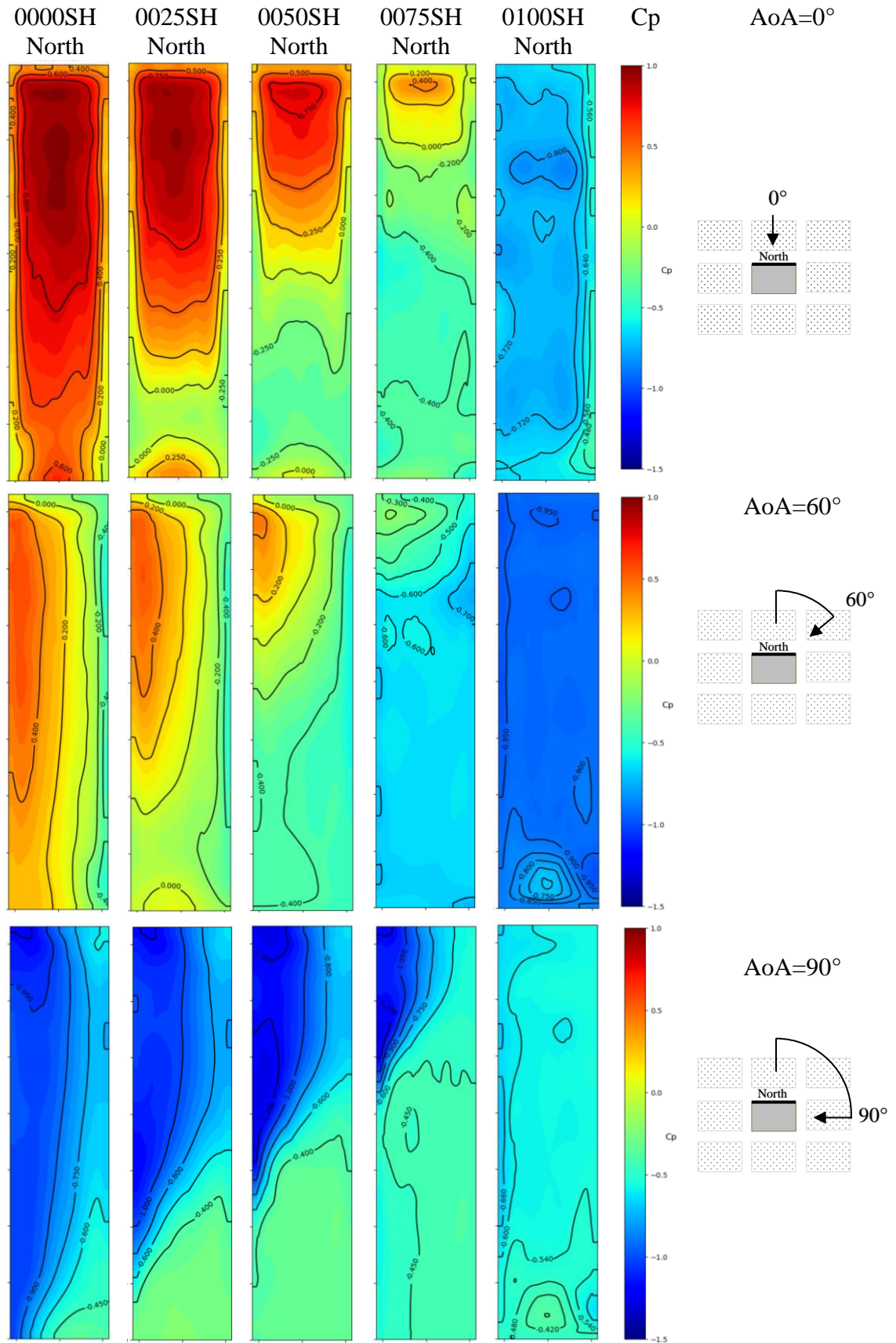


Figure 3-7 Wind flow separation and eddies generation for different AoA hitting (a) frontal wall (b) corner walls.

As the wind changes direction and the flow starts hitting the corners of the study, see Figure 3-7, the location of flow separation changes from case (a) to case (b). This change shifted the positive mean pressures from the center and towards the corners where separation occurs. Similar concept is shown in Figure 3-8 at $AoA = 60^\circ$ with a noticeable decrease in the mean C_p can be seen as it reaches the far end of the building forming a negative pressure

zones of -0.4 on the edges for case 0000SH. As for cases 0025SH and 0050SH, the sheltering buildings obstruct and change the wind flow causing higher fluctuations near the separation zone at the near edge as shown in Figure 3-9. While a decrease in the overall mean C_p was noticed specifically for the shielded part of the building up to a height of $0.2H$ and $0.5H$ respectively. The suction zone causes the mean C_p values to drop from +0.6 for case 0000SH to -0.4 in case 0050SH. Moreover, the positive mean C_p values in the upper parts of the building are reduced approximately by 20%. For cases 0075SH and 0100SH, the whole building windward surface experienced a total suction reaching a mean C_p value of -0.95 in case 0100SH which will affect the wind loading on the building surfaces for cladding design.

For $AoA = 90^\circ$, the northern face of the isolate case 0000SH shows a higher negative mean C_p 's near the windward edge with gradual increases towards the leeward side as shown in Figure 3-8. The pressure distribution seen is due to the separation of wind flow at the windward edge forming a higher suction zone in the range of -0.4 to -1, while the reattachment zone on the leeward edge generated higher C_p values. In cases 0050SH and 0075SH, the sheltering buildings oppose the flow of wind, obstructing the formation of vortices, producing lower negative mean pressures near the base of the study model and up to a height of $0.5H$ and $0.75H$ respectively. However, the unshielded portion of the building showed an increase in negative mean C_p values, reaching a maximum of -1.2 which indicates an increase in speed as wind flows over the upstream buildings. Another observation is that the C_p values on the north face tends to increase near the far edge in the vertical direction which indicates the effect of channeling as shown in Figure 3-8. As a result, it is important to consider the city development in wind loading design for cladding as the building codes mainly consider isolated cases which doesn't fully represent the possible surrounding growth.



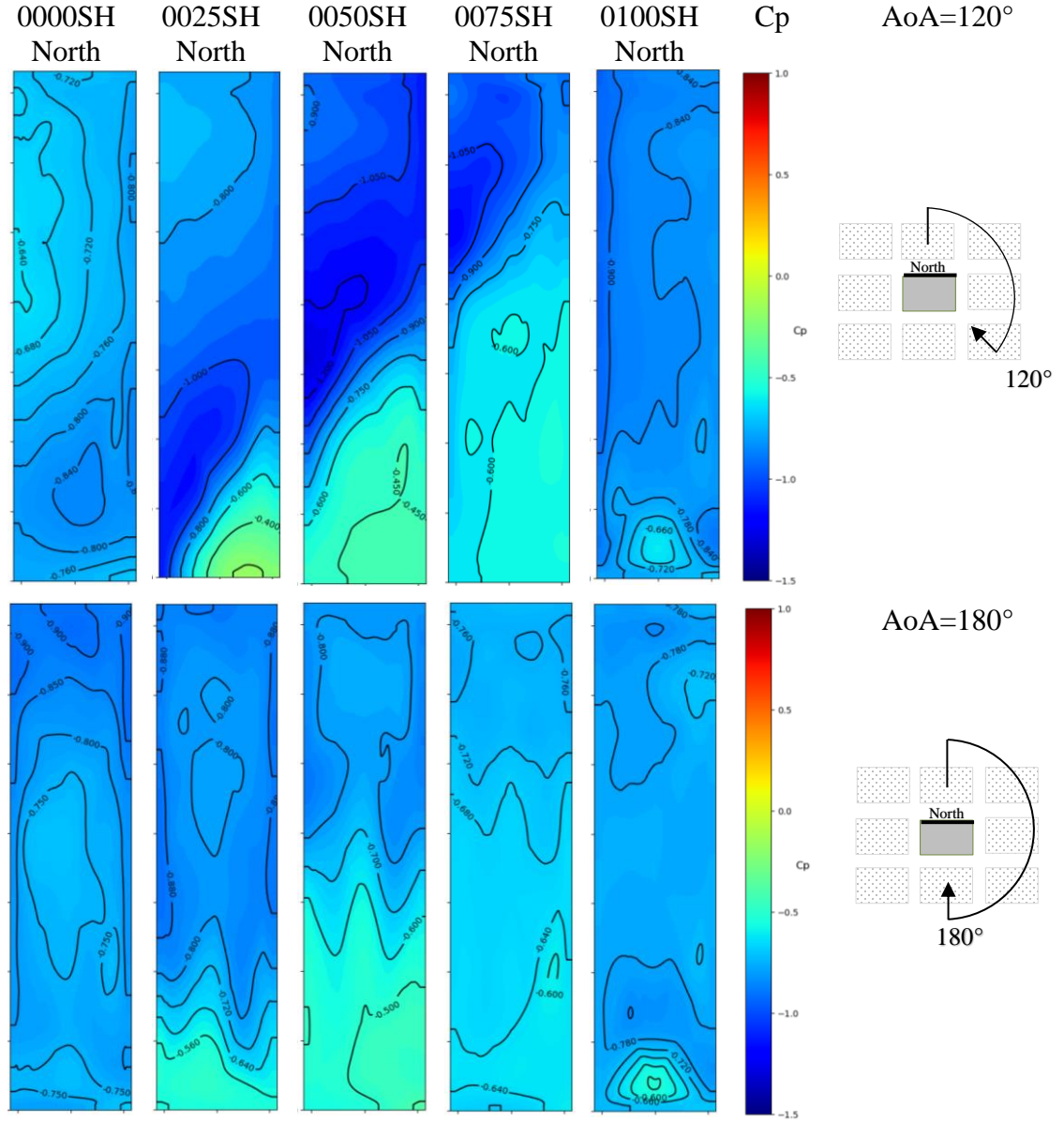
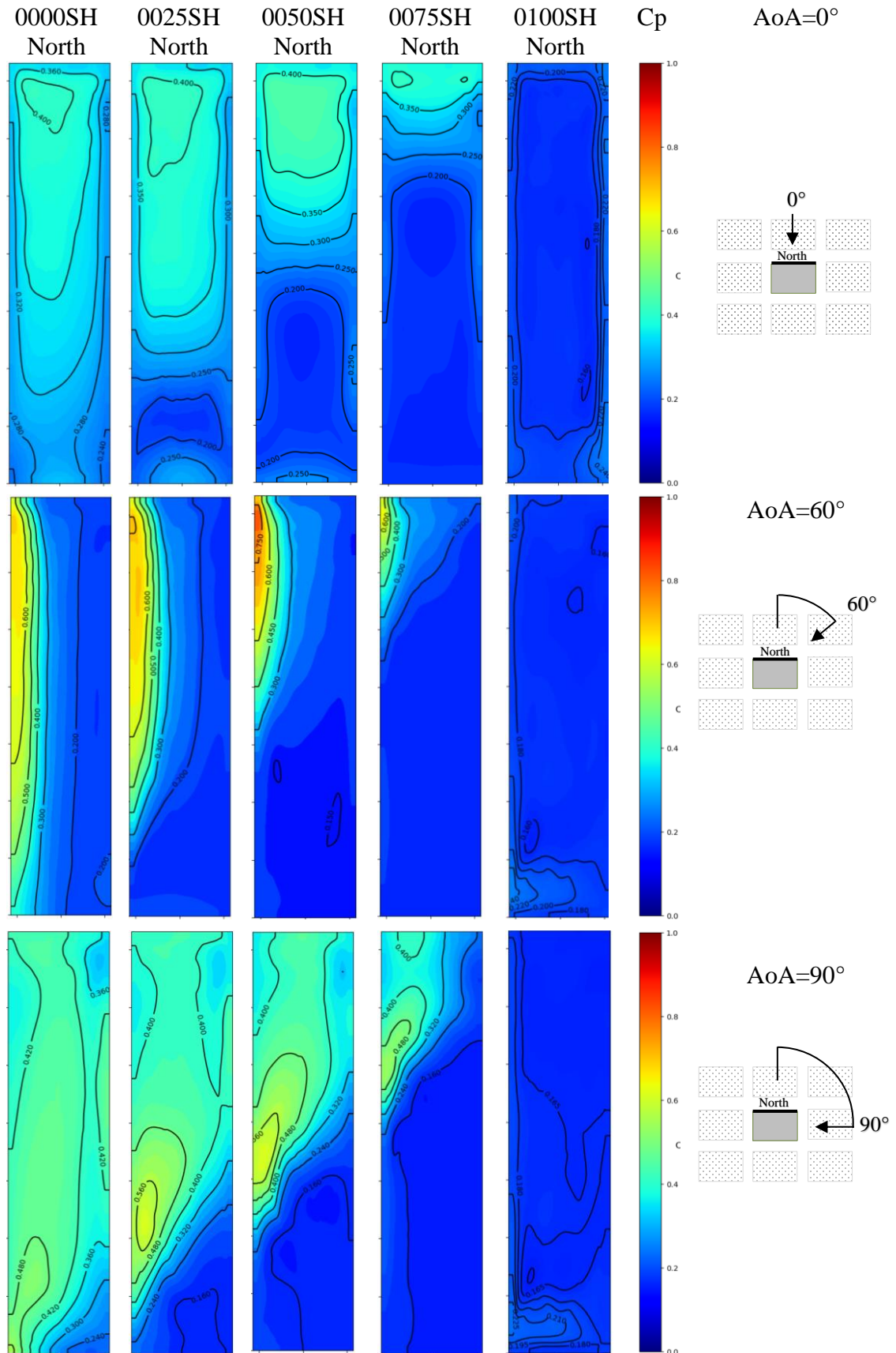


Figure 3-8: Mean pressure coefficients (\bar{C}_p) on the northern wall for all cases at $AoA = 0^\circ, 60^\circ, 90^\circ, 120^\circ, 180^\circ$.



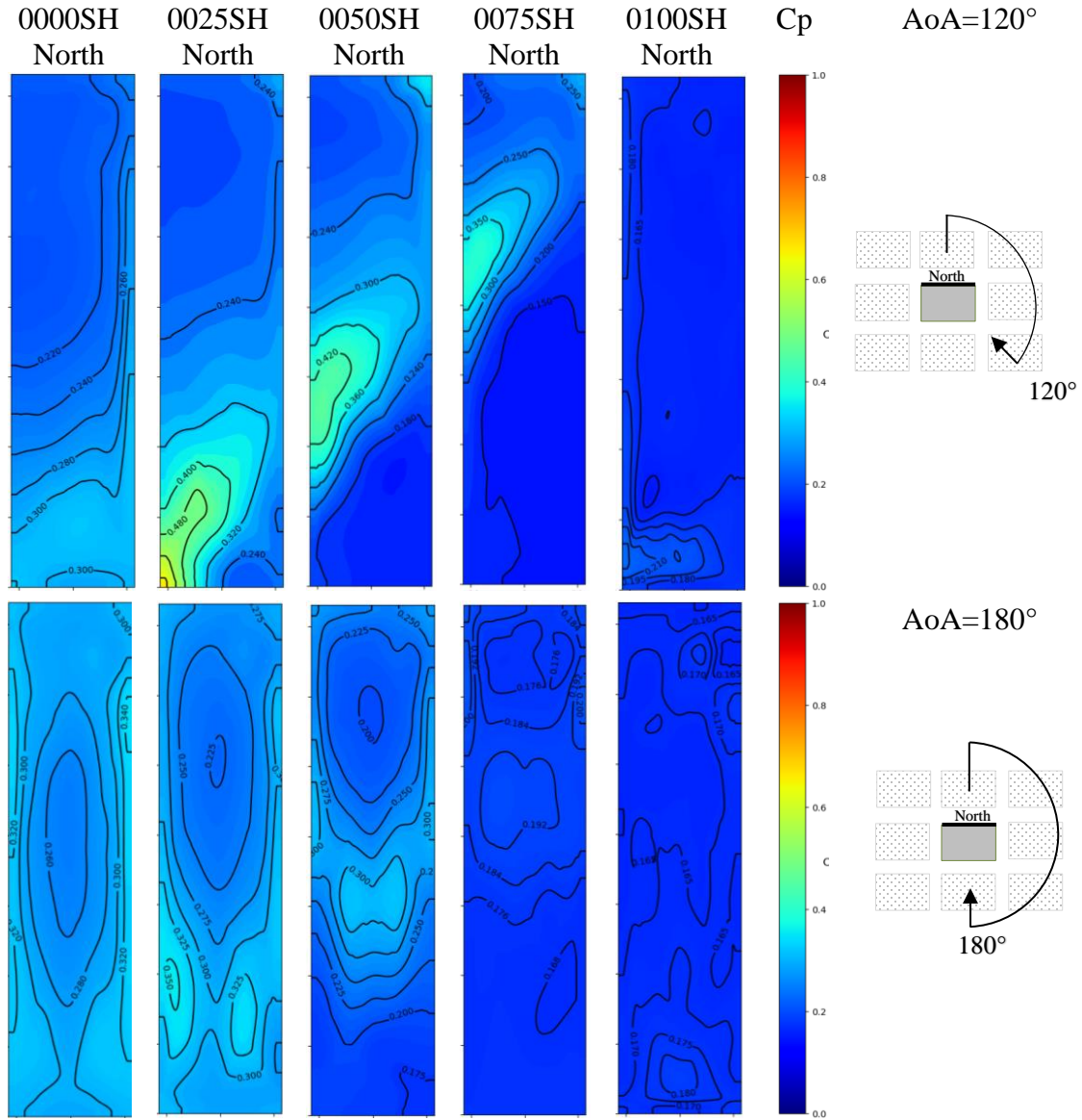


Figure 3-9: Root mean square of pressure coefficients (\bar{C}_p) on the northern wall for all cases at wind directions $\theta = 0^\circ, 60^\circ, 90^\circ, 120^\circ, 180^\circ$.

3.3.2 Peak pressure distribution

In design of cladding, an extreme value analysis is required to obtain the peak values in the pressure data. The Lieblein Best Linear Unbiased Estimator (BLUE) technique was utilized to obtain the extreme peak values by breaking down a sample of records into smaller segments (Lieblein 1974). The observed maximum and minimum values were taken from each of these subsets. Each of the subsets peak is fitted to an extreme value distribution allowing extrapolation of the results to the complete sample length. This provide more reliable results than using the single observed extreme coefficient from the sample record.

The distribution of maximum and minimum peak pressure coefficients on the front (northern) face of the study building for all surrounding cases at wind directions (0° , 60° , 90° , 120° and 180°) are shown in Figure 3-11 and Figure 3-12, respectively. The maximum peak pressure coefficient for the isolated case 0000SH, \hat{C}_p ($\theta=0^\circ$) is found to be around +2.52 located on the central axis of the front face at $0.9H$ of the building height near the stagnation point. It has similar characteristics to the mean C_p values where the highest values at stagnation point decreases and shifts upwards with the increase in surrounding heights. It is obvious that there is a drop in the positive peaks pressures (\hat{C}_p) for ($0^\circ < \theta < 90^\circ$) which reflects the separation of flow at the outer layers of the upstream buildings leaving the downstream building more sheltered inside its wake causing a decrease in \hat{C}_p . While for the minimum \check{C}_p , it was found that the peak minimum \check{C}_p for the isolated case 0000SH, occurs at $AoA=90^\circ$ with a value of -5.43 at $0.03H$ of the building height. The suction zone takes place at the windward bottom corner along the separation edge and diagonally continues up towards the trailing edge. These observations for the isolated case scenario are consistent with previous literature (Cheung 1984). It was also observed that as the height of surroundings increase the largest minimum \check{C}_p was recorded -6.5, occurring for case 0050SH with an increase 20% compared to the isolated case. and for case 0075SH it showed an increase around 40% in the local peak pressure for the lower section of the building at $AoA=120^\circ$. This can describe the flow speeding up resulting in higher-pressure fluctuation due to the shielding effects of the surrounding bodies. Figure 3-10, shows a comparison between case 0050SH and the isolated case 0000SH. The effect of increased pressure fluctuations particularly on some cladding elements, is viewed as a high wind risk due to fatigue damage accumulation, therefore a complete study of the existing and predicted building's surroundings is important for a valid evaluation of cladding risks.

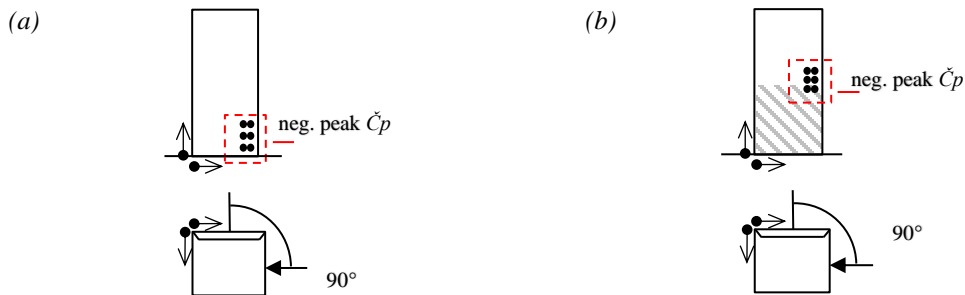
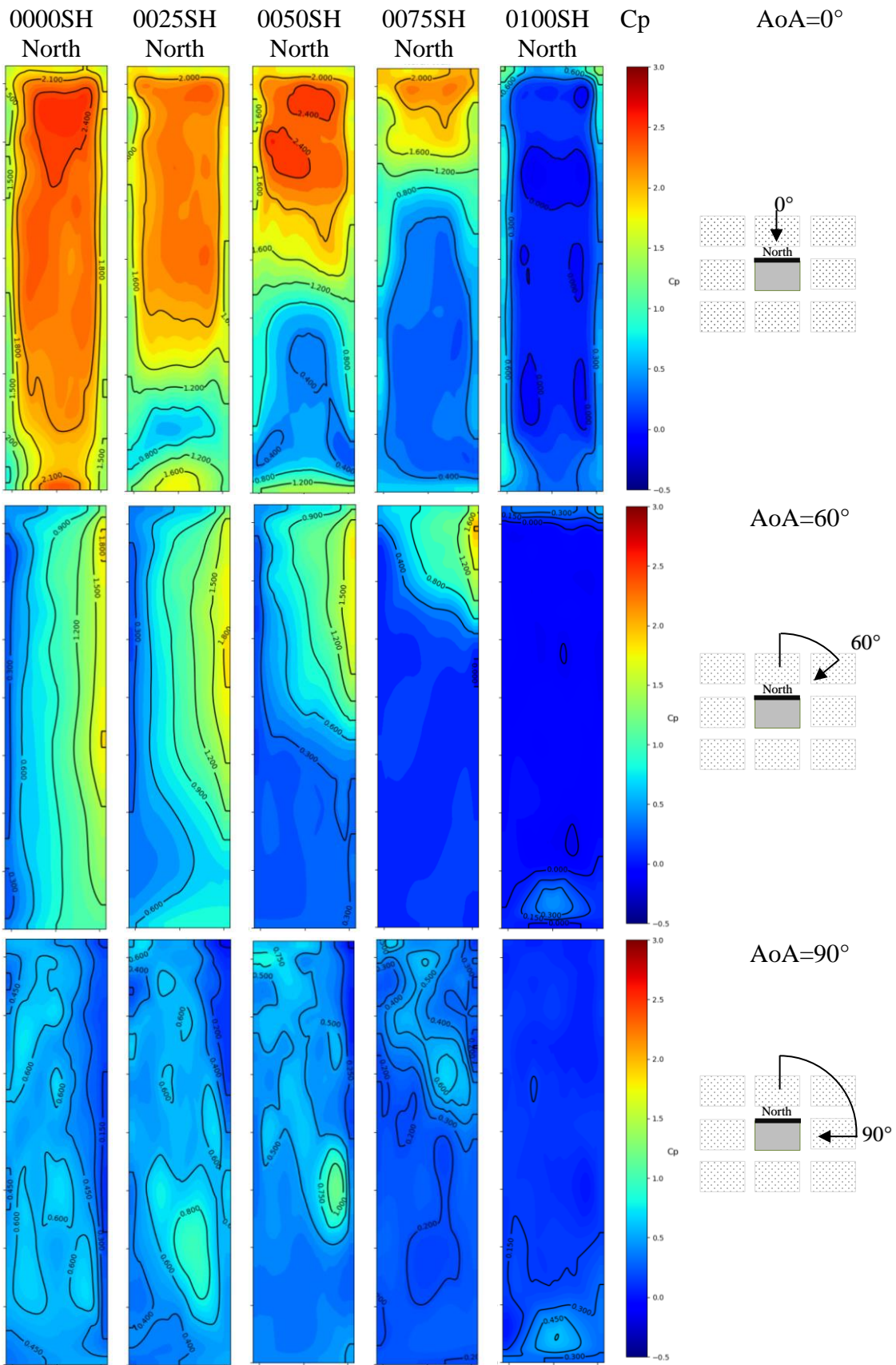


Figure 3-10: Largest minimum \check{C}_p tap locations for a) case 0000SH, b) case 0050SH



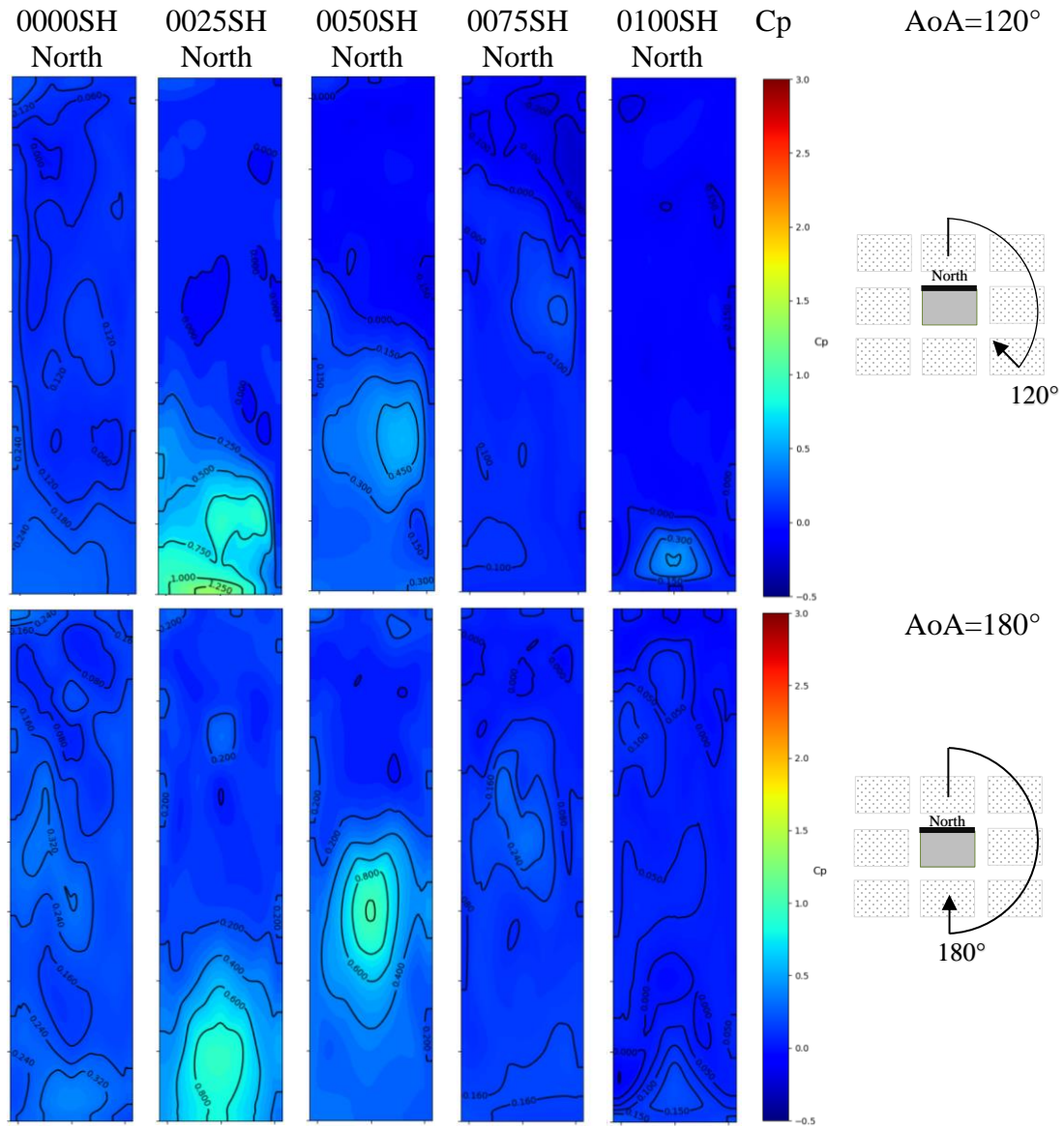
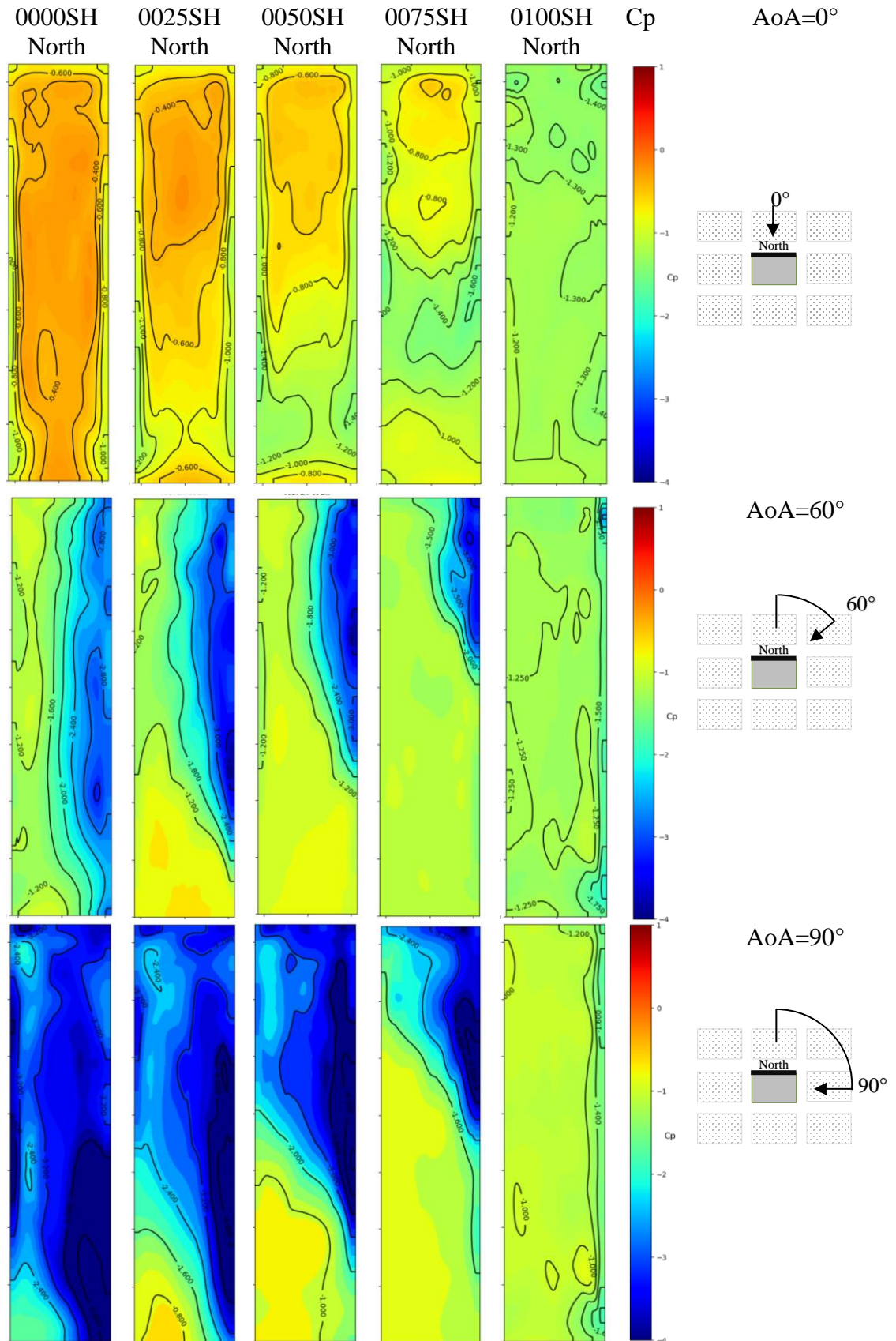


Figure 3-11: Maximum peak pressure coefficients (\hat{C}_p) on the northern wall for all cases at $AoA = 0^\circ, 60^\circ, 90^\circ, 120^\circ, 180^\circ$.



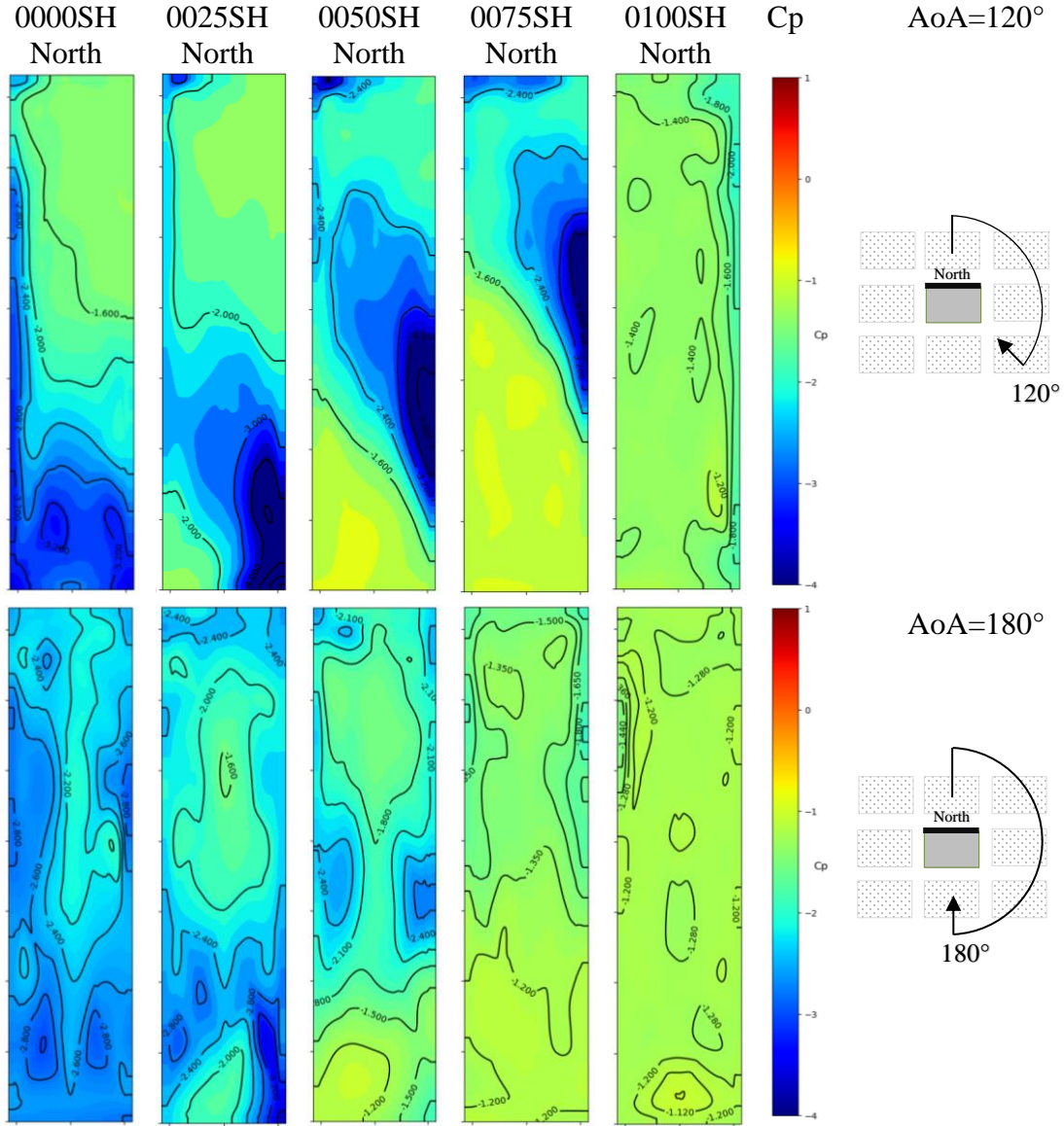


Figure 3-12: Minimum peak pressure coefficients (\check{C}_p) on the northern wall for all cases at $AoA = 0^\circ, 60^\circ, 90^\circ, 120^\circ, 180^\circ$.

3.3.3 Effect of height ratio on the local peak pressure coefficients.

In the current study, the maximum and the minimum peak coefficients are plotted for all the taps found on the building surfaces with varying surrounding heights at wind direction θ , following the expressions

$$\hat{C}_p(\theta) = \max C_{p_i} [\hat{C}_p(i, \theta)] \quad 3-2$$

$$\check{C}_p(\theta) = \min C_{p_i} [\check{C}_p(i, \theta)] \quad 3-3$$

Plotting the maximum and minimum local peaks contribute significantly in the design of cladding and produces a fair comparison between all cases as shown in Figure 3-13. Moreover, being able to trace the overall trend of the maximum \hat{C}_p and minimum \check{C}_p peak pressure coefficients, validates the existing data since it's almost symmetric around $AoA = 90^\circ$. The \hat{C}_p for the isolated case 0000SH are similar irrespective of the wind direction. The \hat{C}_p for both cases 0025SH and 0050SH show higher variation dependent on wind direction compared to the isolated case 0000SH as shown in Figure 3-13. Cases 0025SH and 0050SH show higher \hat{C}_p , reaching +2.9. This is due to the body generate turbulence from the upstream buildings producing higher fluctuations specially around the edge walls of the building and upwind speed up. As the height increases to 0.75H in case 0075SH, the \hat{C}_p decreased and a significant drop occurred near angle 45° . However, when the building is fully surrounded by full height interfering buildings (0100SH), it is obvious that the shielding effect on the study building caused a massive drop in the peaks of almost 50% decrease in the maximum and minimum peak pressures. Similarly in Figure 3-13 (b), cases 0075SH and 0100SH shows lower peak values due to the shielding effect as described earlier. However, the minimum peak pressure coefficients \check{C}_p for cases 0025SH and 0050SH have an overall higher peak suction than the isolated case 0000SH, particularly for case 0025SH at $AoA = 120^\circ$, where the suction at the lower part of the building corner increased by 40% reaching a \check{C}_p value of -7.0.

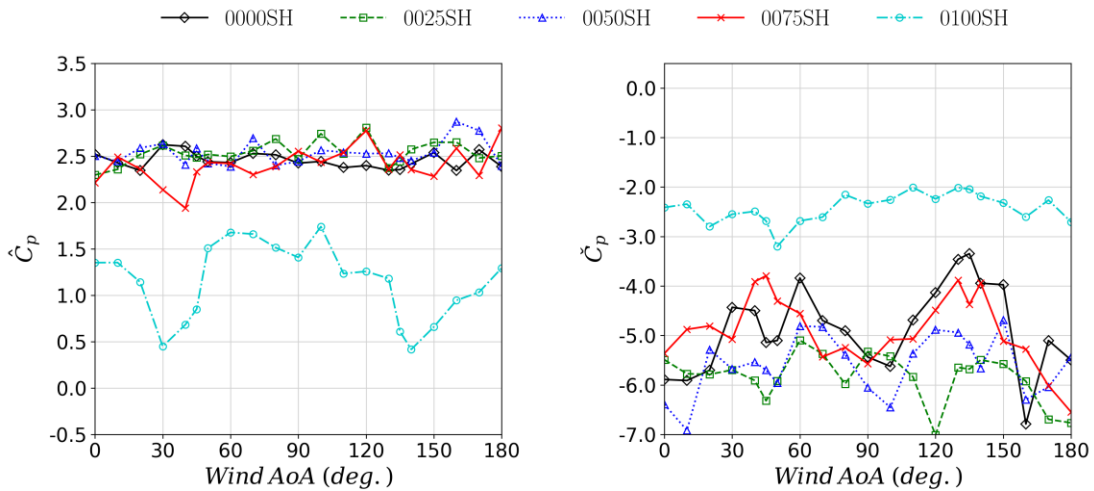


Figure 3-13: Variation in a) Maximum and b) Minimum pressure coefficient peaks for various configurations at AoA (θ).

Positive peak pressures \hat{C}_p and negative peak pressures \check{C}_p were also investigated along on the center line and corner line of the northern and eastern faces of the CAARC study building at three selected tap locations with different heights (0.96H, 0.56H and 0.15H), as shown in Figure 3-14. The plots compared the peaks of the selected taps for all surrounding cases at different wind directions, evaluating the effect of growth on the peak values at critical facade locations. It was observed that the common trend for most cases at tap (A_1) at the center line of the northern face, starts with positive peak values at $AoA = 0^\circ$ with highest \hat{C}_p equal to +2.5 and gradually drops as the wind changes direction reaching a slightly negative \hat{C}_p between 120° and 180° , see Figure 3-15. The recorded \hat{C}_p values were similar for all cases except for case 0100SH where full height shelter was reached, a significant drop in \hat{C}_p was noticed especially for angles (0° to 120°).

As for tap A_2 (located at 0.56 H of the building height), a significant drop in the \hat{C}_p values occurs for cases 0075SH and 0100SH due to the sheltering effect. At tap A_3 (0.15H), an interesting increase in the \hat{C}_p for cases 0025SH for angle between (90° - 180°) which endorses the earlier concept of wake disturbance with higher fluctuations at lower surrounding building heights. In Figure 3-16, the negative peak \check{C}_p for the three tap locations recorded an increase in the negative value for all the cases compared to the isolated case for angles (0° - 60°). However, at angles (60° - 120°) only cases 0025SH and 0050SH exceeded the isolated case for the higher tap locations. On the other hand, a significant decrease in the negative values for almost all the case for tap B_3 were recorded for angles (60° - 180°) except for case 0025SH (0.25H surround) which showed fluctuating peaks for angles (135° – 180°) as described earlier.

According to the behavior of wind around an isolated high-rise building as described by Holmes (2002), the corners are where the separation of wind flow occurs and the formation of small fast vortices are formed. This creates a suction zone with higher fluctuations affecting the negative peak values \check{C}_p at the edges and forming a critical suction zone for cladding to be investigated. Figure 3-17 and Figure 3-18, show the positive and negative pressure peak values for the edge line of the eastern facade for taps C_1 , C_2 and C_3 , see Figure 3-14 for exact locations. It was observed that the surrounding buildings typically increased in the negative peak \check{C}_p when compared to the isolated case 0000SH. Particularly for lower

surrounding heights as for 0025SH, where it reached 40% increase at the mid-level tap C_2 for $AoA = 0^\circ$.

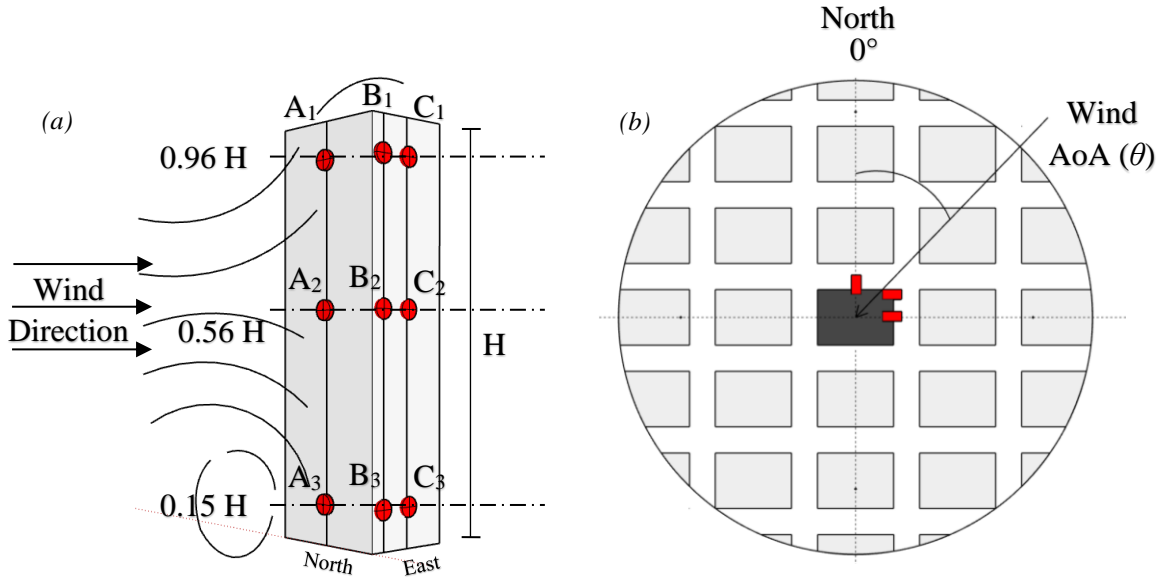


Figure 3-14: a) specific tap locations at the northern and eastern facades and b) $AoA(\theta)$ according to tap location.

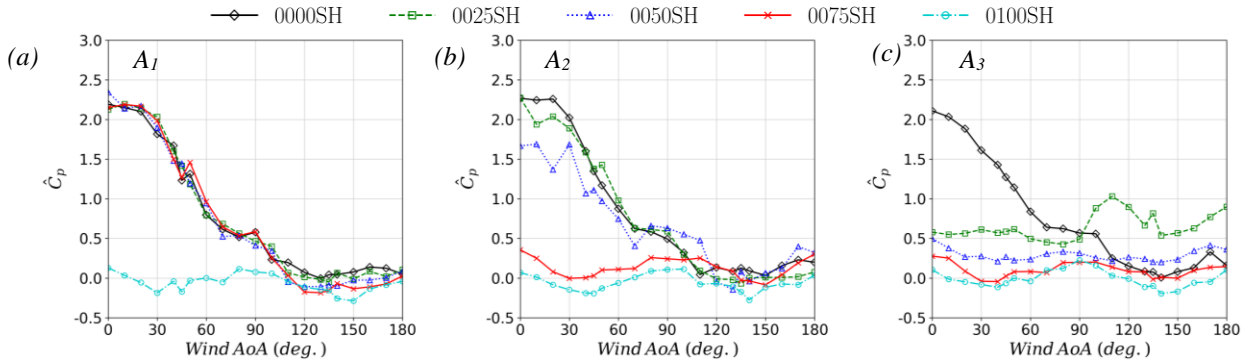


Figure 3-15: Variation of the positive peak pressure (\hat{C}_p) at the center line of the north facade for all cases at different AoA: (a) Tap A_1 ; (b) Tap A_2 ; (c) Tap A_3

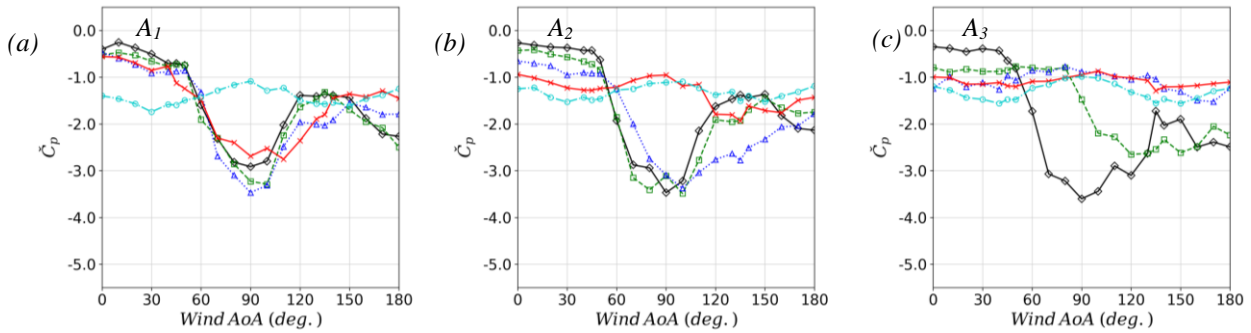


Figure 3-16: Variation of the negative peak pressure (\check{C}_p) at the center line of the north facade for all cases at different AoA: (a) Tap A_1 ; (b) Tap A_2 ; (c) Tap A_3

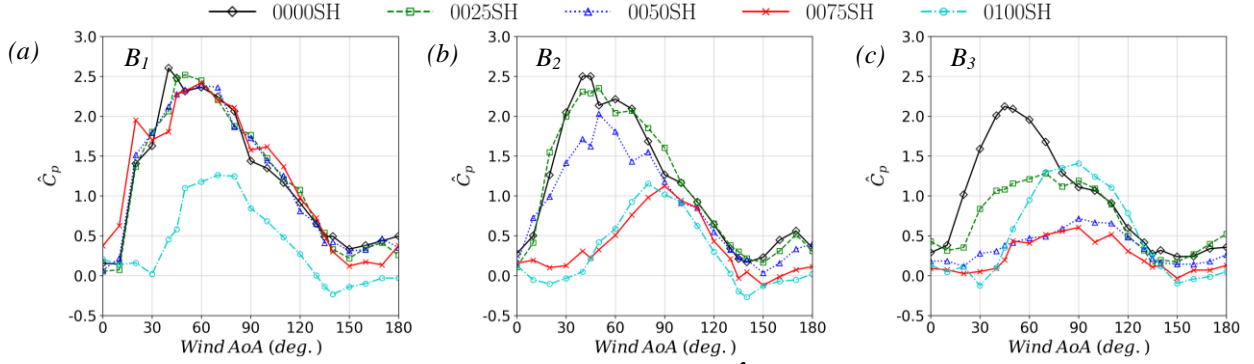


Figure 3-17: Variation of the positive peak pressures (\hat{C}_p) at the corner edge of the east facade for all cases at different AoA: (a) Tap B_1 ; (b) Tap B_2 ; (c) Tap B_3

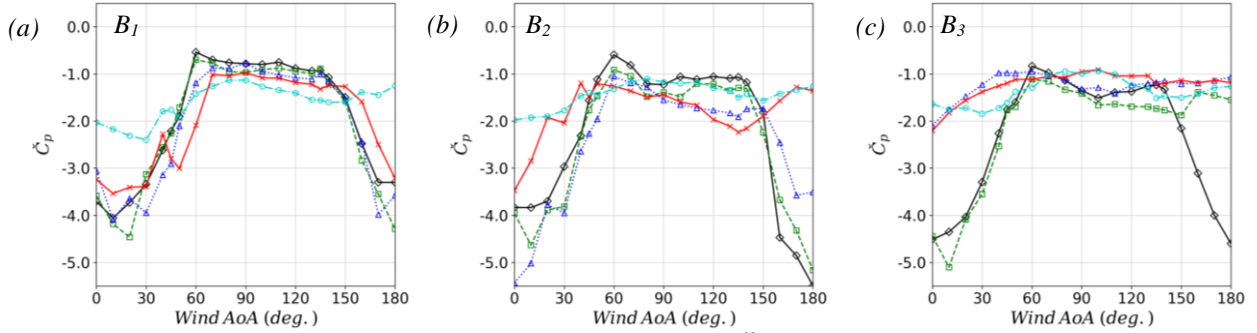


Figure 3-18: Variation of the negative peak pressures (\check{C}_p) at the corner edge of the east facade for all cases at different AoA: (a) Tap B_1 ; (b) Tap B_2 ; (c) Tap B_3

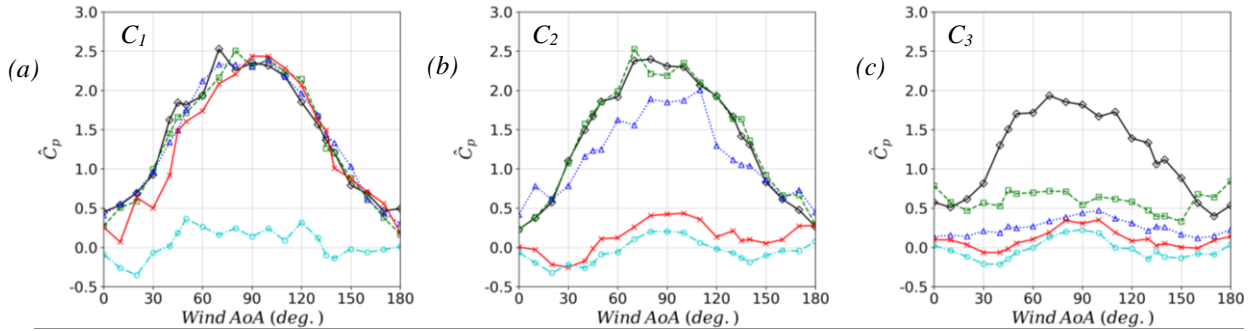


Figure 3-19: Variation of the positive peak pressures (\hat{C}_p) at the center line of the east facade for all cases at different AoA: (a) Tap C_1 ; (b) Tap C_2 ; (c) Tap C_3

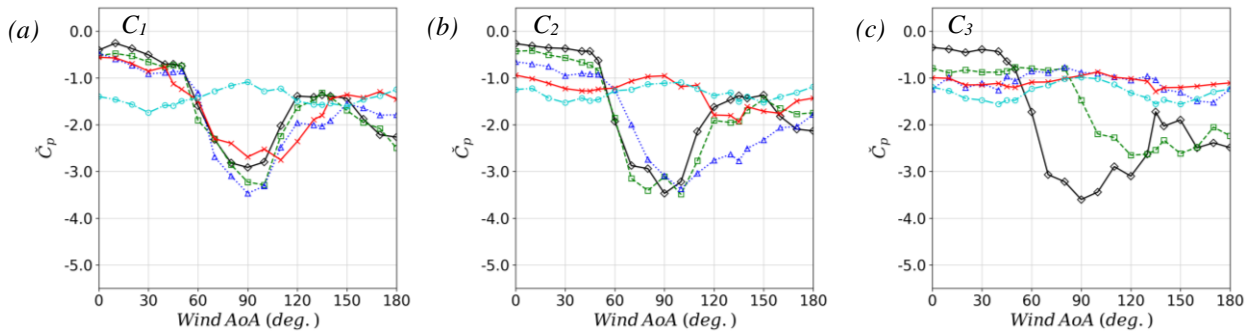


Figure 3-20: variation of the negative peak pressures (\check{C}_p) at the center line of the east facade for all cases at different AoA: (a) Tap C_1 ; (b) Tap C_2 ; (c) Tap C_3

3.3.4 Pressure power spectra

The frequency of the fluctuating surface pressures provides a deep understanding on how the wind react around the building, thus how the energy is distributed. When the flow is obstructed and opposed by sheltering bodies other than the study model, the flow become more complex and the energy distribution fluctuates accordingly. Figure 3-21, Figure 3-22, Figure 3-23, Figure 3-24 and, Figure 3-25 show the difference in pressure fluctuations on a ring of taps located at $2/3H$ of the building height. The spectral densities were demonstrated for all the surrounding cases including the isolated typical case 0000SH in a suburban exposure at $AoA=0^\circ$.

For case 0000SH, it is evident that the wind ward surface at tap points (T_2 , T_3 , T_4) are experiencing a broader energy distribution in comparison with the edges at (T_6 , T_7 and T_{19} , T_{20}) see Figure 3-21, where a sudden increase in energy is spotted forming a spike around the corners, just before the separation occurs. These narrow spikes are due to the fluctuations of the vortex shedding formed inside the wakes. As the wind flows towards the far edges, a slight increase in energy developed due to a possible reattachment at taps (T_9 , T_{10} and T_{16} , T_{17}). The distribution starts then to widen again and become even broader at the leeward surface at (T_{12} and T_{13}). These observations match closely to what have been demonstrated by (Surry and Djakovich 1995) for a high-rise building model.

For case 0025SH, the fluctuations of the surface pressure experience a slight decrease in energy, particularly, the near edge where the formed spikes have lower energy compared to the isolated case 0000SH. Similarly, the far edges were subjected to more disturbance broadening the peaks created through reattachment as shown in Figure 3-22. These alterations occurs due to the opposition of flow with the sheltering bodies, which break up the vortices coming from the upstream wind, see taps for the near edges (T_6 , T_7 and T_{19} , T_{20}) and the far edge where reattachment occurs, see taps (T_{10} and T_{16}). The leeward surface showed a much broader energy distribution compare to case 0000SH, see taps (T_{12} , T_{13} and T_{14}). Similar distribution was also spotted for case 0050SH with lower energy levels compared to case 0025SH and 000SH, see Figure 3-23.

For case 0075SH, the front taps (T₁, T₂, T₃, T₄ and T₅) experience a shift in the energy peak with slightly higher values towards the higher frequencies. and this is due to the positioning of the study model, which is submersed inside the wake of the surrounding buildings colliding with the broken vortices formed by the upstream buildings, see Figure 3-24. As for case 0100SH with full sheltering height, it's obvious that the energy distribution around the surface became very low with no defined energy peaks as result of total shielding around the study building see Figure 3-25.

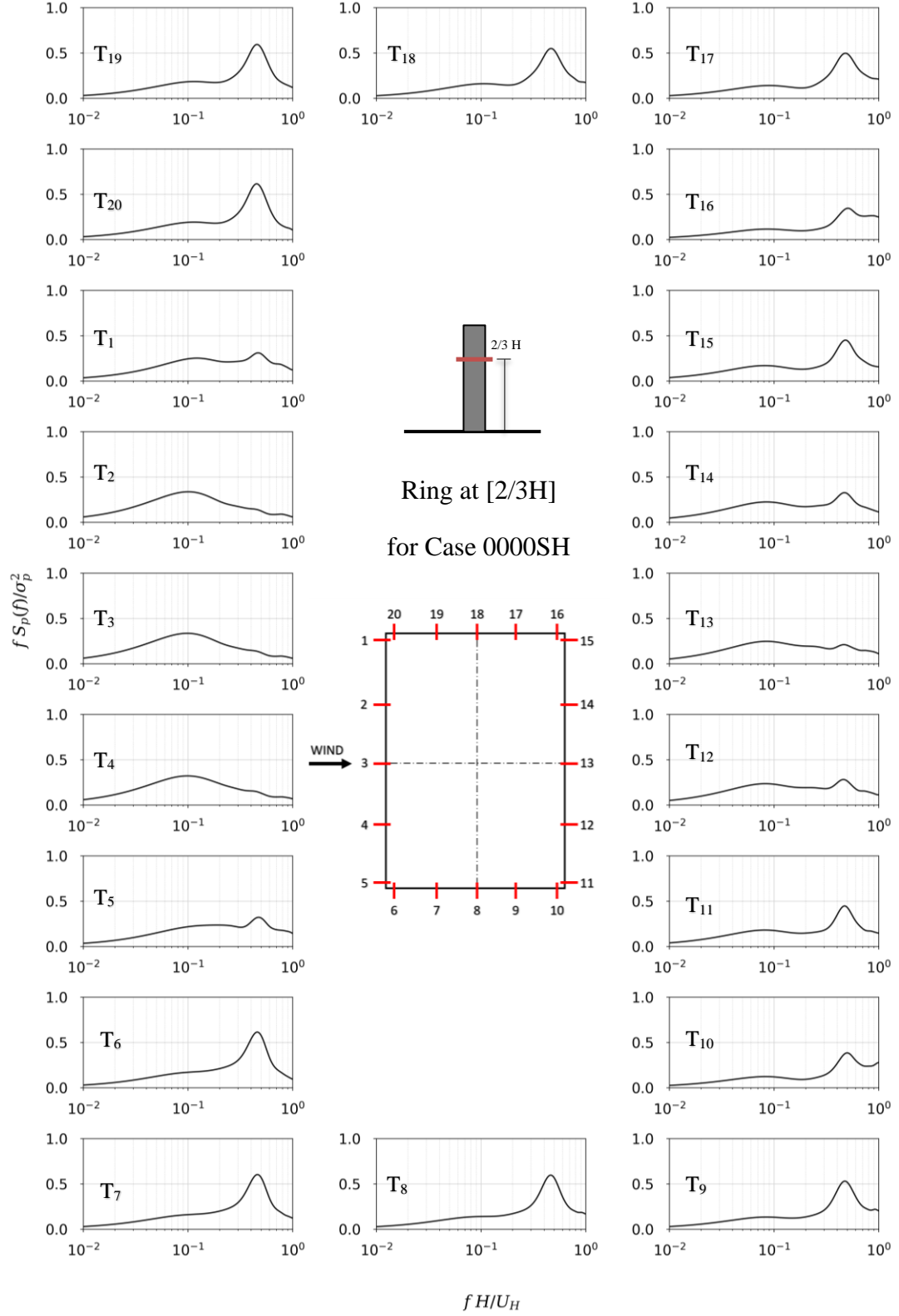


Figure 3-21: Power spectral densities of pressure at model height of $2/3H$ of the study building height for case 0000SH in suburban terrain at $\text{AoA}=0^\circ$.

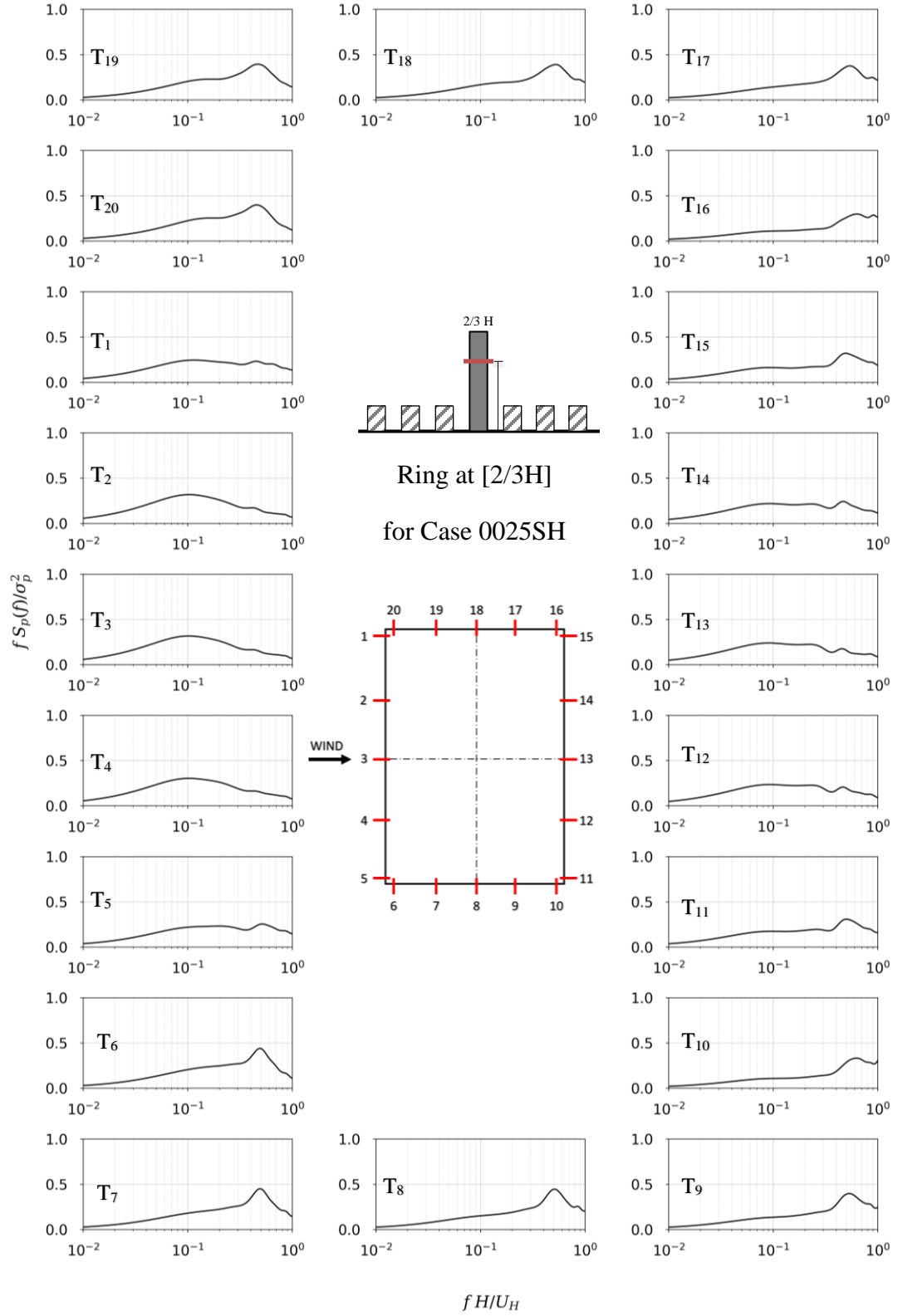


Figure 3-22: Power spectral densities of pressure at model height of $2/3H$ of the study building height for case 0025SH in suburban terrain at $AoA=0^\circ$.

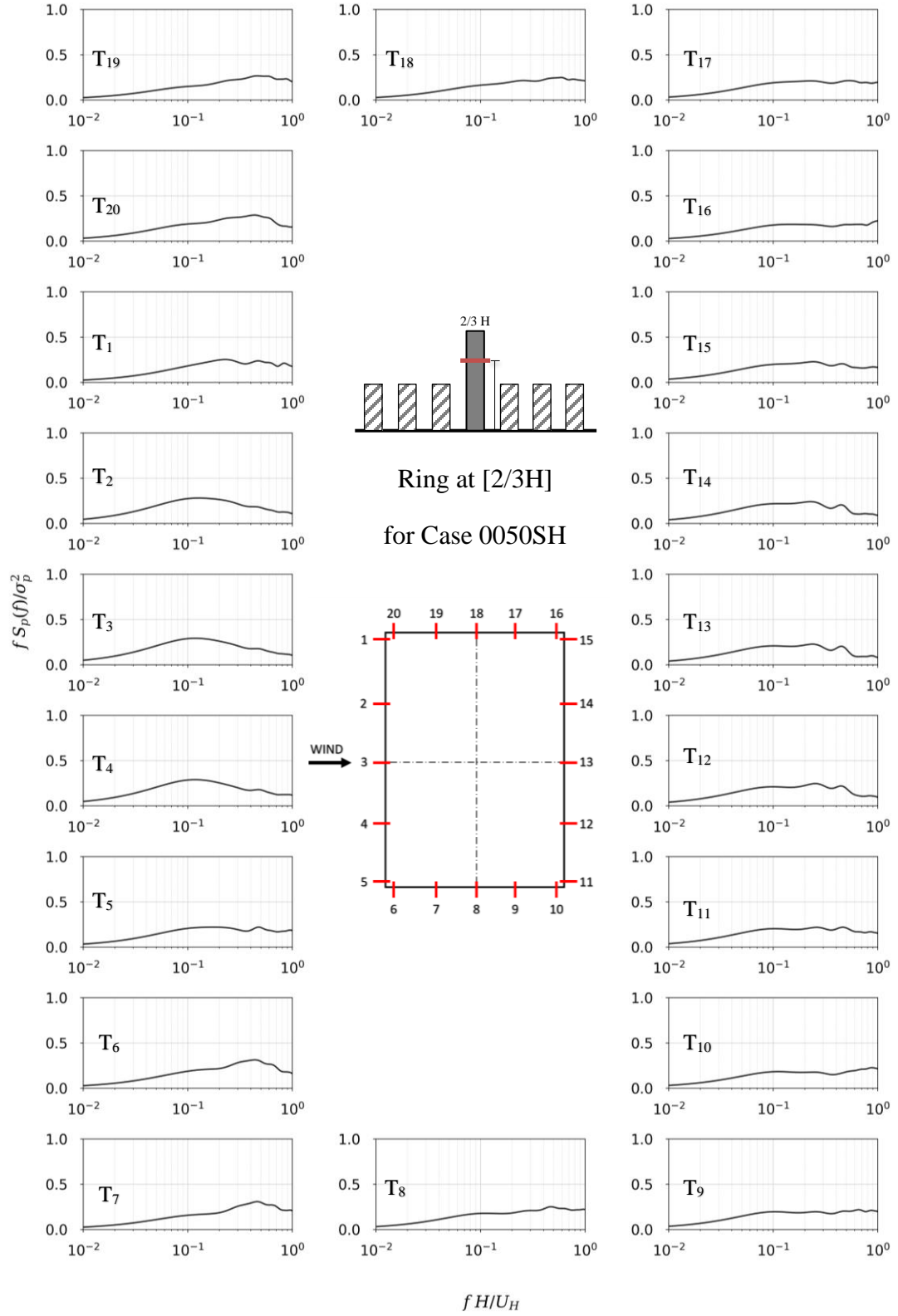


Figure 3-23: Power spectral densities of pressure at model height of $2/3H$ of the study building height for case 0050SH in suburban terrain at $\text{AoA} = 0^\circ$.

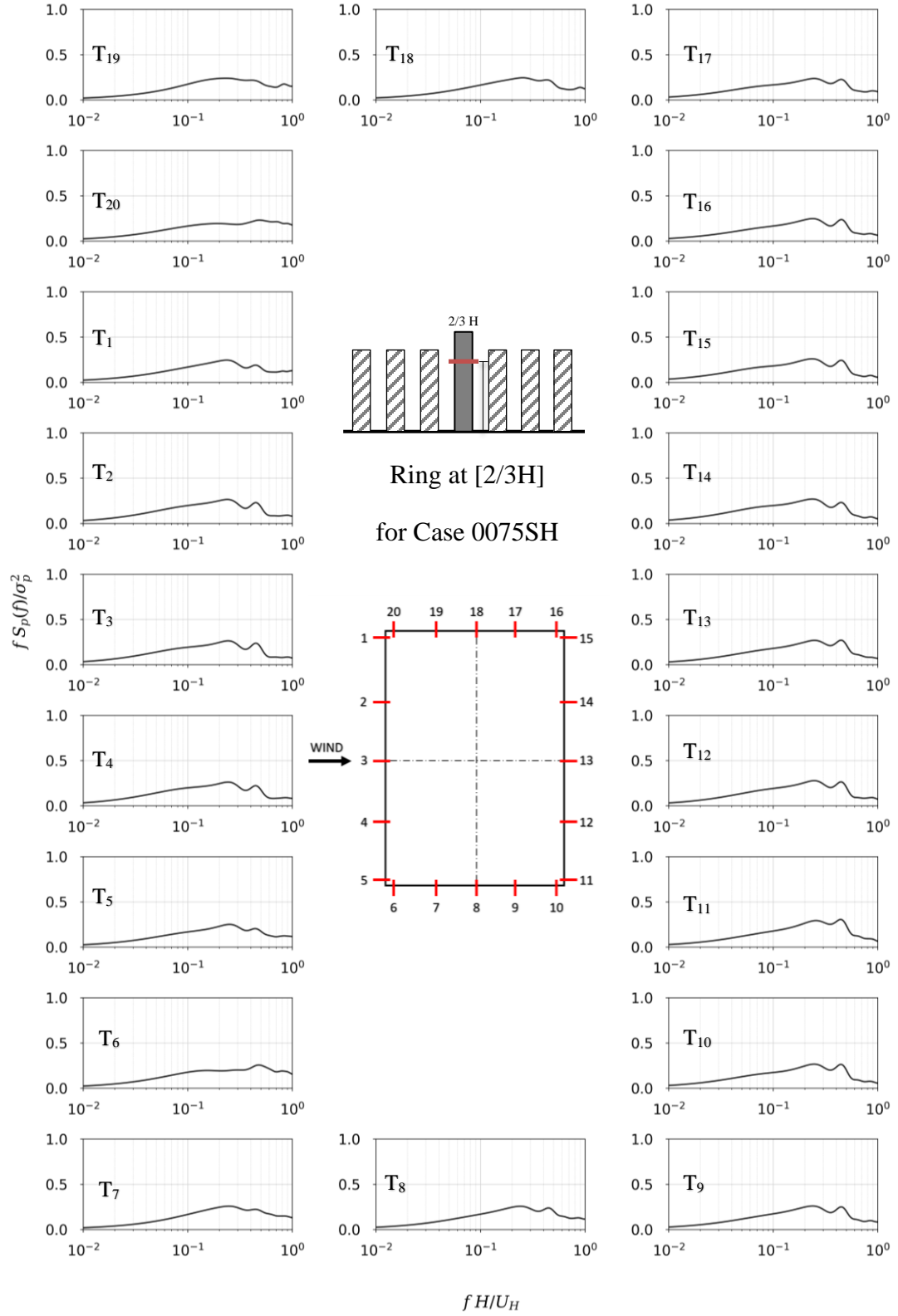


Figure 3-24: Power spectral densities of pressure at model height of $2/3H$ of the study building height for case 0075SH in suburban terrain at $AoA=0^\circ$.

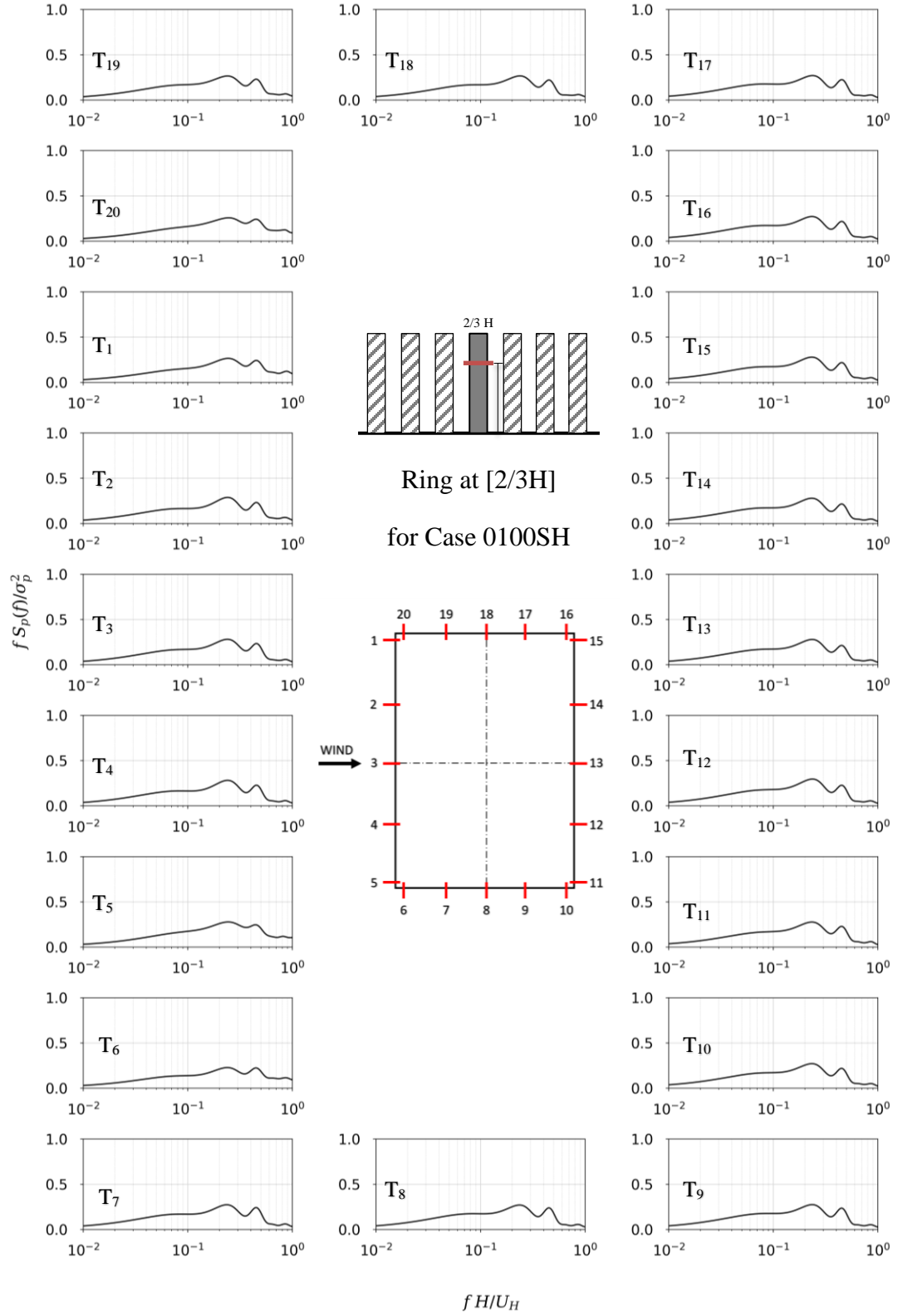


Figure 3-25: Power spectral densities of pressure at model height of $2/3H$ of the study building height for case 0100SH in suburban terrain at $AoA=0^\circ$.

3.4 Conclusion

The previous study aimed to investigate the impact of city growth on high-rise buildings, focusing on cladding loads. High Frequency Pressure Integration (HFPI) tests were conducted at the Boundary Layer Wind Tunnel Laboratory (BLWTL) to assess the complex behavior of wind with sheltering bodies and its impact on surface pressures and cladding loads. These experiments captured the changes in pressure distribution on the CAARC building model within 5 different generic surrounding configurations equally spaced with varying height ratios for real representation of city development. The main observations from the independent local mean pressure distributions are summarized as follows:

- i. The windward surface experience a decrease in the mean pressure distribution while higher fluctuations with the increase in surrounding height. It was observed that the positive mean pressures experienced an upward shift for the windward face at $AoA = 0^\circ$ especially for cases 0025SH and 0050SH. Which also created a suction zone behind the sheltering body. For cases 0075SH and 0100SH, the negative pressure become the dominant on the windward surface altering the $\overline{C_p}$ from +0.8 for the isolated case 0000SH to -0.8 as it reaches Case 0100SH (full height surrounding)
- ii. The parallel surfaces to the flow along the near edge lines experience an increase by 14% in the negative mean $\overline{C_p}$ distribution at $AoA = 90^\circ$, reaching maximum of -1.2 in case 0050SH,
- iii. As for the extreme value analysis, case 0025SH and 0050SH showed around 40% and 20% increase in the largest minimum \check{C}_p at values of -7 and -6.5 compared to the isolated case 0000SH for $AoA = 120^\circ$ and 90° respectively. These high fluctuations are the result of continues wake disturbance with the sheltering body, speeding up the vortices formed there and increasing the fluctuations significantly.

3.5 References

- ASCE. 2012. “Wind Tunnel Testing for Buildings and Other Structures.” In . American Society of Civil Engineers.
- Bailey, P A, and K C S Kwok. 1985. “Interference Excitation of Twin Tall Buildings.” *Journal of Wind Engineering and Industrial Aerodynamics* 21 (3): 323–38.
- Bezabeh, M. A., G. T. Bitsuamlak, M. Popovski, and S. Tesfamariam. 2020. “Dynamic Response of Tall Mass-Timber Buildings to Wind Excitation.” *Journal of Structural Engineering* 146 (10): 04020199. [https://doi.org/10.1061/\(asce\)st.1943-541x.0002746](https://doi.org/10.1061/(asce)st.1943-541x.0002746).
- Chen, Xinzhong, and Ahsan Kareem. 2005. “Dynamic Wind Effects on Buildings with 3D Coupled Modes: Application of High Frequency Force Balance Measurements.” *Journal of Engineering Mechanics* 131 (11): 1115–25. [https://doi.org/10.1061/\(asce\)0733-9399\(2005\)131:11\(1115\)](https://doi.org/10.1061/(asce)0733-9399(2005)131:11(1115)).
- Cheung, J C K. 1984. “Effect of Tall Building Edge Configurations on Local Surface Wind Pressures.” In *3rd International Conference on Tall Buildings, Hong Kong and Guangzhou*, 10–15.
- Codes, National Research Council of Canada. Canadian Commission on Building and Fire. 2015. “National Building Code of Canada: 2015.” National Research Council of Canada. Canadian Commission on Building and Fire Codes.
- Cóstola, D., B. Blocken, and J. L.M. Hensen. 2009. “Overview of Pressure Coefficient Data in Building Energy Simulation and Airflow Network Programs.” *Building and Environment* 44 (10): 2027–36. <https://doi.org/10.1016/j.buildenv.2009.02.006>.
- Dagnew, Agerneh K., and Girma T. Bitsuamlak. 2014. “Computational Evaluation of Wind Loads on a Standard Tall Building Using Les.” *Wind and Structures, An International Journal* 18 (5): 567–98. <https://doi.org/10.12989/was.2014.18.5.567>.
- Davenport, A G. 1967. “The Treatment of Wind Loading on Tall Buildings.” In *Tall Buildings*, 3–45. Elsevier.
- Davenport, Alan G. 2002. “Past, Present and Future of Wind Engineering.” *Journal of Wind Engineering and Industrial Aerodynamics* 90 (12–15): 1371–80. [https://doi.org/10.1016/S0167-6105\(02\)00383-5](https://doi.org/10.1016/S0167-6105(02)00383-5).
- Elshaer, Ahmed, Haitham Aboshosha, Girma Bitsuamlak, Ashraf El Damatty, and Agerneh Dagnew. 2016. “LES Evaluation of Wind-Induced Responses for an Isolated and a Surrounded Tall Building.” *Engineering Structures* 115: 179–95. <https://doi.org/10.1016/j.engstruct.2016.02.026>.
- Elshaer, Ahmed, Anant Gairola, Kimberley Adamek, and Girma Bitsuamlak. 2017. “Variations in Wind Load on Tall Buildings Due to Urban Development.”

- Sustainable Cities and Society* 34 (December 2016): 264–77.
<https://doi.org/10.1016/j.scs.2017.06.008>.
- English, Elizabeth C. 1990. “Shielding Factors from Wind-Tunnel Studies of Prismatic Structures.” *Journal of Wind Engineering and Industrial Aerodynamics* 36: 611–19.
[https://doi.org/https://doi.org/10.1016/0167-6105\(90\)90343-B](https://doi.org/https://doi.org/10.1016/0167-6105(90)90343-B).
- ESDU. 2001. *Engineering Sciences Data Unit. Characteristics of Atmospheric Turbulence near the Ground. Part II: Single Point Data for Strong Winds*. 85320th ed.
- Holmes, John D. 2018. *Wind Loading of Structures*. CRC press.
- Holmes, John D, Yukio Tamura, and Prem Krishna. 2008. “Wind Loads on Low, Medium and High-Rise Buildings by Asia-Pacific Codes,” no. May: 29–31.
- Huang, Peng, and Ming Gu. 2005. “Experimental Study on Wind-Induced Dynamic Interference Effects between Two Tall Buildings.” *Wind and Structures, An International Journal* 8 (3): 147–61. <https://doi.org/10.12989/was.2005.8.3.147>.
- Hui, Yi, Akihito Yoshida, and Yukio Tamura. 2013. “Interference Effects between Two Rectangular-Section High-Rise Buildings on Local Peak Pressure Coefficients.” *Journal of Fluids and Structures* 37: 120–33.
<https://doi.org/10.1016/j.jfluidstructs.2012.11.007>.
- Kareem, Ahsan. 1992. “Dynamic Response of High-Rise Buildings to Stochastic Wind Loads.” *Journal of Wind Engineering and Industrial Aerodynamics* 42 (1–3): 1101–12. [https://doi.org/10.1016/0167-6105\(92\)90117-S](https://doi.org/10.1016/0167-6105(92)90117-S).
- Khanduri, A. C., T. Stathopoulos, and C. Bédard. 1998. “Wind-Induced Interference Effects on Buildings - A Review of the State-of-the-Art.” *Engineering Structures* 20 (7): 617–30. [https://doi.org/10.1016/S0141-0296\(97\)00066-7](https://doi.org/10.1016/S0141-0296(97)00066-7).
- Khanduri, Atul C., Theodore Stathopoulos, and Claude Bédard. 2000. “Generalization of Wind-Induced Interference Effects for Two Buildings.” *Wind and Structures, An International Journal* 3 (4): 255–66. <https://doi.org/10.12989/was.2000.3.4.255>.
- Kijewski, T; Kareem, A. n.d. “Dynamic Wind Effects - A Comparative Study (1998).Pdf.” *Wind & Structures*.
- Kim, Wonsul, Yukio Tamura, and Akihito Yoshida. 2011. “Interference Effects on Local Peak Pressures between Two Buildings.” *Journal of Wind Engineering and Industrial Aerodynamics* 99 (5): 584–600.
<https://doi.org/10.1016/j.jweia.2011.02.007>.
- Krishna, Prem. 1995. “Wind Loads on Low Rise Buildings - A Review.” *Journal of Wind Engineering and Industrial Aerodynamics* 54–55 (C): 383–96.
[https://doi.org/10.1016/0167-6105\(94\)00055-I](https://doi.org/10.1016/0167-6105(94)00055-I).

- Lam, K. M., M. Y. H. Leung, and J. G. Zhao. 2008. "Interference Effects on Wind Loading of a Row of Closely Spaced Tall Buildings." *Journal of Wind Engineering and Industrial Aerodynamics* 96 (5): 562–83. <https://doi.org/10.1016/j.jweia.2008.01.010>.
- Lee, B E, and G R Fowler. 1975. "The Mean Wind Forces Acting on a Pair of Square Prisms." *Building Science* 10 (2): 107–10.
- Lieblein, Julius. 1974. "Efficient Lillithods of Extreme-Value Methodology," no. October.
- Mara, T. G., B. K. Terry, T. C.E. Ho, and N. Isyumov. 2014. "Aerodynamic and Peak Response Interference Factors for an Upstream Square Building of Identical Height." *Journal of Wind Engineering and Industrial Aerodynamics* 133: 200–210. <https://doi.org/10.1016/j.jweia.2014.06.010>.
- Melbourne, W. 1980. "Comparison of Measurements on the CAARC Standard Tall Building Model in Simulated Model Wind Flows." *Journal of Wind Engineering and Industrial Aerodynamics* 6: 73–88.
- Stone, Gary K. 1987. *Aerodynamic Interference Effects on Wind Loads and Responses of Tall Buildings*. Faculty of Engineering Science, University of Western Ontario.
- Surry, D., and D. Djakovich. 1995. "Fluctuating Pressures on Models of Tall Buildings." *Journal of Wind Engineering and Industrial Aerodynamics* 58 (1–2): 81–112. [https://doi.org/10.1016/0167-6105\(95\)00015-J](https://doi.org/10.1016/0167-6105(95)00015-J).
- Surry, David, and William Mallais. 1983. "Adverse Local Wind Loads Induced by Adjacent Building." *Journal of Structural Engineering* 109 (3): 816–20. [https://doi.org/10.1061/\(asce\)0733-9445\(1983\)109:3\(816\)](https://doi.org/10.1061/(asce)0733-9445(1983)109:3(816)).
- Taniike, Yoshihito. 1991. "Turbulence Effect On Mutual Interference Of Tall Buildings By Yoshihito Taniike 1." *Engineering Mechanics* 117 (3): 443–56.
- Xie, J, and P A Irwin. 1998. "Application of the Force Balance Technique to a Building Complex." *Journal of Wind Engineering and Industrial Aerodynamics* 77: 579–90.
- Xie, Z. N., and M. Gu. 2007. "Simplified Formulas for Evaluation of Wind-Induced Interference Effects among Three Tall Buildings." *Journal of Wind Engineering and Industrial Aerodynamics* 95 (1): 31–52. <https://doi.org/10.1016/j.jweia.2006.05.003>.
- Xie, Z. N., and Minggu Gu. 2004. "Mean Interference Effects among Tall Buildings." *Engineering Structures* 26 (9): 1173–83.
- Zhang, Aishe, and Ming Gu. 2008. "Wind Tunnel Tests and Numerical Simulations of Wind Pressures on Buildings in Staggered Arrangement." *Journal of Wind Engineering and Industrial Aerodynamics* 96 (10–11): 2067–79.

Chapter 4

4 Implications of city development on structural loads

4.1 Introduction

Modern cities are rapidly developing, and the need for vertical expansion has led to the construction of taller and more slender buildings. The performance of these structures is mainly governed by wind loads. As cities become denser, the wind phenomenon become more complex and the typical understanding of wind behavior around a bluff body in its isolated form changes significantly (Khanduri et al. 1998). This interaction with the built environments, alters the flow of wind and change its aerodynamic characteristics, which in return influence the distribution of wind loads on the building surfaces (Holmes et al. 2008). Due to the complexity of wind behavior, wind tunnel testing has been significantly involved over the past decades to assure the accuracy of wind loads, especially with code limitations with respect to building height, shape, and surrounding configurations, (Davenport 2002).

Several Experimental and numerical approaches were performed on Highrise buildings emphasizing the importance of surroundings and its effect on wind-induced loads on structural and non-structural elements. For instance, (Bailey and Kwok 1985) studied the effect of a twin neighboring building on the dynamic response of a square based Highrise study model through a series of boundary layer wind tunnel tests. (Taniike 1991) examined the impact of increasing the neighboring building size ratio to the study building. It was noticed in this study a significant increase in the fluctuating drag of the examined building as the neighboring building width increase. (Khanduri et al. 2000) investigated the behavior of drag and lift coefficients over several wind tunnel experiments of varying aspect ratios, height of surrounding buildings at different terrain exposures. (Huang and Gu 2005) investigated the effect of surrounding on the dynamic response of a Highrise building model through comparing multiple wind tunnel model types (i.e. force balance test, aeroelastic test). (Xie and Gu 2004) and (Xie and Gu 2007) investigated the effects of two tall buildings in different relative positions on the study building mean and fluctuating wind loads. (Lam et al. 2008) studied the sheltering effect on a row of five square-plan tall

buildings arranged in either parallel or diamond patterns. The results show excitation of wind at the diamond patterned row due to a “wind catchment effect” leading to a significant magnification of mean wind loads. (Dagnew and Bitsuamlak 2014), (Elshaer et al. 2016) and (Elshaer et al. 2017) followed a numerical approach through performing CFD simulations to evaluate the aerodynamic response of a typical tall building with and without surrounding buildings (i.e. isolated building, two adjacent buildings, 1 layer of surrounding buildings) showing a good agreement of pressure, top displacement, top accelerations and base moments with wind tunnel results. From cladding design perspective (Surry and Mallais 1983), (Irwin 1998), (Hui et al. 2013), (Kim et al. 2011) studied the local peak pressures with different statistical methods for twin arrangement of surrounding buildings. (Kim et al. 2015) recorded high local peak pressures at the sides and corners of the study building near the top of the building with an increase of 84% near the building top height compared to the isolated form.

Table 4-1: Scope and main findings of previous studies focused on the effect of surroundings on high-rise buildings

Authors	Model	Study purpose	Surrounding Environment	Comments
Bailey and Kwok (1985)	BLWT	Structural design	2 buildings	Studied the dynamic response of a squared based high-rise under the effect of a neighboring buildings in different arrangements
Taniike (1991)	BLWT	Structural design	2 buildings	Investigated the effect of a changing the size ratio of an upstream building on the aeroelastic response of a high-rise square downstream building under low and high turbulence flow
Khanduri et al. (2000)	BLWT	Structural design	2 buildings	Investigated the structural response of a high-rise building surround by an interference building with different aspect ratios, height of surrounding building and terrain exposures)
Huang and Gu (2005)	BLWT	Structural design	2 buildings	Compared the dynamic response of a downstream building surrounded by an adjacent a

				typical building with different experimental techniques (i.e. HFFB, aeroelastic)
Zhao and Lam (2008)	BLWT	Structural design	Row of square buildings	Studied the structural response on a high-rise building surrounded by a set of square-based buildings closely spaced in a row
Hui et al. (2013)	BLWT	Structural design	2 buildings	Investigated the flow field and the pressure distribution of interference effects on external pressures between two high-rise buildings of exact height
Dagneu and Bitsuamlak (2014)	CFD	Structural design	2 buildings	Investigated the effect of sheltering of a neighboring building. Also, examined three different turbulence models showing agreement of the synthetic method with the BLWT than the random and the recycling flow methods.
Elshaer et al (2016)	CFD	Structural design	Isolated and Complex building surroundings	Investigated the aerodynamic response of a typical tall building with and without surrounding buildings showing a decrease in mean by 50% and a higher rms by 40%.Difference
Elshaer et al (2017)	CFD	Structural design	Complex building surroundings	Examined the changes in the design of wind loads on tall buildings with urban development showing a reduction in the mean and fluctuating base moments by 50% and 20%, respectively, with the increase in surrounding height .

Although several studies discussed the impact of the existing surroundings on the aerodynamics of tall buildings. However, the effect of future possible changes in the surrounding conditions is not investigated thoroughly. It is very rare for buildings to be demolished completely from the surrounding, but the prediction is more likely towards further construction and denser developments. This scenario is more favorable and can have significant changes over newly developed cities. Moreover, most of the previously

mentioned literature where adopting the effect of surrounding with restricted configurations in terms of number of buildings, the area of the sheltering region and the variation in the aspect ratios. In this study, generic configurations of the predicted city growth are presented through a series of wind tunnel testing conducted at the University of Western Ontario, Boundary Layer Wind Tunnel I (BLWTI). The study building is being adopted from the Commonwealth Advisory Aeronautical Council (CAARC) building model (Melbourne 1980) where a High frequency integration test is being applied to investigate the impact surrounding configurations on wind-induced loads for aerodynamic structural analysis. The city growth is represented by five different generic surrounding configurations, varying in height ratios compared to the study building forming a sheltering region with a radius of 500 m in full scale from the study model. The configuration includes an isolated case scenario 0000SH, 25% increase in Surrounding Height (0025SH), 50% increase (0050SH), 75% increase (0075SH) and 100% full height increase (0100SH) of surrounding buildings.

4.2 Experimental setup methodology

4.2.1 Wind tunnel testing

High Frequency Pressure Integration (HFPI) test was adopted for the current study to investigate the impact of city development on wind-induced loads applied on a Highrise building model. The study model was adopted from the Commonwealth Advisory Aeronautical Research Council (CAARC). It has a geometrical scale of 1:400 with a rectangular footprint of (Depth D * Width B * height H), where $D = 45.72$ m (150 ft), $B = 30.48$ m (100 ft), and $H = 182.88$ m (600ft) in full scale. The experimental tests were performed at the University of Western Ontario's Boundary Layer Wind Tunnel Laboratory (BLWTL I) as shown in Figure 4-1. The tunnel has a working section of approximately 2.44 m in width by 2.3 m in height and a length of 24.4 m. The test was carried out in suburban exposure for all the surrounding configurations to represent the city-profile. The exposure was generated by the combined effect of the three 0.8 m high trapezoidal spires and the random arrangement of the roughness blocks, see Figure 4-1. The mean wind speed, turbulence intensity and spectral density profiles are adjusted according to the

acquired geometrical scale (1:400) and matched with the ESDU profiles of the simulated suburban exposure, see Figure 4-2.

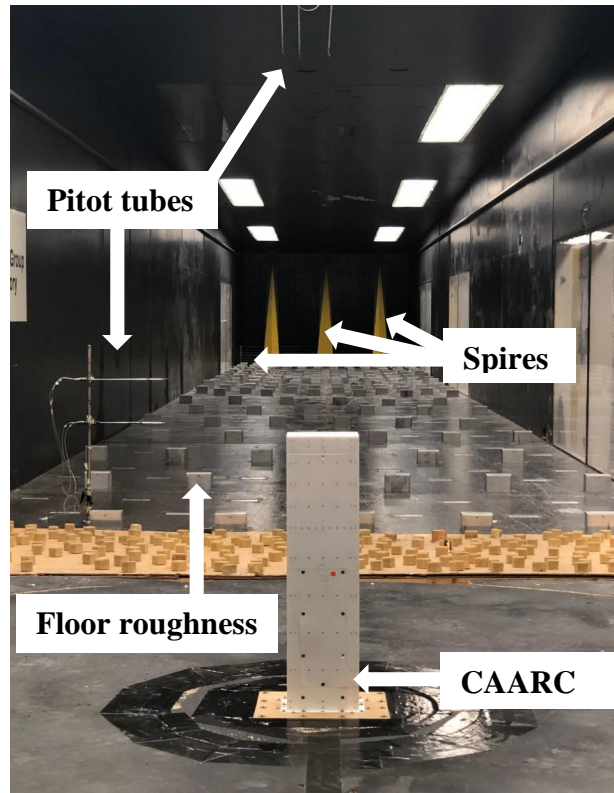


Figure 4-1: Experimental model in BLWTL for the isolate case 0000SH for a wind $AoA=0^\circ$

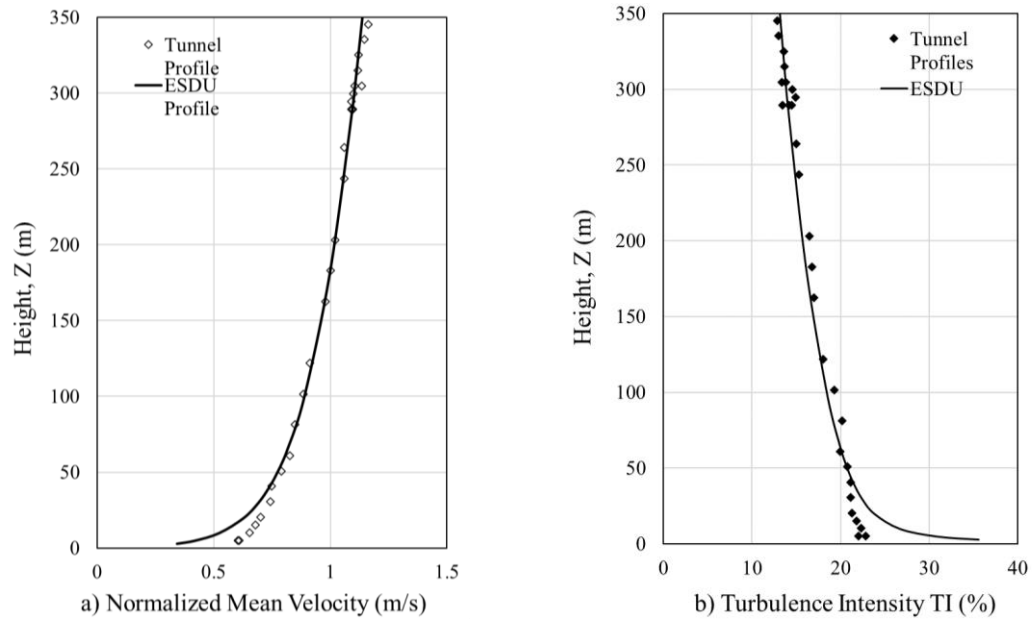


Figure 4-2: Wind tunnel profiles for suburban terrain: (a) normalized mean wind speed, (b) turbulence intensity profiles (TI%)

4.2.2 Pressure measurements

The CAARC model was 3D printed at Western University Machine Shop using acrylic powder. The model was printed into 3 levels (upper, Middle, and lower parts) and connected with a wooden base board for support. It was also constructed to have a hollow interior for proper installation of the applied pressure system, see Figure 4-3. The exact locations of the pressure taps were marked on the model, leaving holes on the printed model for Installation of the plastic tubing. Each tube is 600mm long that connects the model surface with multiple pressure electronic scanner.

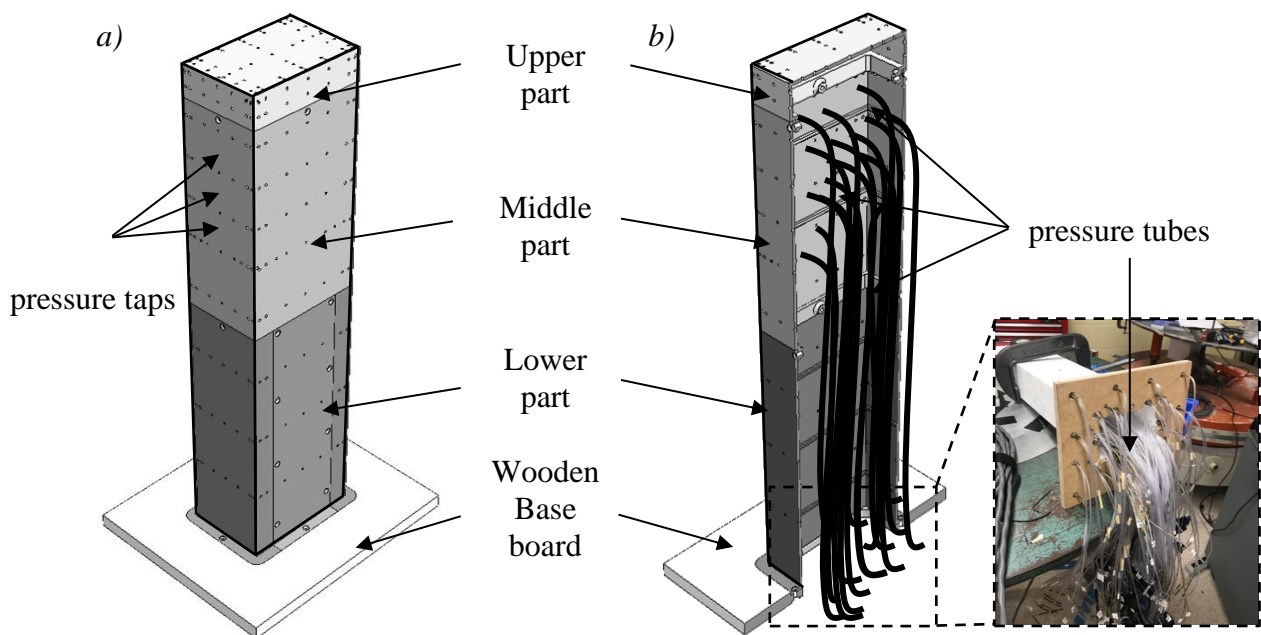


Figure 4-3: a) perspective view and b) a longitudinal section of the constructed 3D printed model

The total number of taps installed were 367 taps including 51 roof taps and the rest are distributed over 12 layers on the building surfaces. Denser points were placed more densely near the edges of the buildings to allow capturing the strong pressure gradients that commonly occur at the corners according to the expected distribution of C_p 's. Pressure readings were extracted from the tests for each wind direction of a total of 23 wind directions from 0° to 180° at 10° increment plus the corner angles. The exact locations of the taps were recorded in an excel sheet and given specific numbers which correspond to their attached scanners, see Appendix. The pressure time history for all taps was measured simultaneously at a sampling frequency of 400Hz, where continuous sampling of 20 The

pressure time history for all taps were measured simultaneously at a sampling frequency of 400 Hz. The pressure time histories for each wind direction was recorded for 128s at model scale which corresponds to 3.5 hours at full-scale. Different pressure coefficients are obtained for analysis and comparisons including mean, root mean-square values as expressed below.

$$\bar{C}p_i = \frac{p_i - p_0}{\frac{1}{2} \rho_a \bar{U}_h^2} \quad \hat{C}p_i = \frac{\sqrt{p_i^2 - p_0}}{\frac{1}{2} \rho_a \bar{U}_h^2} \quad 4-1$$

where the denominator represent the dynamic pressure found from the mean wind speed at building height \bar{U}_h and the air density ρ_a . The reference pressure is denoted by p_0 , while the varying pressure p_i is specified to each tap location i . To obtain the wind-induced responses on the CAARC study building, the force for each pressure tap is computed using the following equations.

$$f_{xi}(t) = \frac{1}{2} \rho \bar{U}_h^2 C p_i(t) a_{xi} \quad 4-2$$

$$f_{yi}(t) = \frac{1}{2} \rho \bar{U}_h^2 C p_i(t) a_{yi}$$

$$f_{zi}(t) = \frac{1}{2} \rho \bar{U}_h^2 C p_i(t) a_{zi}$$

where, ρ is the air density, \bar{U}_h is the mean wind velocity at building height, , and a_{xi} , a_{yi} are the tributary areas at pressure tap i projected from x and y respectively. The building base moment time histories are calculated for all the building surrounding configurations using the computed forces as follows.

$$\begin{aligned} M_x &= \sum_{i=1}^N f_{xi}(t) h_i \\ M_y &= \sum_{i=1}^N f_{yi}(t) h_i \\ M_z &= \sum_{i=1}^N f_{zi}(t) r_i \end{aligned} \quad 4-3$$

where h_i is the height of the pressure and r_i is the moment arm for pressure tap i .

Table 4-2: Dynamic properties of the study building

Study building properties	Value
Height H , Width B , Depth D	182.88m, 30.48m, 45.7m
Natural frequency	0.2 Hz (x & y), 0.35Hz (torsional)
Damping ratio (percentage)	1% for all modes
Mass per unit volume m	192.22kg/m ³

the tributary area of the model surface pressures was defined using a simple grid mesh covering the entire surfaces of the CAARC model. The mesh is created so that it divides the space between each two adjacent taps in x and y-directions to forms an enclosed cell around each tap

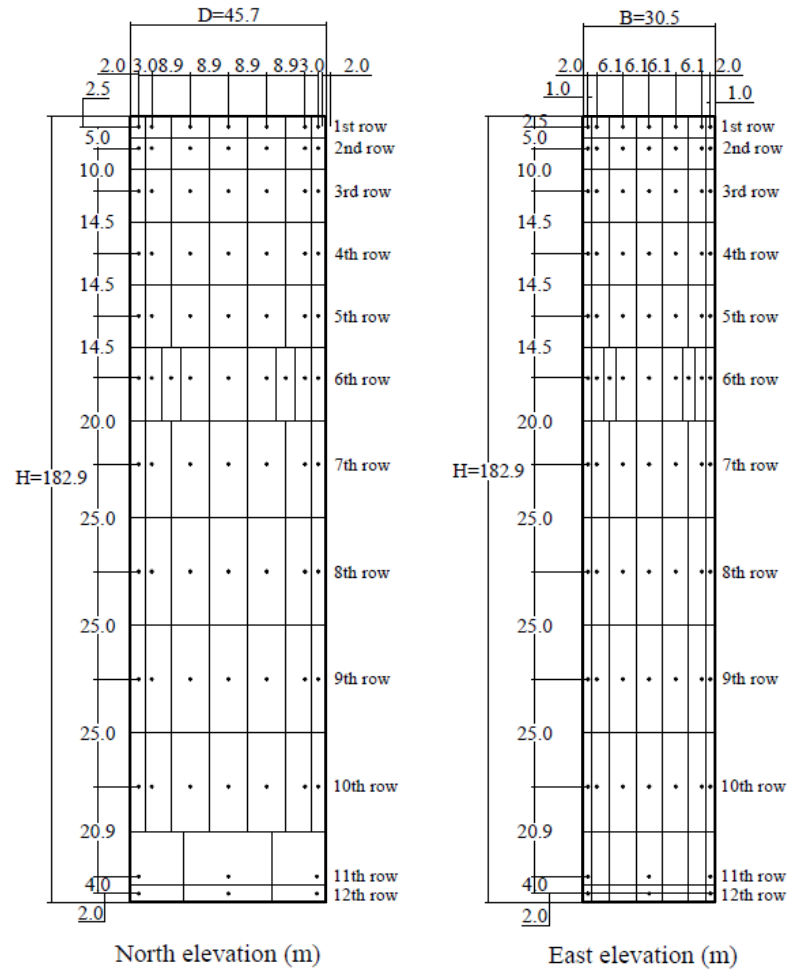


Figure 4-4: Tributary area distribution on the pressure layout for the north and east elevations.

4.2.3 Dynamic response evaluation

The dynamic response of the study building is evaluated to investigate the impact of the surrounding growth. Table 2 provides a summary of the dynamic properties used to determine the peak top floor accelerations. The first two sway modes were assumed to be linear while the torsional mode was constant. The center of mass and rigidity of the building are assumed to coincide. The structural response of the building is computed using random vibration theory. The building is approximated by a discrete lumped mass system as shown in Figure 4-5. Each lumped mass has three degrees-of-freedom, two sway and one rotation. It is assumed that the modes shapes are orthogonal and can be considered uncoupled. The uncoupled system can be represented in modal coordinate using the following equation.

$$\ddot{q}_j + 2\xi_j\omega_j\dot{q}_j + \omega_j^2q_j = \frac{F_j(t)}{m_j} \quad 4-4$$

where ξ_j , ω_j are the j th mode damping and circular frequency, respectively. q_j is the j th mode generalized displacement vector, $F_j(t)$ is the j th mode generalized force, computed using the modes shapes and the forces at each pressure tap

$$F_j(t) = \int f_x(t) \phi_{xj}(h)dh + \int f_y(t) \phi_{yj}(h)dh + \int f_z(t) \phi_{zj}(h)dh \quad 4-5$$

m_j is the j th mode generalized mass which was computed from the mode shapes, discretized mass $m(h)$ and story mass of inertia, $I(h)$

$$m_j = \int m(h) \phi_{xj}^2(h)dh + \int m(h) \phi_{yj}^2(h)dh + \int I(h) \phi_{zj}^2(h)dh \quad 4-6$$

Using random vibration theory, the variance of the j th mode generalized acceleration $\sigma_{\ddot{q}_j}^2$ was computed using the spectral density of the generalized forces $S_{FFj}(\omega)$

$$\sigma_{\ddot{q}_j}^2 = \int_0^\infty \omega^4 \left| \frac{1}{m_j} \left(\frac{1}{(\omega_j^2 - \omega^2) + 2i\xi_j\omega_j\omega} \right) \right|^2 S_{FFj}(\omega) d\omega \quad 4-7$$

The peak response was evaluated using Eq.

$$\hat{R} = \bar{R} + g_f \hat{R} \quad 4-8$$

where R is the response, g_f is a gust factor which is assumed to be 3.5 and σ_R the rms of the response. For acceleration response of the building, the mean component is zero.

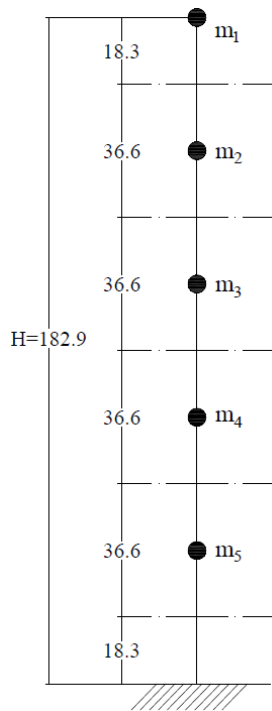


Table 4-3: Mass distribution

No. of elements	Mass distribution	Length L (m)	Mass m (kg)
1	m_1	18.3	4898758
2	m_2	36.6	9797516
3	m_3	36.6	9797516
4	m_4	36.6	9797516
5	m_5	36.6	9797516

Figure 4-5: Mass distribution layout on the CAARC building

4.2.4 Surrounding configurations

The CAARC model was tested over two phases: a) isolated case scenario without surrounding buildings and b) with surrounding configurations of a regular pattern varying in height ratios with respect to the study model. Suburban exposure was adopted for all the surrounding configurations to mimic the city profile, see Table 4-4

Table 4-4: Test phases and configurations at different wind directions.

Configurations	Case	Height of surrounds H_s (m)	Height Ratios ($H_r=H_s/H$)	Exposure (z_o)
Isolated	0000SH	0.00	0.00	Suburban (0.30)
With	0025SH	45.72	0.25	Suburban (0.30)
Surrounding	0050SH	91.44	0.50	Suburban (0.30)
Buildings	0075SH	137.16	0.75	Suburban (0.30)
	0100SH	182.88	1.00	Suburban (0.30)

Note: wind pressure measurements were taken for 0-180° AoA @10° increment to additional AoA (45°, 135°, 225°, 315°) were also tested.

Generic configurations for the predicted city growth were conducted to represent five different growth levels varying in height ratios (Isolated, 0.25 H, 0.50 H, 0.75 H and 1H full height) of surrounding blocks covering an area around the building with a radius of 500m in full scale. These surroundings were constructed using high-density foam blocks as shown in Figure 4-6

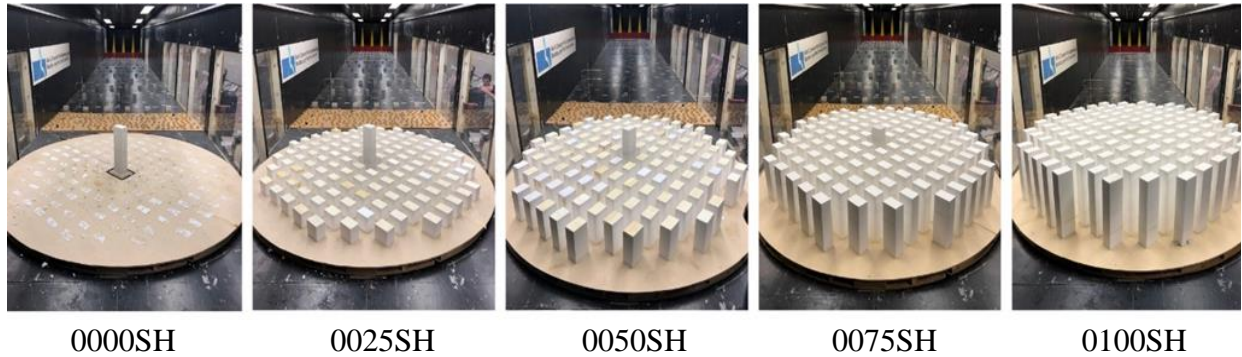


Figure 4-6: Installation of the CAARC model and the five different surrounding configurations of at the University of Western Ontario Boundary layer wind tunnel I (BLWT I).

4.3 Results and discussion

Wind loading

The following section describes the dynamic loading determined from the simultaneously measure external point pressures. where the generalized forces are determined from the pressure measurements and are then used in a standard random vibration analysis to provides estimates of the total dynamic loads and responses of the building structure.

4.3.1 Mean and rms pressure distribution

The altered flow field developed by change in urban topology result in different surface pressure distributions. Figure 4-7 and Figure 4-8 show the mean (C_p) pressure distribution contours for the 5 different surrounding configurations at wind directions (0° , 45°). For $AoA = 0^\circ$, it is observed that the isolated case 0000SH recorded the highest mean C_p value of +0.8 at 0.6H of the northern wall. As the surrounding buildings increase in height (cases 0025SH and 0050SH), the highest mean value at the northern wall; near the stagnation point; witnesses a gradual decrease in size accompanied with an upward shift in the location. The area of high positive mean pressure is reduced by approximately 25% and 50% for cases 0025SH and 0050SH, respectively, compared to the isolated case. These

reductions are not directly seen in the computed base moments since majority of the load reduction is experienced in the lower portions of the building where the moment arms are smaller. Additionally, the regions of high positive pressures are shift upwards which would increase the moment arms, resulting in an increase in the base moment for the x and y axis. For the southern (leeward) face, the negative pressures are reduced significantly in the lower sections. As for cases 0075SH, the reduction of positive pressures outweighs the impact of the upwards shift. The leeward face shows a notable reduction in the negative pressure along the height of the building, leading to a lower moment in the along wind direction. For case 0100SH, the study building is shielded from the upwind flow and therefore only experience negative pressure (suction) on exterior surfaces. As seen in Figure 4-7, case 0100SH shows a reduction in negative pressures along the western edge of the north face. The unsymmetric nature of pressure distribution can lead to an increase in the mean torsional loads. This pressure distribution can be a result of the wind flow between buildings, specifically channeling down street canons can interact with windward edge of study building.

Figure 4-9 and Figure 4-10 show the rms of the pressure distributions for both $AoA = 0^\circ$ and 45° . For the windward (north) face, the fluctuating component of the pressures reduce in the regions shielded by the upstream buildings. The region of high fluctuations near the top of the of the building increases in size as upstream buildings increase in height as seen for case 0025SH and 0050SH. For case 0075SH, the high fluctuation region near the top reduced significantly compared to the previous case. The rms of the pressure distribution for the 0100SH case is lower than the isolated case and is constant along the entire windward face. The leeward (south) side also shows are reduction in the fluctuating component of the pressures. For the isolated case 0000SH, the lowest rms C_p value is located in the center of the south face. As the surroundings increase in height, the low fluctuation region decreases in magnitude and shifted upwards, as seen in cases 0025SH and 0050SH. Cases 0075SH and 0100SH, the rms C_p values are significantly reduced, and the distributions are constant throughout the surface. For $AoA = 0^\circ$, the rms distribution of the pressures along the eastern face contribute to the across wind response. As seen in Figure 4-9, the region of high fluctuations is shifted upwards as the surroundings increase

in height. An area of lower fluctuations develops below the region of high fluctuations. The net result is a reduction in the peak across wind moment.

For $AoA = 45^\circ$, the wind flow is directed towards the corner of the building (northern-east direction) applying positive pressure on both the north and east side corners, while separation occurs at the far ends of both surfaces forming an area of negative pressures at the leeward edge, see Figure 4-10. The areas of high positive pressure are reduced as the surroundings increase in height while the upwards shift is not as distinct as seen in $AoA = 0^\circ$. The region of negative pressures seen on leeward edge experience a reduction in size, similar to positive pressures. As a result, the reduction in base moments in the x and y direction are lessened. For the 0100SH, the region of lower suction along outer edge of the building is not observed since street canon are not parallel with the flow. Figure 4-10 shows the rms C_p distribution for the $AoA = 45^\circ$ direction. The region of high fluctuations is located along the windward edge as seen on the northern and eastern face. As the upstream buildings increase in height, the high fluctuation region is shifted upwards. As the region moves upwards, the maximum rms value increases, as shown in cases 0025SH and 0050SH. For case 0075SH, the maximum rms C_p value reduced compared to the previous case. For the case 0100SH, the rms values become constant throughout the surface. For case 0000SH, rms C_p distribution on the leeward (south) is constant through the surface. The introduction of upstream buildings causes a region of high fluctuations to develop close to the roof height of the upstream buildings. As a result, the rms base moment values in the x and y direction remain unchanged between cases 0000SH, 0025SH and 0050SH for $AoA = 45^\circ$. The large reduction in the rms C_p distribution for the windward faces leads to the lower rms base moment values in the x and y direction for case 0075SH. The following section will investigate the impact of the surrounding growth on the base moments.

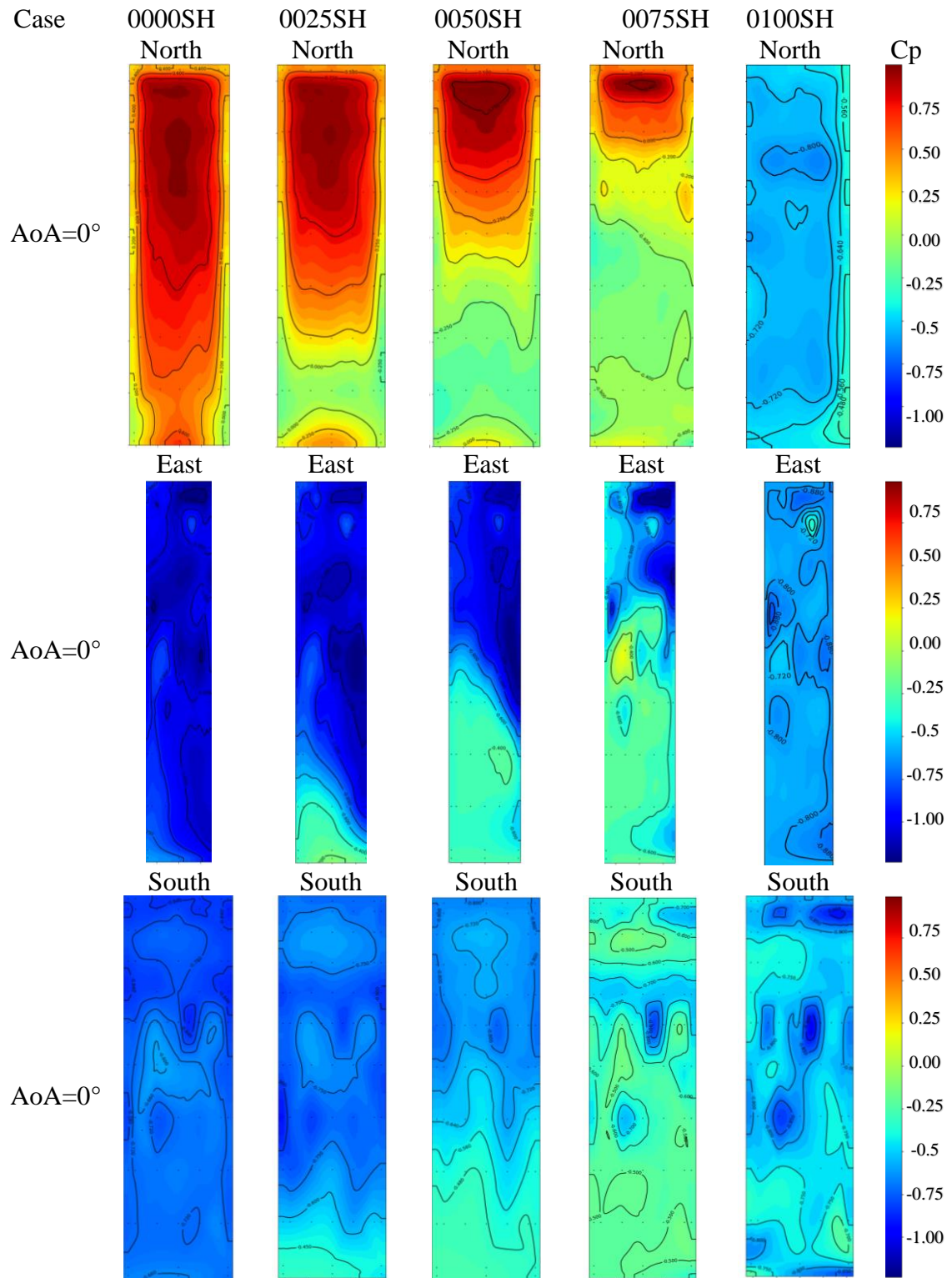


Figure 4-7: mean pressure distribution (C_p) for the north, east and south facades at $AoA=0^\circ$

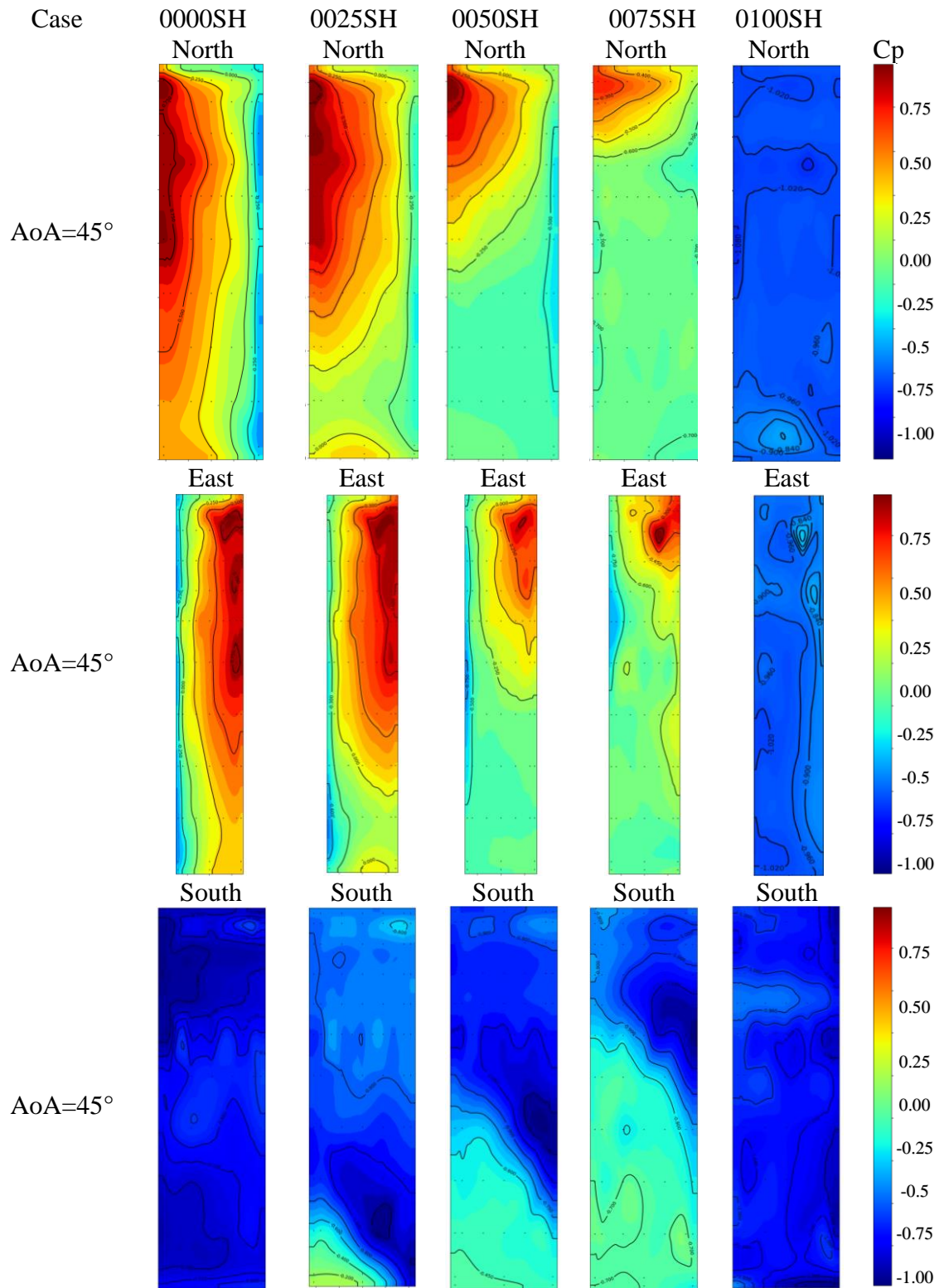


Figure 4-8: mean pressure distribution (C_p) for the north, east and south facades at $AoA=45^\circ$

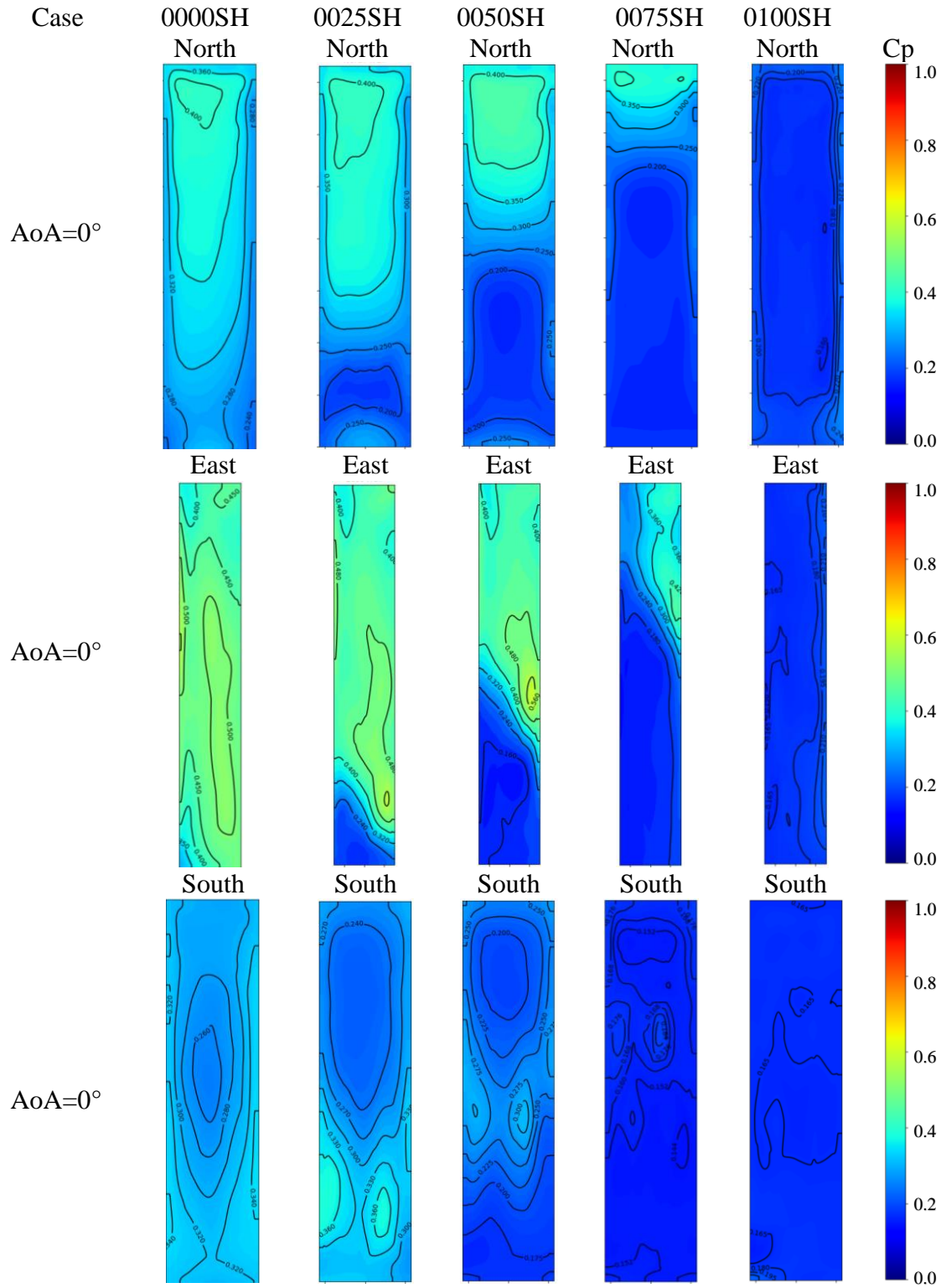


Figure 4-9: Rms pressure distribution (\hat{C}_p) for the north, east and south facades at AoA=0°

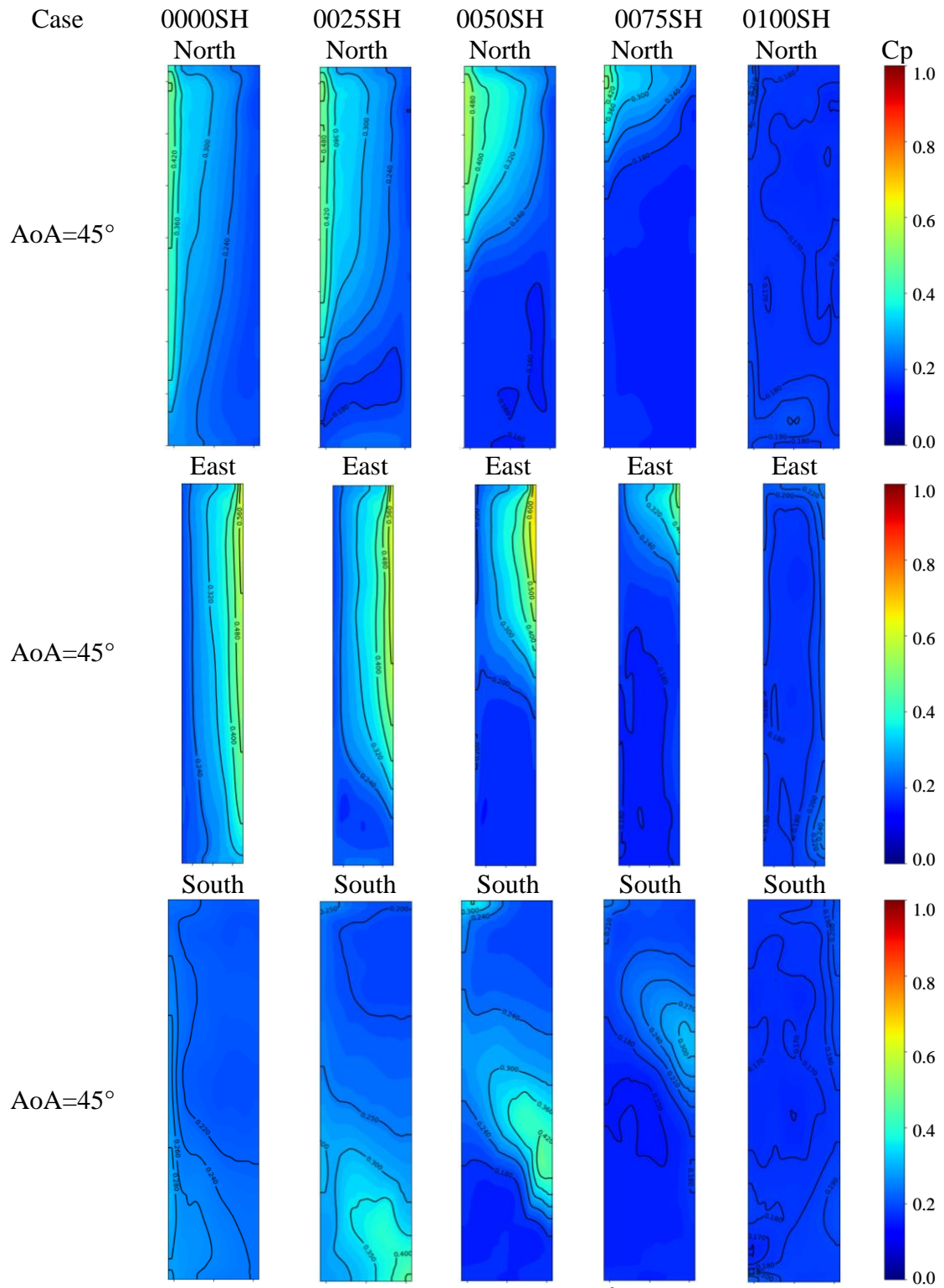


Figure 4-10: Rms pressure distribution (\hat{C}_p) for the north, east and south facades at AoA=45°

4.3.2 Base moment time histories and spectra

Figure 4-12, shows the base moment time histories around x, y and z-axis in the along wind, across wind and torsional directions as corresponding to the defined axis orientation, see Figure 4-11. It is noted that, the overall building moments decreases as the surrounding buildings increase in height ratios. This decrease in the along-wind moment specifically is derived due to the sheltering effect of the upstream surrounding buildings, causing a breakdown of the frontal large eddies into smaller ones which lead to a decrease in the across wind base moments as well.

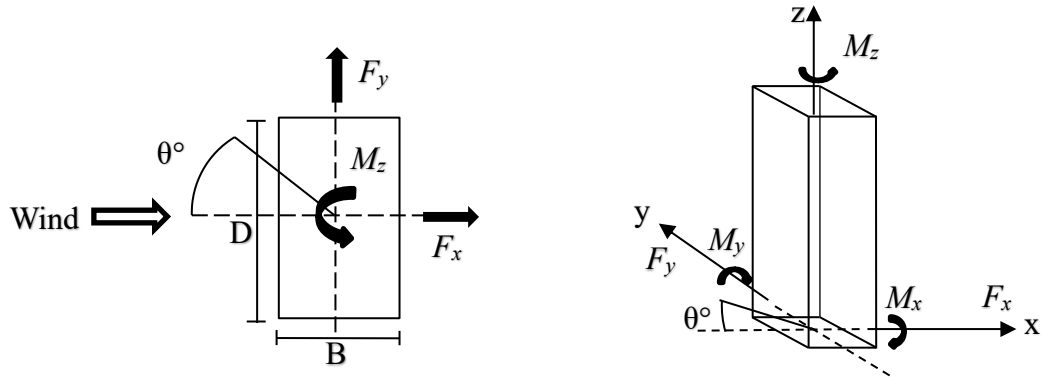


Figure 4-11: CAARC building axis definition

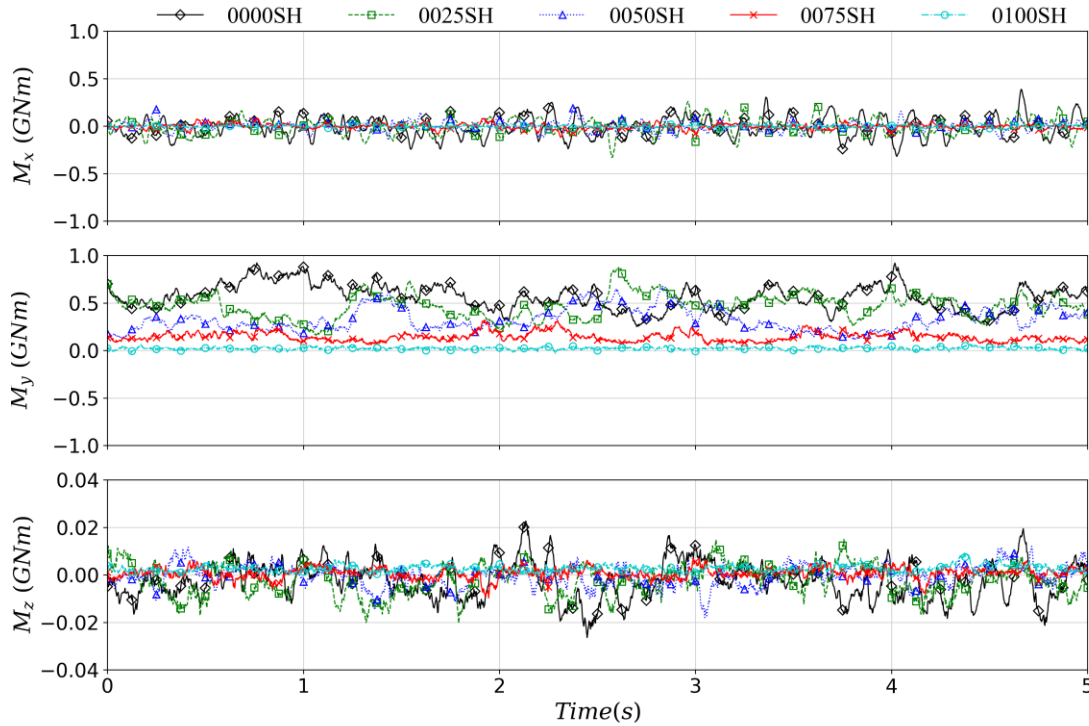


Figure 4-12: Base moments time histories for M_x , M_y and M_z at $AoA=0^\circ$

Figure 4-13 shows the power spectral densities (PSD) of base moments in the along-wind and the across-wind directions for different surrounding configurations. The along wind moment power spectra of the isolated case (0000SH) generally reflects the characteristics of the upstream wind corresponding to Von Karman spectrum with the energy distributed broadly. As the surrounding increase in height ratios for cases 0025SH, 0050SH and 0075SH, the high frequency vortices generate by the upstream buildings increases the amount of energy seen in the high frequency range of the spectra. For case 0100SH where the surrounding buildings totally cover the study building height, the spectra show a shift towards the high frequencies range. For this case, large scale eddies from the upstream exposure are unable to reach the study building, leaving the smaller scale eddies to interact with the buildings. This can also be further understood through observing the mean, rms and peak base moment plots described earlier, where case 0100SH has the lowest values compared to cases 0025SH, 0050SH and 0075SH in all directions. For the power spectra of the across wind base moment as shown in Figure 4-13 generally the isolated case has a sharp peak near the Strouhal number of 0.1. However, when the surrounding buildings increase in height ratios, the distribution of the vortex shedding changed, and the sharp peak dampened and distributed over a wider range of frequencies.

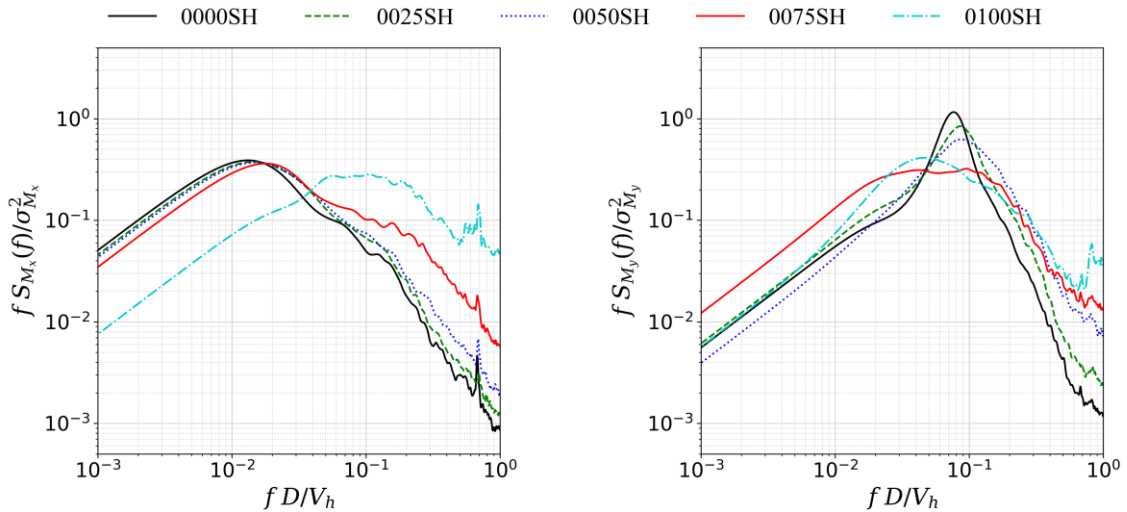


Figure 4-13: Power spectral density of the base moment for a) M_x and b) M_y at $AoA=0^\circ$

4.3.3 Mean, rms and peak base moments

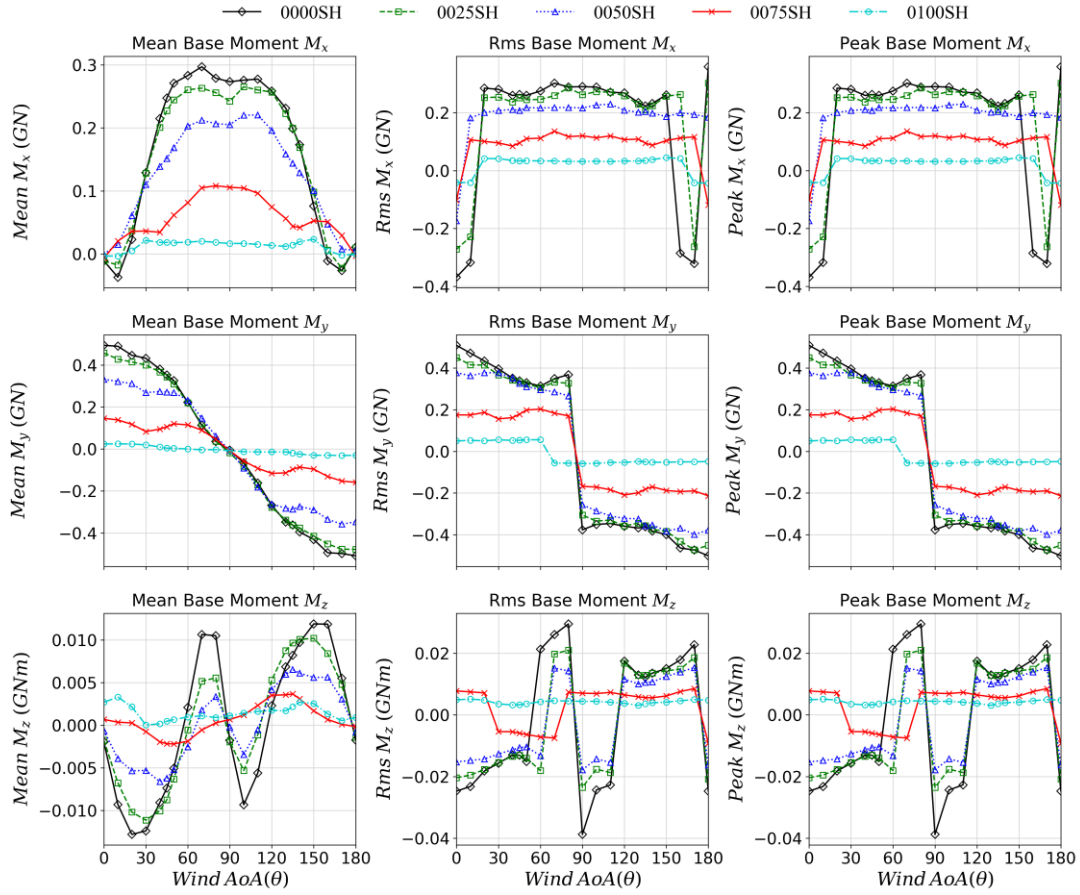


Figure 4-14: Mean, rms, and peak base moment for M_x , M_y , M_z for different surrounding configurations for different wind AoA

For further comparison, the mean, rms and peak of the base moments were plotted for each configuration in x, y and z directions for all angles of attack, see Figure 4-14. It is observed that cases 0000SH, 0025SH and 0050SH have closer values in terms of mean, rms and peak base moments. Although, there is a slight decrease in values compared to the isolated case 0000SH, they still follow the same trend and behavior which endures previous discussion. As for case 0075SH, it is obvious that the plots are more flattened with a significant drop in the mean, rms and peak base moments in the along wind, across wind and torsional directions. This can be due to the shielding effect of the surrounding buildings as it covers almost 75% of the building height. This disturbance of the upstream wind lead to breaking down of large eddies into smaller eddies which dramatically changed the aerodynamic behavior of wind. For case 0100SH the mean, rms and peak base moments

are almost zero which indicates a total coverage around the study building which breaks up the large vortices in the upcoming wind and alter their movement.

4.3.4 Top floor acceleration

This section presents the results of the dynamic analysis of the study for the different surrounding configurations under a 1-in-10-year wind speed. Figure 4-15, shows the accelerations for each wind AoA for each surrounding configuration. The peak top floor acceleration seems to be significantly reduced once the surrounding buildings reach %75 of the study building's height. Case 0025SH has a similar response to the isolated case 0000SH since the upstream buildings only shield the lower section of the study building, a region which has little impact on the top floor acceleration. Case 0050SH shows a reduction in the across wind motion as less of the building is exposed to the upstream flow. The reduction is only seen for the across wind motion which indicates that the vortex shedding mechanism is altered by the upstream surrounding conditions. For case 0075SH, the peak top floor acceleration caused by vortex shedding to be similar in magnitude as along wind responses. Finally, the shield effect of the surroundings causes the acceleration in case 0100SH to drop significantly compared to the previous case

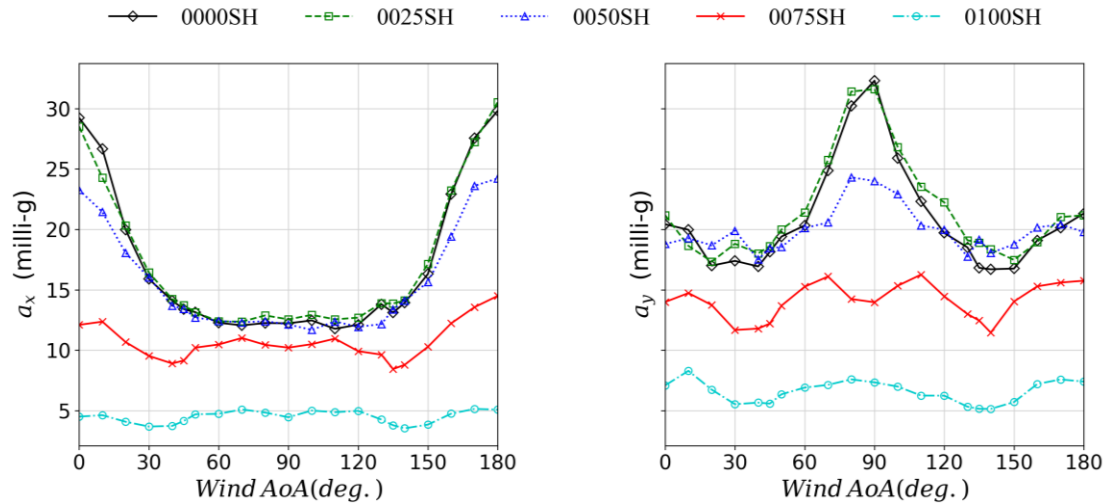


Figure 4-15: Top floor acceleration along the x-axis, y-axis and the torsional.

4.4 Conclusion

The previous study aimed to investigate the impact of city growth on high-rise buildings, focusing on response prediction under wind loads. High Frequency Pressure Integration (HFPI) tests were conducted in the Boundary layer wind tunnel to assess the complex behavior of wind with sheltering bodies and its impact on wind induced responses. These tests captured the building's pressure coefficients (Cps) and base moments within 5 different generic surrounding configurations equally spaced with varying height ratios for real representation of city development. The contribution of this study can be summarized as follows:

- i. A reduction of 25% and 50% in the area of high positive mean pressure are noticed in cases 0025SH and 0050SH respectively. However, these reductions did not affect the computed base moments for those cases since the majority of the load reduction is experienced in the lower portions of the building where the moment arms are smaller.
- ii. Cases 0075SH and 0100SH show reduction in the negative pressure in the leeward face along the height of the building and pressures along the western edge of the north face respectively.
- iii. Introduction of upstream buildings also caused higher fluctuation regions close to the roof height of the surrounding buildings which in turn kept the rms base moments unchanged to slightly decrease for cases 0000SH, 0025SH and 0050SH. For case 0075SH and 0100SH, the high fluctuation region near the top reduces significantly compared to cases 0025SH and 0050SH. s
- iv. The peak top floor acceleration showed a reduction as the surrounding height increases. Showing a drop of top peak acceleration of 6 times at case 0100SH when comparing to the reference isolated building.

4.5 References

- ASCE. 2012. “Wind Tunnel Testing for Buildings and Other Structures.” In . American Society of Civil Engineers.
- Bailey, P A, and K C S Kwok. 1985. “Interference Excitation of Twin Tall Buildings.” *Journal of Wind Engineering and Industrial Aerodynamics* 21 (3): 323–38.
- Bezabeh, M. A., G. T. Bitsuamlak, M. Popovski, and S. Tesfamariam. 2020. “Dynamic Response of Tall Mass-Timber Buildings to Wind Excitation.” *Journal of Structural Engineering* 146 (10): 04020199. [https://doi.org/10.1061/\(asce\)st.1943-541x.0002746](https://doi.org/10.1061/(asce)st.1943-541x.0002746).
- Chen, Xinzhong, and Ahsan Kareem. 2005. “Dynamic Wind Effects on Buildings with 3D Coupled Modes: Application of High Frequency Force Balance Measurements.” *Journal of Engineering Mechanics* 131 (11): 1115–25. [https://doi.org/10.1061/\(asce\)0733-9399\(2005\)131:11\(1115\)](https://doi.org/10.1061/(asce)0733-9399(2005)131:11(1115)).
- Cheung, J C K. 1984. “Effect of Tall Building Edge Configurations on Local Surface Wind Pressures.” In *3rd International Conference on Tall Buildings, Hong Kong and Guangzhou*, 10–15.
- Codes, National Research Council of Canada. Canadian Commission on Building and Fire. 2015. “National Building Code of Canada: 2015.” National Research Council of Canada. Canadian Commission on Building and Fire Codes.
- Cóstola, D., B. Blocken, and J. L.M. Hensen. 2009. “Overview of Pressure Coefficient Data in Building Energy Simulation and Airflow Network Programs.” *Building and Environment* 44 (10): 2027–36. <https://doi.org/10.1016/j.buildenv.2009.02.006>.
- Dagnew, Agerneh K., and Girma T. Bitsuamlak. 2014. “Computational Evaluation of Wind Loads on a Standard Tall Building Using Les.” *Wind and Structures, An International Journal* 18 (5): 567–98. <https://doi.org/10.12989/was.2014.18.5.567>.
- Davenport, A G. 1967. “The Treatment of Wind Loading on Tall Buildings.” In *Tall Buildings*, 3–45. Elsevier.
- Davenport, Alan G. 2002. “Past, Present and Future of Wind Engineering.” *Journal of Wind Engineering and Industrial Aerodynamics* 90 (12–15): 1371–80. [https://doi.org/10.1016/S0167-6105\(02\)00383-5](https://doi.org/10.1016/S0167-6105(02)00383-5).
- Elshaer, Ahmed, Haitham Aboshosha, Girma Bitsuamlak, Ashraf El Damatty, and Agerneh Dagnew. 2016. “LES Evaluation of Wind-Induced Responses for an Isolated and a Surrounded Tall Building.” *Engineering Structures* 115: 179–95. <https://doi.org/10.1016/j.engstruct.2016.02.026>.
- Elshaer, Ahmed, Anant Gairola, Kimberley Adamek, and Girma Bitsuamlak. 2017. “Variations in Wind Load on Tall Buildings Due to Urban Development.”

- Sustainable Cities and Society* 34 (December 2016): 264–77.
<https://doi.org/10.1016/j.scs.2017.06.008>.
- English, Elizabeth C. 1990. “Shielding Factors from Wind-Tunnel Studies of Prismatic Structures.” *Journal of Wind Engineering and Industrial Aerodynamics* 36: 611–19.
[https://doi.org/https://doi.org/10.1016/0167-6105\(90\)90343-B](https://doi.org/https://doi.org/10.1016/0167-6105(90)90343-B).
- ESDU. 2001. *Engineering Sciences Data Unit. Characteristics of Atmospheric Turbulence near the Ground. Part II: Single Point Data for Strong Winds*. 85320th ed.
- Holmes, John D. 2018. *Wind Loading of Structures*. CRC press.
- Holmes, John D, Yukio Tamura, and Prem Krishna. 2008. “Wind Loads on Low, Medium and High-Rise Buildings by Asia-Pacific Codes,” no. May: 29–31.
- Huang, Peng, and Ming Gu. 2005. “Experimental Study on Wind-Induced Dynamic Interference Effects between Two Tall Buildings.” *Wind and Structures, An International Journal* 8 (3): 147–61. <https://doi.org/10.12989/was.2005.8.3.147>.
- Hui, Yi, Akihito Yoshida, and Yukio Tamura. 2013. “Interference Effects between Two Rectangular-Section High-Rise Buildings on Local Peak Pressure Coefficients.” *Journal of Fluids and Structures* 37: 120–33.
<https://doi.org/10.1016/j.jfluidstructs.2012.11.007>.
- Kareem, Ahsan. 1992. “Dynamic Response of High-Rise Buildings to Stochastic Wind Loads.” *Journal of Wind Engineering and Industrial Aerodynamics* 42 (1–3): 1101–12. [https://doi.org/10.1016/0167-6105\(92\)90117-S](https://doi.org/10.1016/0167-6105(92)90117-S).
- Khanduri, A. C., T. Stathopoulos, and C. Bédard. 1998. “Wind-Induced Interference Effects on Buildings - A Review of the State-of-the-Art.” *Engineering Structures* 20 (7): 617–30. [https://doi.org/10.1016/S0141-0296\(97\)00066-7](https://doi.org/10.1016/S0141-0296(97)00066-7).
- Khanduri, Atul C., Theodore Stathopoulos, and Claude Bédard. 2000. “Generalization of Wind-Induced Interference Effects for Two Buildings.” *Wind and Structures, An International Journal* 3 (4): 255–66. <https://doi.org/10.12989/was.2000.3.4.255>.
- Kijewski, T; Kareem, A. n.d. “Dynamic Wind Effects - A Comparative Study (1998).Pdf.” *Wind & Structures*.
- Kim, Wonsul, Yukio Tamura, and Akihito Yoshida. 2011. “Interference Effects on Local Peak Pressures between Two Buildings.” *Journal of Wind Engineering and Industrial Aerodynamics* 99 (5): 584–600.
<https://doi.org/10.1016/j.jweia.2011.02.007>.
- Krishna, Prem. 1995. “Wind Loads on Low Rise Buildings - A Review.” *Journal of Wind Engineering and Industrial Aerodynamics* 54–55 (C): 383–96.
[https://doi.org/10.1016/0167-6105\(94\)00055-I](https://doi.org/10.1016/0167-6105(94)00055-I).

- Lam, K. M., M. Y. H. Leung, and J. G. Zhao. 2008. "Interference Effects on Wind Loading of a Row of Closely Spaced Tall Buildings." *Journal of Wind Engineering and Industrial Aerodynamics* 96 (5): 562–83.
- Lee, B E, and G R Fowler. 1975. "The Mean Wind Forces Acting on a Pair of Square Prisms." *Building Science* 10 (2): 107–10.
- Lieblein, Julius. 1974. "Efficient Lillithods of Extreme-Value Methodology," no. October.
- Mara, T. G., B. K. Terry, T. C.E. Ho, and N. Isyumov. 2014. "Aerodynamic and Peak Response Interference Factors for an Upstream Square Building of Identical Height." *Journal of Wind Engineering and Industrial Aerodynamics* 133: 200–210. <https://doi.org/10.1016/j.jweia.2014.06.010>.
- Melbourne, W. 1980. "Comparison of Measurements on the CAARC Standard Tall Building Model in Simulated Model Wind Flows." *Journal of Wind Engineering and Industrial Aerodynamics* 6: 73–88.
- Stone, Gary K. 1987. *Aerodynamic Interference Effects on Wind Loads and Responses of Tall Buildings*. Faculty of Engineering Science, University of Western Ontario.
- Surry, D., and D. Djakovich. 1995. "Fluctuating Pressures on Models of Tall Buildings." *Journal of Wind Engineering and Industrial Aerodynamics* 58 (1–2): 81–112.
- Surry, David, and William Mallais. 1983. "Adverse Local Wind Loads Induced by Adjacent Building." *Journal of Structural Engineering* 109 (3): 816–20. [https://doi.org/10.1061/\(asce\)0733-9445\(1983\)109:3\(816\)](https://doi.org/10.1061/(asce)0733-9445(1983)109:3(816)).
- Taniike, Yoshihito. 1991. "Turbulence Effect on Mutual Interference of Tall Buildings." *Engineering Mechanics* 117 (3): 443–56.
- Xie, J, and P A Irwin. 1998. "Application of the Force Balance Technique to a Building Complex." *Journal of Wind Engineering and Industrial Aerodynamics* 77: 579–90.
- Xie, Z. N., and M. Gu. 2007. "Simplified Formulas for Evaluation of Wind-Induced Interference Effects among Three Tall Buildings." *Journal of Wind Engineering and Industrial Aerodynamics* 95 (1): 31–52. <https://doi.org/10.1016/j.jweia.2006.05.003>.
- Xie, Z. N., and Minggu Gu. 2004. "Mean Interference Effects among Tall Buildings." *Engineering Structures* 26 (9): 1173–83. <https://doi.org/10.1016/j.engstruct.2004.03.007>.
- Zhang, Aishe, and Ming Gu. 2008. "Wind Tunnel Tests and Numerical Simulations of Wind Pressures on Buildings in Staggered Arrangement." *Journal of Wind Engineering and Industrial Aerodynamics* 96 (10–11): 2067–79. <https://doi.org/10.1016/j.jweia.2008.02.013>.

Chapter 5

5 Conclusion

5.1 Summary

In this research study the impact of city growth on building response is represented by experimentally testing five different surrounding configurations. The configuration includes 25% increase in Surrounding Height (0025SH), 50% increase (0050SH), 75% increase (0075SH) and 100% increase (0100SH) in surrounding building heights, along with an isolated case scenario (0000SH) arranged regularly for generic assessment. The changes in surroundings ratios are found to have different impacts on structural and non-structural elements from wind hazard perspective. Firstly, the cladding loads evaluation showed that the overall recorded mean wind pressures are reduced while fluctuations within these pressures are increasing as the urban environment becomes denser. Due to Bernoulli and venturi, local pressure increases are observed for certain cases. The results show showed 40% increase for case 0025SH at a value of -7.0 compared to the isolated case 0000SH for the lower corner of the building and 20% increase in the negative peak pressures \check{C}_p for case 0050SH at a value of -6.5 compared to the isolated case scenario 0000SH at $AoA=90$ with an upward shift. These high fluctuations are the result of continues wake disturbance with the sheltering body, speeding up the vortices formed there and increasing the fluctuations significantly which subject the building to higher risks of cladding failure.

In addition, the structural load evaluation has shown an overall reduction in base moments. However, the reduction of mean pressure did not affect the computed base moments for cases 0025SH and 0050SH since the majority of the load reduction is experienced in the lower portions of the building where the moment arms are smaller. Moreover, the upward shift of the positive pressures produced a contradicting effect to the moments lost at the base. On the contrary, the reduction of positive pressures in cases 0075SH and 0100SH outweighs the impact of the upwards shift showing a significant drop by almost 50% in base moments. Furthermore, The Introduction of upstream buildings also caused higher fluctuation regions close to the roof height of the surrounding buildings which in turn kept

the rms base moments unchanged to slightly decrease for cases 0000SH, 0025SH and 0050SH while cases 0075SH and 0100SH, they experienced significant drop in fluctuations. Finally, the peak top floor acceleration showed similar trends as the base moments with slight a reduction in peak acceleration for cases 0025SH and 0050SH while a significant drop was notices for case 0100SH by 6 times less acceleration compared to the reference isolated building 0000SH.

5.2 Recommendation for future work

The current thesis discusses several topics related to urban city development and the effect of generic configurations development on the structural and non-structural elements of tall buildings. For future research, the following investigations are suggested:

- Investigate the effect of different surrounding orientations and spacing between the study model and surrounding buildings
- Include the impact of city growth considering a realistic/future surrounding conditions and climate types.
- Investigate different urban layouts and street patterns other than the regular grid pattern.



- Study the effect of city growth on the pedestrian level wind (PLW).

Curriculum Vitae

Name:	Hadil Abdallah
Post-secondary Education and Degrees:	University of Alexandria Alexandria, Egypt 2012-2016, B.Sc. Architecture and Construction Engineering
Honours and Awards:	NSERC- Canada Graduate Scholarship (CGSM) 2019-2021 SOSCIP Ontario Centres of Excellence TalentEdge and IBM Canada 2018-2019
Related Work Experience	Teaching Assistant The University of Western Ontario 2018-2020 Research Assistant The University of Western Ontario 2018-2021
Publications:	

Elshaer, A., Abdallah, H., Bitsuamlak, G., (2019). Variation in wind load and flow of a low-rise building during progressive damage scenario. *Wind and Structures* 28(6), 389-404.